UNIVERSITÉ DE SHERBROOKE

Faculté de génie
Département de génie civil

SERVICEABILITY OF CONCRETE MEMBERS REINFORCED WITH FRP BARS

ÉTUDE DU COMPORTEMENT EN SERVICE DE MEMBRURES EN BÉTON RENFORCÉES DE BARRES DE PRF

Thèse de doctorat
Spécialité : génie civil

Jury: Prof. Brahim BENMOKRANE, directeur de recherche
Prof. Amr ELRAGABY, Examinateur
Prof. Adel EL SAFTY, Examinateur
Prof. Ammar YAHIA, Rapporteur

Amr Maher El-Nemr

Sherbrooke (Québec) Canada **January 2013**

Your file Votre référence
ISBN: 978-0-494-93230-8

Our file Notre référence
ISBN: 978-0-494-93230-8

ABSTRACT

The deterioration of Canadian infrastructure due to corrosion of steel reinforcement is one of the major challenges facing the construction industry. Recent advances in polymer technology have led to the development of new generations of fiber-reinforced-polymer (FRP) reinforcing bars. These corrosion resistant bars have shown promise way to further protect bridges and public infrastructure from the devastating effects of corrosion. The recently published [CAN/CSA-S807, 2010] "*Specification for fibre-reinforced Polymers*" along with the FRP bars being produced of the highest quality strongly supported the FRP reinforcement as a realistic and cost-effective alternative to traditional steel reinforcement for concrete structures under severe environmental conditions.

The design of concrete members reinforced with FRP bars is typically governed by serviceability state rather than ultimate state. Thus, there is a need to investigate the flexural performance and the deflection and crack width behaviour, the two terms of serviceability criteria. In addition, recent developments in the FRP industry led to introducing FRP bars with different surface configurations and mechanical properties as well. These developments are expected to affect their bond performance and, consequently, the crack width in FRP-reinforced concrete members. The design codes and guidelines, however, provide a unique value for the bond-dependent coefficient (k_b) considering the surface configurations and neglecting FRP bar type, bar diameter, and concrete type and strength.

This research program aims at investigating the flexural behaviour and serviceability performance of concrete members reinforced with different types and ratios of carbon and glass FRP bars and fabricated using normal-and high-strength concretes. In addition, it evaluates the bond-dependent coefficient (k_b) of glass and carbon FRP bars in normal- and

high-strength concrete beams. The experimental program included fabricating and testing of thirty three full-scale simply-supported beams measuring 4250-mm long × 200-mm wide × 400-mm deep. Twenty seven concrete beams were reinforced with glass FRP bars, four concrete beams were reinforced with carbon FRP bars, and two beams were reinforced with steel bars. All beams were tested in four-point bending over a clear span of 3750 mm. The test parameters were: reinforcement type and ratio, FRP bar diameter and surface configurations, number of FRP layers, and concrete strength. The test results of these beams were presented and discussed in terms of flexural capacity and mode of failure, concrete and reinforcement strains, deflection, and crack widths through three journal papers presented in this thesis.

Among the three papers presented in this thesis, two investigated the flexural behaviour and serviceability performance of carbon and glass FRP-reinforced concrete beams fabricated with normal- and high-strength concretes. These two papers investigated GFRP bars of different grades, diameters, and surface configurations. While the third one evaluated the current design recommendations for bond-dependent coefficient (k_b) values and checked the dependency of the k_b values on FRP bar type (glass and carbon), diameter, and concrete type and strength. The cracking moments and flexural capacity were compared against the provisions of the North American codes and guidelines [ACI 440.1R-06, 2006; ISIS Manual No.3, 2007; CAN/CSA-S6.1S1, 2010; CAN/CSA-S806, 2012]. In addition, the experimental results were employed in assessing the accuracy of the current deflection and crack-width prediction equations and the k_b values in the FRP design codes and guidelines in North America [ACI 440.1R-06, 2006; ISIS Manual No.3, 2007; CAN/CSA-S6.1S1, 2010; CAN/CSA-S806, 2012]. The results introduced the effect of different parameters on the flexural behaviour and serviceability performance of the FRP- reinforced concrete members.

Furthermore, the findings did not support the unique k_b value for FRP bars of different types (carbon and glass) with similar surface configurations and was found to be dependent on bar diameter.

RÉSUMÉ

La détérioration des infrastructures au Canada due à la corrosion des armatures est l'un des défis majeurs de l'industrie de la construction. Les progrès récents dans la technologie des polymères ont conduit au développement d'une nouvelle génération de barres d'armature à base de fibres renforcées de polymères (PRF), (en particulier les fibres de verre). Ces barres, résistant à la corrosion, ont montré un grand potentiel d'utilisation pour mieux protéger les infrastructures en béton armé contre les effets dévastateurs de la corrosion. Avec la publication du nouveau code S807-10 "*Spécifications pour les polymères renforcés de fibres*" et la production de barres en PRF de très haute qualité, celles-ci représentent une alternative réaliste et rentable par rapport à l'armature en acier pour les structures en béton soumises à de sévères conditions environnementales.

La conception des éléments en béton armé de barres en PRF est généralement gouvernée par l'état de service plutôt que l'état ultime. Par conséquent, il est nécessaire d'analyser les performances en flexion et le comportement en service en termes de déflexion et de largeur de fissures des éléments en PRF sous charges de service et de vérifier que ces éléments rencontrent les limites des codes.

Aussi, de récents développements dans l'industrie des PRF ont conduit à l'introduction des barres en PRF avec des configurations de surface et des propriétés mécaniques différentes. Ces développements sont susceptibles d'affecter leur performance d'adhérence et, par conséquent, la largeur des fissures dans les éléments en PRF. Cependant, les codes de conception et les guidelines de calcul fournissent une valeur unique pour le coefficient

d'adhérence (k_b) en tenant compte des configurations de surface et en négligeant le type de barre en PRF, le diamètre de la barre, et le type de béton et de sa résistance.

En outre, le code canadien S807-10 "*Spécifications pour les polymères renforcés de fibres*" fournit une étape en classant les barres en PRF par rapport à leur module d'élasticité (E_{frp}). Ces classifications ont été divisées en trois classes : Classe I (E_{frp} <50 GPa), Classe II (50 GPa ≤ E_{frp} < 60 GPa) et Classe III (E_{frp} ≥ 60 GPa)

Ce programme de recherche vise à étudier expérimentalement le comportement en flexion des éléments en béton en service armé avec différents paramètres sous charges statiques. Le programme expérimental est basé sous plusieurs paramètres, dont les différents ratios de renforcement, différents types de barres (différentes classes comme classifiées par le CAN/CSA S807-10), le diamètre et la surface de la barre, la configuration ainsi que la résistance du béton.

De plus, les recommandations actuelles de design pour les valeurs de k_b et la vérification de la dépendance des valeurs de k_b sur le type de barres (verre ou carbone), le diamètre des barres et le type de béton et sa résistance ont été étudiées

Le programme expérimental comprenait la fabrication et les essais sur 33 poutres à grande échelle, simplement appuyées et mesurant 4250 mm de long, 200 mm de large et 400 mm de hauteur. Vingt et sept poutres en béton ont été renforcées avec des barres en PRF à base de verre, quatre poutres en béton ont été renforcées avec des barres de PRF à base de carbone, et deux poutres ont été renforcées avec des barres en acier. Toutes les poutres ont été testées en flexion quatre points sur une portée libre de 3750 mm.

Les paramètres d'essai étaient: le type de renforcement, le pourcentage d'armature, le diamètre des barres, configurations de surface et la résistance du béton. Les résultats de ces essais ont été présentés et discutés en termes de résistance du béton, de déflection, de la largeur des fissures, de déformations dans le béton et l'armature, de résistance en flexion et de mode de rupture.

Dans les trois articles présentés dans cette thèse, le comportement en flexion et la performance des poutres renforcées de barres en PRFV et fabriquées avec un béton normal et un béton à haute performance ont été investigués, ainsi que les différentes classes de barres en PRFV et leurs configurations de surface. Les conclusions des investigations expérimentales et analytiques contribuent à l'évaluation des équations de prédiction de la déflection et des largeurs de fissures dans les codes de béton armé de PRF, pour prédire l'état de service des éléments en béton renforcés de PRF (déflection et largeur de fissures)

En outre, à la lumière des résultats expérimentaux de cette étude, les équations de service (déflection et largeur des fissures) incorporées dans les codes et guidelines de design [ACI 440.1R-06, 2006; ISIS Manual No.3, 2007; CAN/CSA-S6.1S1, 2010; CAN/CSA-S806, 2012] ont été optimisées. En outre, les largeurs de fissures mesurées et les déformations ont été utilisées pour évaluer les valeurs courantes de k_b fournies par les codes et les guidelines de calcul des PRF. En outre, les conclusions ne prennent pas en charge la valeur unique de k_b pour les barres en PRF de types différents (carbone et verre) avec des configurations de surface similaires et s'est avéré être dépendant du diamètre de la barre.

ACKNOWLEDGEMENTS

The author yields sincere gratitude and thanks to Prof. Brahim Benmokrane, NSERC Research Chair Professor in Innovative FRP Composites for Infrastructures (Ph.D. advisor); Dr. Ehab Ahmed, Post-doctoral fellow at the Department of Civil Engineering, University of Sherbrooke.

The author would also like to thank the structural laboratory technical staff at the Department of Civil Engineering at the University of Sherbrooke, especially, Mr. François Ntacorigira, Simon Kelly, and Martin Bernard for their help in constructing and testing the specimens.

The finical support received from the Natural Sciences and Engineering Research Council of Canada (NSERC), Fonds Québécois de la recherché sur la nature et les technologies (FQRNT), Pultrall Inc. (Thetford Mines, Quebec, Canada), the Ministry of Transportation of Quebec (MTQ), the Network of Centres of Excellence on the Intelligent Sensing of Innovative Structures (ISIS Canada), and the University of Sherbrooke is greatly acknowledged.

Sincere gratitude and respect is given to Dr. Ehab Ahmed, Dr. Ahmed Sabry, Dr. Mathieu Robert, Dr. Patrice Cousin, Mr. Fadi Yassa, Mrs. Ghada Eloraby, Mrs. Nayera Mohamed, Mr. Mathieu Montaigu, Mr. Jean-François Claude, Mr. Patrick Vincent and Mr. Mohammed Osama for their genuine help while conducting this PhD program.

Special thanks to *Fadi Yassa* who always fulfill the wisdom saying "*a friend in need is a friend indeed*". He was always there when I needed him. He taught me to be responsible for myself and my acts. I am very lucky to know a humble person like him.

This Thesis is dedicated to *my parents and my future wife* (*Lina Mohammed El-Beltagy*), to my brothers and sister for their patience, support, and encouragement. This support cannot be praised enough. There are no words that can fulfill their support. Special thanks to my Father, *Prof. Maher El-Nemr*, who believed in me and in my ability that "*I can do it*".

TABLE OF CONTENTS

LIST OF FIGURES

LIST OF TABLES

NOMENCLATURE

A = effective tension area of concrete surrounding the flexural tension reinforcement and bearing the same centroid as that reinforcement, divided by the number of bars (mm^2);

a = shear span (mm);

A_f = area of FRP tension reinforcement (mm^2);

b = effective width of beam (mm);

c = neutral axis depth (mm);

c/d = neutral axis-to- depth ratio;

d = distance from the extreme compression fiber to the centroid of tension force (mm);

d_b = bar diameter (mm);

d_c = distance from extreme tension fiber to the centre of the longitudinal bar or wire located closest thereto according to the code or guideline (mm);

E_c = modulus of elasticity of concrete (MPa);

E_f = modulus of elasticity of longitudinal FRP reinforcement (MPa);

E_s = modulus of elasticity of longitudinal steel reinforcement (MPa);

f'_c = compressive strength of the concrete (MPa);

f_f = stress in FRP reinforcement under specified loads (MPa);

f_{frpu} = characteristic tensile strength (average – 3 standard deviation (SD))

f_{fu} = ultimate strength of FRP longitudinal reinforcement (MPa);

f_G = guaranteed tensile strength (average – 3 standard deviation (SD));

f_r = modulus of rupture (MPa);

f_r = modulus of rupture (MPa);

f_s = stress in reinforcement at serviceability limit state and shall be calculated on the basis of a cracked section;

f_t = tensile strength from cylinder-splitting test (MPa);

f_y = yield strength of steel longitudinal reinforcement (MPa);

h_1 = distance from neutral axis to center of tensile reinforcement (mm);

h_2 = distance from neutral axis to extreme tension fiber (mm);

I_{cr} = transformed moment of inertia of cracked reinforced concrete section (mm^4);

I_e = effective moment of inertia (mm^4);

I_g = gross moment of inertia of un-cracked section (mm^4);

J = Deformability factor.

k_b = bond-dependent coefficient;

L = length of clear span (mm);

L_g = length of the un-cracked section (mm);

M_a = applied moment (kN.m);

M_{cr} = cracking moment (kN.m);

M_{cr} = cracking moment (kN.m);

M_n = nominal moment of the reinforced-concrete section (kN.m);

M_S = Service moment at a corresponding concrete strain of 1,000 microstrains or 2,000 microstrains in the FRP reinforcement as defined by Newhook *et al.*, [2002] (kN.m);

M_U = Ultimate moment (kN.m);

M_y = moment corresponding to the yield stress of the steel bars (kN.m);

P = applied load (kN);

s = spacing between the longitudinal reinforcement bars (mm);

SD = standard deviation;

w = maximum crack width (mm);

y_t = distance from centroid axis of cross-section to the extreme fiber in tension (mm);

z = maximum stresses at crack width initiated adopted by CAN/CSA-S806, [2012] (N/mm);

δ = mid-span deflection (mm);

ε_{cu} = ultimate strain of concrete;

ρ_f = longitudinal reinforcement ratio;

ρ_{fb} = balanced longitudinal reinforcement ratio.

ψ = curvature;

Ψ_S = curvature at a corresponding concrete strain of 1,000 microstrains or 2,000 microstrains in the FRP reinforcement as defined by Newhook *et al.*, [2002];

Ψ_U = curvature at ultimate state.

CHAPTER 1
INTRODUCTION

1.1 Background and Problem Definition

Considerable damage of reinforced concrete structures occurs due to the corrosion of steel reinforcement and related deteriorations. This problem is a major challenge for the construction industry, especially, when the reinforced concrete structures are subjected to harsh environmental conditions. These conditions normally accelerate the need of costly repairs and may lead to catastrophic failures. Due to its non-corrosive nature, the fiber-reinforced polymer (FRP) reinforcement is being used as an alternative to steel bars to overcome the common corrosion problems and deteriorations. The recent advancement in the FRP technology led to introducing FRP bars with enhanced mechanical properties and surface configurations, which is expected to increase the use of FRP. In addition, the recently published standards for the FRP specifications [CAN/CSA-S807, 2010] provided a step forward for increasing the use of FRP materials and for introducing them to new applications.

The FRP bars have different mechanical and bond properties compared with those of steel bars. The FRP bars are characterized by very high tensile strength, relatively low modulus of elasticity, and linear stress-strain behaviour until failure. The lower modulus of FRP bars yields large strains being developed in the bars at low load levels creating large crack widths and deflections. As a result, the design of concrete members reinforced with FRP materials is governed by the serviceability limit state (SLS) rather than the ultimate limit state (ULS) [Mathys and Taerwe, 2000; Nanni, 2003]. Due to lack of standards, a wide variety of FRP products with different properties and surface configurations are commercially available.

The FRP bars could vary significantly because their properties are relying on type of fiber, type of resin, and manufacturing process in addition to the surface and/or coating characteristics [Ceroni *et al.*, 2006; Baena *et al.*, 2009]. Consequently, the design models and guidelines are required to cope with all the available FRP products. Furthermore, most of the FRP design codes and guidelines are based on adopting the design equations for steel reinforced members with some modifications to account for the different mechanical and/or bond properties. Thus, the design equation may yield good results with one type of FRP bars and discrepancy with any other type.

Serviceability (deflection and crack width) is also one of the most important issues in designing the FRP reinforced concrete members due to the lower modulus of elasticity of FRP than that of steel. For deflection, coefficients were proposed to modify Branson's equation used in steel design codes [ACI 318, 2008], while other suggestions were introduced to use the modified equivalent moment of inertia derived from the integration of curvatures along the beam. These different approaches were adopted in various FRP design codes and guideline for predicting the deflection of FRP reinforced concrete beams [ACI 440.1R-06, 2006; ISIS Manual No.3, 2007; CAN/CSA-S806, 2012]. On the other hand, cracking behaviour of FRP reinforced concrete elements, design equations and prediction models are generally based on similar formula to that of steel reinforced concrete such as Gerlgy-lutz and Frosch formula with coefficient that depends on the different characteristics of the bars and their interaction with concrete, however, the design formula for crack width is still under discussion even for steel reinforced concrete [Beeby, 2004; Beeby *et al.*, 2005; fib., 2010]. In addition, the crack width calculations include the effect of bond between the FRP bars and the surrounding concrete; which is normally included in the FRP design codes and guidelines through what-so-called bond-dependent coefficient (k_b), while the interpretation of this coefficient remains

ambiguous [McCallum et Newhook, 2012]. The FRP design codes and guidelines provide unique values for the bond-depended coefficient (k_b) depending on the surface characteristics of the bar only and neglecting FRP bar type, diameter, and surrounding concrete type and strength.

Based on the results from the literature and considering the different available FRP products, there is a need for further investigation concerning the flexural response and serviceability performance of FRP reinforced concrete members using normal- and high-strength concretes.

1.2 Research Objectives

This study aims at investigating the flexural behaviour and serviceability behaviour of FRP reinforced concrete beams reinforced with different types of FRP bars and fabricated using normal- and high-strength concretes. The study focused on three types of glass FRP bars and one type of CFRP bars as they are being used extensively in Canada. Few studies were conducted on high-strength concrete beams; however, many extensive studies were conducted by normal-strength concrete. Thus, this study included both normal- and high-strength concretes. The specific objectives of this study are:

- To investigate the flexural of concrete beams reinforced with different types and ratios of glass and carbon FRP bars using normal- and high-strength concretes;
- To investigate the serviceability (cracking and deflections) performance of normal- and high-strength concrete beams reinforced with FRP bars;

- To evaluate the current design approaches of the FRP reinforced concrete beams at service and ultimate load levels (SLS and ULS) and to evaluate the applicability of the design provisions on both concrete types (normal and high-strength);
- To evaluate the bond dependent coefficient (k_b) recommended by current design codes and guidelines and check the dependency of k_b values on FRP bar type (glass and carbon), FRP diameter, and concrete strength.

1.3 Methodology

To achieve the aforementioned objectives, an extensive experimental program was conducted. The program included full-scale simply supported concrete beams reinforced with different types and ratio of FRP bars. The beams measured 4250-mm long x 200-mm wide x 400-mm deep. The test parameters were the type of FRP reinforcing bars, reinforcement ratio, bar diameter. The beams specimens were fabricated with normal- and high concrete strengths (NSC and HSC). The experimental program aspects (materials, specimens, testing, and analysis are summarized in this section:

a- Materials:

Reinforcement:

(i) GFRP-1: Sand Coated glass FRP bars of diameters 13, 15, 20, 22, and 25 mm having fiber content ratio (by weight) of 80.8%, 81.4%, 82.7%, 82.5% and 82.3%, with two different grades of modulus of elasticity (46.4 to 53.2 GPa);

(ii) GFRP-2: Sand Coated glass FRP bars of diameters 13, 15, 20, and 25 mm having fiber content ratio (by weight) of 81.7%, 81.4%, 81.6%, and 82.4%, with two different grades of modulus of elasticity (52.5 to 69.3 GPa);

(iii) GFRP-3: Helically-grooved glass FRP bars of 15, and 25 mm diameter having fiber content ratio of 86.7% and 88.6%, with standard modulus of elasticity close to 60 GPa;

(iv) CFRP-1: Sand Coated carbon FRP bars of diameter 10, and 13 mm having fibre content ratio of 78.8% and 75.9%, with standard modulus elasticity around 140 GPa;

(v) Conventional 10M and 15M steel of diameter 15.9 mm as well as smooth steel bars of 10 mm diameter for steel stirrups, with standard modulus of elasticity of 200 GPa.

Concrete:

Ready-mixed normal- and high-strength concretes (NSC and HSC) with 28-day target compressive strengths of 30 and 65 MPa, respectively, were used. The composition of the concrete mix of both concrete types was as follows:

(i) Normal Concrete Strength: A cubic meter of the NSC contained 350 kg of cement, 813 kg of sand, and 1032 kg of aggregate with a water/cement ratio (*w/c*) of 0.44 and air entrained ratio of 5-6%. The maximum aggregate size was 20 mm.

(ii) High Concrete Strength: A cubic meter of HSC contained 490 kg of cement, 813 kg of sand, and 1032 kg of aggregate with a water/cement ratio (*w/c*) of 0.32 and 0% of air entrained. The maximum aggregate size was 14 mm.

b- Instrumentation and testing:

(i) 500 KN hydraulic actuator used for applying the load with stroke-controlled rate of 0.6 mm/min. The Beams were tested in four-point bending over a clear span of 3750-mm.

(ii) Electrical strain gauges of 10 and 60 mm length and 120 ohm resistance manufactured by Kyowa limited for measuring strains along the reinforcing bars.

(iii) Six high precision linear variable displacement transducers (LVDTs) for measuring deflection along the beam at different load levels as well as the crack width evolution during the test after determining their initial widths using a hand-held microscope of 50X magnifying power.

(iv) A data acquisition system comprising 60 channels controlling the loading, strain gauges, and LVDTs for cracking and deflection.

c- Analysis:

(i) Analyzing the flexural behaviour and serviceability performance of the beams and discussing the test results in the light of the codes and guidelines recommendations and requirements. Strains, crack widths, and deflections were compared and conclusions were drawn. The bond dependent coefficient k_b for cark width prediction was also assessed and evaluated. The codes' equations were compared against the experimental results and conclusions were drawn.

1.4 Structure of the Thesis

The thesis comprises seven chapters; three of them (chapters 3 to 5) presents papers accepted/submitted to Journals. The following is a brief description of each chapter's content:

Chapter 1: This chapter defines the problem and presents the main objectives of this study. The methodology followed to achieve the objectives of this research program is also highlighted and the structure of the thesis is presented.

Chapter 2: This chapter provides a literature review on the serviceability of FRP reinforced concrete members. This chapter also presents the main factors influencing the deflection and crack width of FRP reinforced concrete beams. The currently available equations for flexural capacity, deflection and cracking in the design codes and guidelines in North America are also summarized.

Chapter 3: This chapter includes a paper submitted to the ACI Structural Journal. The paper investigated the flexural behaviour and serviceability performance of GFRP reinforced concrete beams in terms of deflection, crack width, strains in concrete and reinforcement, flexural capacity, and mode of failure. The results were verified against the current deflection and crack-width prediction equations in the North American FRP design guidelines and Canadian codes.

Chapter 4: This chapter includes a paper submitted to the ASCE Journal of Construction Composites. The paper aimed at investigating the current design recommendations for the bond-depended coefficient (k_b) values and verifying the dependency of the k_b values on FRP bar type, diameter, and concrete type and strength. The findings did not support the unique k_b

value for FRP bars of different types with similar surface configurations. Moreover, k_b was found to be dependent on bar diameter.

Chapter 5: This chapter includes a paper submitted to the Canadian Journal of Civil Engineering. This paper evaluates the flexural behaviour and serviceability performance of concrete beams reinforced with GFRP bars of different grades and surface configurations. The results were presented in terms of serviceability and flexural performance and verified against the current serviceability prediction equations of North American FRP design guidelines and Canadian codes. The Deformability of FRP reinforced concrete beams are also evaluated and discussed in the lights of the codes' requirements.

Chapter 6: This chapter includes the overall conclusions of this study based on the findings. In addition, recommendations for further research work are also presented.

CHAPTER 2

LITERATURE REVIEW

2.1 Background

Concrete material is strong in compression and weak in tension. Thus, the behaviour presents a brittle behaviour in tension. Reinforcing concrete with steel has been traditional solution to the brittle act of concrete under tension. Because of its mechanical properties, steel provides well flexure behaviour when used as reinforcement in concrete members.

Although its adequate bond transfer as reinforcement, the steel corrodes rapidly under aggressive conditions such as severe weather where deicing salts are used. Thus, with the development of composite materials, Fiber reinforced polymer (FRP) emerged an alternative substitute were used instead of steel, especially when durability under aggressive conditions is required.

These materials have different mechanical properties from steel, in addition, to their surface textures which affect the bond transfer mechanism between the bar and the surrounding concrete. This chapter includes a review of the basic aspects that affect the flexural behaviour of FRP reinforced concrete members.

The chapter is describing the main mechanical properties of concrete and FRP bars as internal reinforcement of reinforced concrete in according to CAN/CSA-S807 [2010] classification. In addition, the chapter gives a brief summary about the FRP manufacturer and its new development. Also, a brief summary on service limit states adopted by different codes and guidelines is presented.

Then after, an overview of the flexural capacity of reinforced concrete beams in terms of current equations available in codes and guidelines were validated. Moreover, the design prediction equations for deflection and crack width recently adopted by codes and guidelines were presented and described with their limitations.

2.2 Material properties

2.2.1 Concrete:

Several test books provides many information and models on concrete properties [Neville, 1970] but most were limited to quasi-static and one-dimensional states of stress-strain. More review of this information is given by Aoyama et Noguchi, [1979]. Furthermore, extensive reviews have also been given by Newman [1966], Brooks et Newman [1968] and Shah [1980] on high concrete strength.

Concrete forms a large number of micro cracks, especially at interfaces between coarser aggregates and mortar even before any load has been applied [Chen et Saleeb, 1982]. Thus, the propagation of these micro cracks during loading contributes to nonlinear behaviour of concrete at a low stress level and causes the volume expansion near failure. These micro cracks may be caused by segregation, shrinkage or thermal expansion in mortar developed during loading through the differences in stiffness between aggregates and mortar. The mechanical behaviour of concrete is strong in compression and weak in tension due to the aggregate mortar interface that has lower tensile strength.

The constitutive relationship of concrete under uniaxial is commonly derived from experimental tests on cylinders with a height to diameter ratio of 2. From this test, a typical

stress-strain relationship can be deduced for concrete when subjected to uni-axial compression as shown in Figure 2.1.

The stress-strain curve has nearly linear-elastic behaviour up to about 30% of its maximum compressive strength $f_c^{'}$. For stresses above this point, the curve shows a gradual increase in curvature up to about $0.75 f_c^{'}$ to $0.90 f_c^{'}$ according to the concrete strength (normal - or- high concrete strength), then after it bends sharply and approaches the peak point at $f_c^{'}$. Beyond this peak, the stress-strain curve is descending till crushing failure occurs at the ultimate strain ε_u. This stress-strain curve (Figure 2.2) has been studied extensively and several models were proposed to describe such curve depending on several factors [Hognestad, 1951; Hognestad *et al.*, 1955; Todeschini *et al.*, 1964].

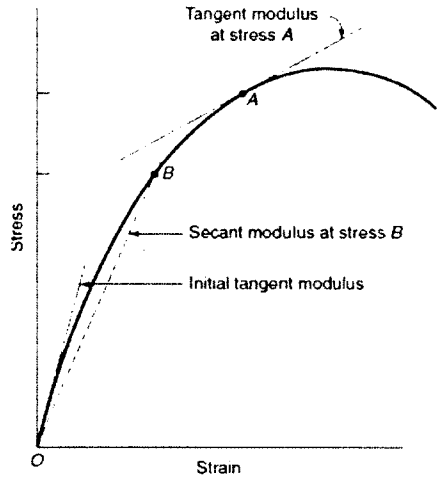

Figure 2.1 The concrete compressive stress-strain curve [MacGregor 1997]

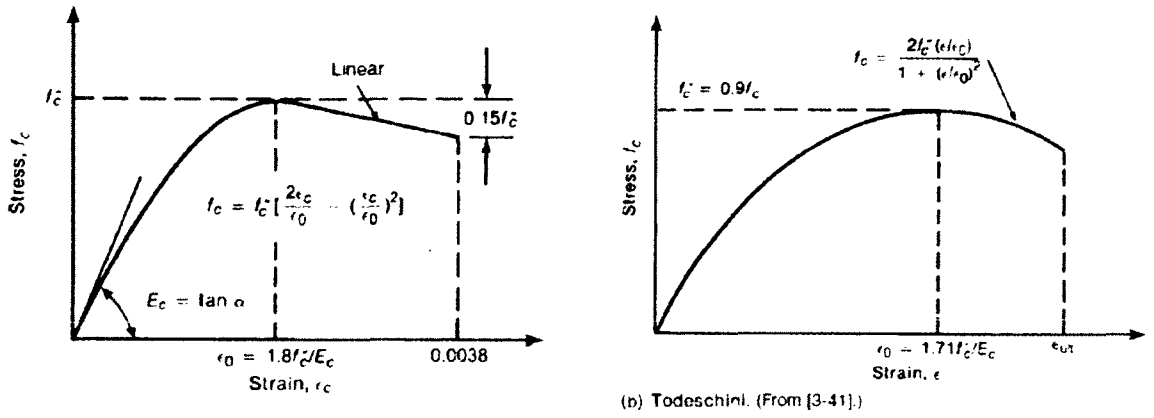

(a) Modified Hognestad (b) Todeschini.

Figure 2.2 Analytical approximation to the concrete compressive stress-strain curve [MacGregor 1997]

Most codes and guidelines [ACI 318, 2008; CAN/CSA-A23.3, 1994; ACI 318, 1999] adopted the model proposed by Collins and Mitchell (1993). The expression relates the stress f_c and strain at that stress, ε_c. Many other models were provided by Model Code 90 [CEB-FIP. 1990], Euro Code 2[CEN. 2004], [fib. 2007]. All of them were limited to concrete with characteristic strengths of up to 65 MPa, except that adopted by Euro code 2 [CEN. 2004] which is limited to concrete strength was up to 90 MPa.

On the other hand, the concrete behaves linearly under tensile stress until it reaches its ultimate tensile strength [MacGregor 1997]. For values of strain larger than that corresponding to the ultimate tensile strength, the stress decreases with an increase of the measured strain.

Since cracking is a discrete phenomenon and cannot locate cracking position, the strain along tensile reinforced element is not constant [Barris 2010]. In cracked concrete element, the

concrete zone between two consecutive cracks contributes to load-carrying capacity through the bond stress transfer between the concrete and reinforcement. This phenomenon produces an increment of the stiffness of the element and is extensively known as tension stiffening that will be discussed later in this chapter.

2.2.2 Fibre reinforced polymer (FRP):

Composite materials can be defined on those materials resulting from the contribution of two or more components or constituents. FRPs have been used for decades in the aeronautical, aerospace, automotive and other fields [ISIS Manual No.3, 2007]. The first applications of glass fiber FRP in structural engineering application were not successful due to its poor performance within thermosetting resins cured at high moulding pressure [Parkyn, 1970]. Since their early application, many FRP materials are still developed including different types of fibers and their improvements. Glass, carbon and aramid are major fiber type used manufacturing of reinforcing bars and could be used in reinforcing structural element although the aramid are still in debate [Wallenberger *et al.*, 2001; Walsh, 2001; Chang, 2001]. These fibres were formed from roving, tow, mat, woven fabrics.

Thus, bars made of FRP are considered as innovative material in structural engineering. Their physical and mechanical properties are widely ranged. FRPs are fabricated by choosing the type and quantity of fiber sand matrix resulting in different characteristics of products depending on the manufacturing process and ratio between fiber and matrix. In addition, FRP bars can have different surface configuration with varying performances in their bond behaviour with concrete, which in turn affect many behavioural aspects such as crack width and deflection.

2.2.3 FRP constituents

FRP products are composite materials consisting of continuous fibres impregnated with polymeric resins. As clear, continuous fibres with high strength and high stiffness are embedded and boned together by low modulus polymeric matrix. The reinforcing fibres represents the backbone of material in which determines strength and stiffness in the directions of fibres, thus, the matrix act as physical and environmental protection [ISIS Manual No.3, 2007].

Carbon fibres are similar to steel in stiffness, durable and expensive in cost. From field application [El-Gamal *et al.*, 2005], the carbon has proven quite resistant to most environmental conditions and can with stand high sustained and fatigue loading conditions. In contrast, glass fibre has lower strength and significantly lower stiffness. One of recent concerns is to check the durability of glass fibres. Unprotected glass fibre degrades against most environments, especially hot/wet or highly alkaline environments [Barris *et al.*, 2009]. In addition, it is subjected to creep rupture phenomenon which results in the eventual failure of the materials under sustained loads of fraction from the instantaneous ultimate load. The polymeric matrix (i.e. resin) act as coat for fiber to avoid damage and ensure the alignment of fibre resulting is distributing the load uniformly among many of the individual fibres in composite.

Two types of resins were used in FRP composites: thermosetting and thermoplastic resins. In construction and structural application, the most utilized resins are the thermosetting, such as epoxy and vinyl ester. The resins are flowable material with low viscosity that should be cured to a final solid form. Most of these resins are sensitive to heat and ultra-violet

exposure. As mentioned earlier, one of the factors that affect mechanical properties of FRP materials is manufacturing processes. Three common processes are available, such as Pultrusion, braiding, and filament winding [ISIS Manual No.3, 2007]. However, Pultrusion is the common technique for manufacturing continuous lengths of FRP bars of constant or nearly constant profile. This technique is schematically represented in Figure 2.3 and Figure 2.4 [fib., 2007]. Continuous fibres of reinforcing material are drawn from curls through a resin tank where they are saturated with resin and then through a number of wiper rings into the mouth of heated die. Thereafter, the surface of the bars is usually braided or sand-coated.

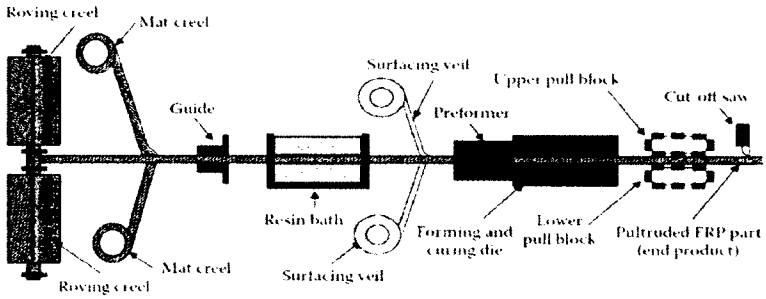

Figure 2.3 Schematic of a Pultrusion process [fib., 2007]

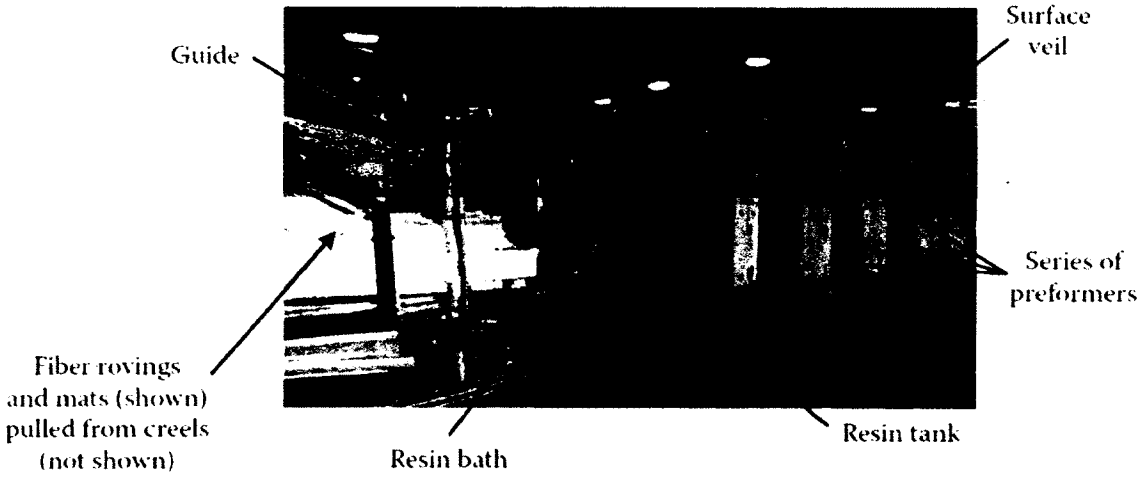

Figure 2.4 Pultrusion process: fibers/fabrics passing through guidelines and into the resin bath (left and middle part); resin tank at the bottom of the resin bath (middle portion); addition of surface veils (right part) [fib., 2007].

2.2.4 Mechanical properties of FRP bars

The mechanical properties of the FRP products are specified by fibre quality, orientation, shape, and volumetric ratio, adhesion to the matrix and on the manufacturing process. For example, to provide functioning reinforcing bars the fibre volume fractions should be more than 55%. ACI 440.6M-08 [2008] stated that fibre content should be measured according to ASTM Standards [ASTM D7205, 2011] in which represents the procedure of measuring fibre content in FRP bars or FRP girds. Both them conquered fibre content should at least not be less than 55%. FRP materials, in general, are anisotropic and brittle in nature. Therefore, they are characterised by high tensile strength with no yielding and only in one direction of reinforcing bars.

FRPs bar have linear stress-strain behaviour under tension up to failure, however, they have lower modulus of elasticity and no ductility like the steel bars. Figure 2.5 shows stress-strain curves for different types of FRP bars in the lieu of that of steel bars. Table 2-1 provides some typical ranges of mechanical properties for each FRP type. This anisotropic behaviour of FRP bars affects the shear strength and dowel action as well as their bond performance [Nanni, 2003]. The use of FRP bars as reinforcing bars offers several advantages in comparison to steel reinforcement.

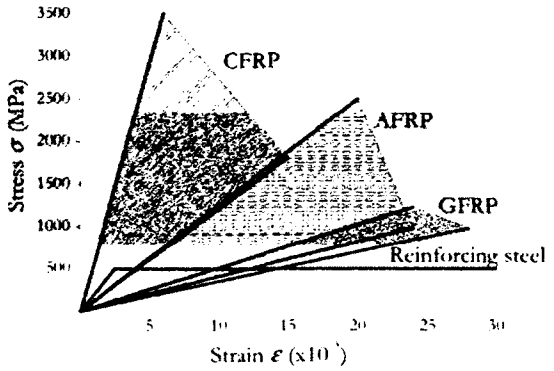

Figure 2.5 Stress-Strain curves of FRP and Steel materials [Pilakoutas *et al.*, 2002]

FRP bars are corrosion resistant, electromagnetic permeability, high cuttability and lighter in weight.

Table 2-1 Typical tensile properties of FRP and steel reinforcing bars [fib., 2007]

Property	Material			
	Steel	GFRP	CFRP	AFRP
Longitudinal modulus (GPa)	200	35 to 60	100 to 580	40 to 125
Longitudinal tensile strength (MPa)	483 to 690	450 to 1600	600 to 3500	1000 to 2500
Ultimate tensile strain (%)	6.0 to 12.0	1.2 to 3.7	0.5 to 1.7	1.9 to 4.4

All these advantages have led the FRP to emerge as an alternative substitute of steel reinforcing in several projects such as marine reinforced concrete structures, MRI rooms in hospitals and mobile telecommunications industry, finally as a temporary diaphragm walls

which can be partially destroyed by tunnel boring machines. In addition, they facilitate transportation and speeds construction [ACI 440.1R-06, 2006; fib., 2007; Pilakoutas *et al.*, 2007].

The unique mechanical properties of FRP represented in lower elastic modulus have significant influence on the structural behaviour of FRP reinforced concrete element. This yielded to large strains being mobilized in bars at low load levels which in turns lead to larger crack width and deflections. As a result, serviceability requirements often govern the design of FRP reinforced concrete members [Mathys and Taerwe 2000; Nanni, 2003]. Finally, the wide range of commercially available products can differ substantially in terms of mechanical properties and surface characteristics imposes difficulty to develop or implement simple design rules that can model adequately the mechanical performance of composite bars in concrete. Despite several design guidelines, codes and recommendations have been recently been published for FRP reinforced concrete members [ACI 440.1R-06, 2006; ISIS Manual No.3, 2007; CAN/CSA-S6.1S1, 2010; JSCE., 1997; IStructE., 1999], the lack of well standards for design and manufacturing is still perceived as a barrier to the extensive use of FRPs in construction.

However, many attempts were proposed to classify the FRP bars product into categories such as surface textures, so that each category has their own rules and models. Recently, the CAN/CSA-S807 [2010] classified the FRP bars by considering their elastic modulus. This classification was refereed by Grade I, II, and III. Grade I being the lowest value of elastic modulus and Grade III being the highest value of elastic modulus. Table 2-2 shows the ranges for each grade, in addition, typical ranges of tested samples included in this research program. Yet, the table did not specify certain rules and laws for each grade.

Table 2-2 Grades of FRP bars corresponding to their minimum modulus of elasticity, (GPa) with typical tested samples

Property	Grade I		Grade II		Grade III	
	Assigned by CSA S807	Typical tested samples	Assigned by CSA S807	Typical tested samples	Assigned by CSA S807	Typical tested samples
AFRP	$50 \le E_{frp}^{*}$	-	$70 \le E_{frp}^{*} < 90$	-	$90 \le E_{frp}^{*}$	-
CFRP	$80 \le E_{frp}^{*}$	-	$110 \le E_{frp}^{*} <$ 140	-	$140 \le E_{frp}^{*}$	-
GFRP	$40 \le E_{frp}^{*}$	46.4±1.5 to 48.7±0.6	$50 \le E_{frp}^{*} \le 60$	52.5±1.7 to 53.2±2.1	$60 \le E_{frp}^{*}$	60.3±2.9 to 69.3±3.2

* E_{frp} is the actual elastic modulus of FRP bars resulted from testing.

2.3 Maintaining service state

Serviceability limit states (SLS) are limits for reinforced concrete members to ensure their structural integrity under service conditions. As mentioned in the previous section, FRP reinforced concrete members are governed by service limit state rather than ultimate limit state due to their lower elastic modulus and different bond behaviour.

The service limit state is defined generally through many aspects as concurred by researchers, codes and guidelines [ACI 440.1R-06, 2006; ISIS Manual No.3, 2007; CAN/CSA-S806, 2012; JSCE., 1997; IStructE., 1999; CNR-DT 203., 2006]. These aspects are limiting the strains in FRP by fraction from their ultimate strains each according to FRP type,

30 % of ultimate load, deflection and crack width limits. Also, the situation can be extended to other materials such as concrete.

Stresses in concrete usually limited the developed compressive stress to prevent the longitudinal cracks and micro-cracks from occurrence. No codes or guidelines, prescribed explicitly a specific limits on concrete compression stresses, however, from the design of flexural capacity. It can be understood that the linear range in which equal to a value of $0.45f'_c$ is the appropriate limit for concrete stresses under service condition. On other hand, stresses in FRP reinforcing bars are limited explicitly in two terms reduction for environmental deterioration and limits under sustained loads.

Table 2-3 shows the limits assigned by different existing codes and guidelines.it is clear that both factors, environmental conditions and sustained loads, leads to serve reductions from the ultimate strength of bar which means slight portion of the FRP strength were used (values are between 0.2 to 0.55 times the ultimate strength).

Other limits were specified such as 30 % of the ultimate load. This limit was deduced from that of steel. The steel reinforced concrete members are governed by strength or ultimate limit state. Thus, giving $M_a = \varphi/(\alpha_{load})\ M_n = 0.67M_n$ when the strength reduction factor $\varphi = 0.9$ and the load factor [$\alpha_{load} = 1.33$ *for dead-to-live load ratio of 2:1*] which correspond to roughly 30% of nominal moment capacity M_n for FRP reinforced concrete sections to ensure that serviceability requirements (crack width and deflection) are satisfied.

Table 2-3 Reduction factor used in the existing guidelines

Factor	FRP Type	ACI 440.1R-06 C_E	CAN/CSA S806-12 φ_{FRP}	JSCE 1997 $1/\gamma_{fm}$	IStructE $1/\gamma_m$	CNR-DT-203 η_a
Reduction for environmental deterioration	GFRP	0.70-0.80	0.50	0.77	"material factor"	0.70-0.80
	AFRP	0.80-0.90	0.60	0.87		0.80-0.90
	CFRP	0.90-1.0	0.75	0.87		0.90-1.0
Stress limit for sustained load	GFRP	0.20	0.25	0.8 x "creep failure strength" ≤ 0.7	Stress limits not specified	η_l 0.30
	AFRP	0.30	0.35			0.50
	CFRP	0.55	0.65			0.90

However, [Bischoff 2005] suggested to lower service load levels to about $0.30M_n$ or less to ensure strains in FRP reinforcement are within the acceptable limit especially where service load related to strength requirement ($M_a = 0.49M_n$ *when* $\varphi = 0.65$ *for* $\rho \geq 1.4\rho_b$). Other limits such as crack width and deflection limits were used to control serviceability of FRP reinforced member. These limits were discussed in the following sections.

Control of cracking:

In general, cracking usually controlled to prevent leakage of fluid in structures that support water or any other liquids and to prevent corrosion of reinforcement which in turn weakened the durability of structure. In steel reinforced concrete members, the primary reason for crack

width limitations is the corrosion of reinforcement. As FRP reinforcing bars are corrosion resistant, thus, the crack width limit was relaxed by all codes and guidelines. For the steel reinforced concrete member, most codes and guidelines limited the maximum crack width to about 0.3 mm, however, others relaxed the limit to 0.4 mm in case of no aggressive exposure by means no risk of corrosion or attack. In the ACI 318 [2008], the crack width limit was replaced by bar spacing closet to tension force of the beam. CAN/CSA-A23.3 [2004] distinguishes between exterior and interior exposures, by values of 0.3 and 0.4 mm as limit for maximum crack width, respectively.

The limitation for FRP reinforced member was relaxed to 0.5 mm for exterior exposure and 0.7 mm for interior exposure [ACI 440.1R-06, 2006; ISIS Manual No.3, 2007]. Other codes and guidelines used the limit of 0.5 mm only in both cases [JSCE, 1997]. Furthermore, ISIS Manual No.3 [2007] suggested controlling the crack width by limiting the maximum strain in FRP to 2000 microstrains. This was obtained through comparing with steel crack width limit. In steel reinforced concrete member, the stress limit in steel reinforcement at service is at 60% of f_y. When f_y = 400 MPa, the allowable strain in steel bars in service ε_s is equal to 1200 microstrains. At the same time, the crack width was limited by 0.4 and 0.3 mm for interior and exterior exposure in comparison to 0.7 and 0.5 mm for FRP reinforced elements.

Thus, the allowed crack width in FRP reinforced members is about 1.5 to 1.7 times that of steel reinforced. For that reason, it was assumed the strain limit should be around 2000 microstrains for FRP reinforced concrete member which represents 5/3 ratio from 1200 microstrains for steel reinforced concrete member. This ratio was deduced from crack width

limit difference. Likewise, CAN/CSA-S806 [2012] defines the quantity z not to exceed 45 kN/mm for interior exposure and 38 kN/m for exterior exposure.

Control of deflection:

Codes and guidelines proposed different deflection limitations for relative parts of elements to the supports. All limitations were provided so that the deformation of a member or structure shall not affects its proper functioning or appearance. Thus to control deflection the codes and guidelines suggested minimum thickness calculated empirically (Table 2-4).

Some of these codes and guidelines set an equation to calculate the thickness required [ACI 440.1R-06, 2006; CEB-FIP., 1990].

Table 2-4 shows the minimum thickness required through typical codes and guidelines to control the deflection

Structural system		Eurocode 2 [CEN. 2004]		ACI 318-08, CAN/CSA A23.3 94	ACI 440.1R-06
		$\rho = 0.5\%$	$\rho = 1.5\%$		
Simply supported	Beam	*L/d = 20*	*L/d = 14*	*L/h = 16*	*L/h = 10*
	One-way slab			*L/h = 20*	*L/h = 13*
One end continuous	Beam	*L/d = 26*	*L/d = 18*	*L/h = 18.5*	*L/h = 12*
	One-way slab			*L/h = 24*	*L/h = 17*
Both ends continuous	Beam	*L/d = 30*	*L/d = 20*	*L/h = 21*	*L/h = 16*
	One-way slab			*L/h = 28*	*L/h = 22*
Cantilever	Beam	*L/d = 8*	*L/d = 6*	*L/h = 8*	*L/h = 4*
	One-way slab			*L/h = 10*	*L/h = 5.5*

Table 2-5 shows the deflection limits adopted from steel reinforced members codes and guidelines [ACI 318, 2008]

Type of member	Deflection to be considered	Deflection limitation
Flat roofs not supporting or attached to non-structural elements likely to be damaged by large deflections.	Immediate deflection due to live load *L*	*l/180*[*]
Floors not supporting or attached to non-structural elements likely to be damaged by large deflections.	Immediate deflection due to live load *L*	*l/360*[*]
Roof or floor construction supporting or attached to non-structural elements likely to be damaged by large deflections.	That part of the total deflection occurring after attachment of non-structural elements (sum of long-term deflection due to all sustained loads and the immediate deflection due to any additional live load)[†]	*l/480*[‡]
Roof or floor construction supporting or attached to non-structural elements not likely to be damaged by large deflections.		*l/240*[§]

[*] Limit not intended to safeguard against ponding. Ponding should be checked by suitable calculations of deflection, including added deflections due to ponded water, and considering long-term effects of all sustained loads, camber, construction tolerances, and reliability of provisions for drainage.

[†] Long-term deflection shall be determined in accordance with 9.5.2.5 or 9.5.4.3, but may be reduced by amount of deflection calculated to occur before attachment of non-structural elements. This amount shall be determined on basis of accepted engineering data relating to time-deflection characteristics of members similar to those being considered.

[‡] Limit may be exceeded if adequate measures are taken to prevent damage to supported or attached elements.

[§] Limit shall not be greater than tolerance provided for non-structural elements. Limit may be exceeded if camber is provided so that total deflection minus camber does not exceed limit

These values used to design the thickness of the members whether it is a beam or one way slab to control the deflection from exceeding the limits assigned by codes and guidelines used of steel reinforced concrete members. In most codes and guidelines, the deflection was limited according the type of structure attached to the member in question.

In fib. [2007], the deflections were calculated to limit the mid-span total deflection to *L/250*. However, ACI 440.1R-06 [2006] adopted the limits developed in ACI 318 [2008] for steel reinforced as well as the CAN/CSA-S806 [2012] counterparts the one used in CAN/CSA-A23.3 [2004] which are seen in the following Table 2-5

2.4 Serviceability performance of FRP Reinforced concrete beam

The deflection and cracking of FRP-reinforced concrete members have been extensively investigated and incorporated in many design codes and guidelines. However, due to the variety of the FRP products which are characterized by different mechanical properties and surface configuration there is no reliable model to predict the serviceability of the FRP-reinforced concrete member considering all the affecting parameters. Furthermore, the validation of these models was not enough to yield a rational model due to the lack of well-established standards, a wide variety of FRP bars are currently marketed, ranging from the simple smooth and helically-deformed bars to bars treated with external features such as sand-coating. These FRP products have a wide range of mechanical properties as well as different surface configurations. Besides, most of the design codes and guidelines use equations for the steel-reinforced members with some modifications to account for the differences in the mechanical properties between FRP and steel bars.

Extensive research has been conducted on the serviceability of FRP-reinforced concrete members especially the simply supported beams under one or two point loading conditions. The detailed literature review on this issue can be found in the ACI state-of-the-art [ACI 440.R-07, 2007]. This extensive research work lead to developing some models and equations to predict the deflection and the crack width in FRP- reinforced concrete members. However, as mentioned earlier, due to the lack of experimental work concerning the rapid development of FRP products there is an urgent need for refined/new models. In this chapter, the overall behaviour of FRP- reinforced concrete members concerning the deflection and cracking and the main parameters affecting them will be summarized. Besides, the design code provisions for the deflection and cracking will be listed and the relevant evaluation, based on the previous research work from the literature, of these provisions will be presented.

2.5 Cracking and the Affecting Parameters

The mechanism of the progressive cracking starts with the formation of primary cracks when the strain in the tension zone of the concrete section is equal to the ultimate concrete tensile strain, the first crack appears. At this point, the concrete is subjected to excessive lengthening of the reinforcement and the bond between the reinforcement and concrete transfers the tensile force from the reinforcement bar to the surrounding concrete in between the primary cracks [Goto, 1971]. Therefore, more cracks would appear (i.e. secondary cracks) as shown in Figure 2.6.

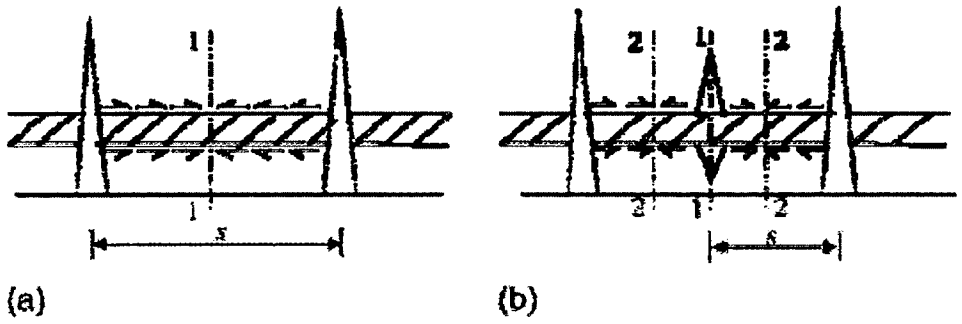

Figure 2.6: Primary and secondary cracking in concrete: (a) section of highest concrete tension; (b) next section of highest concrete tension

At a certain distance between the crack (i.e. S), deformation compatibility between the reinforcement and concrete is restored. Theoretically, it is through this distance where the ultimate concrete tensile strength again reached, thus, a new crack formed. A third crack between the first two cracks can occur only if the bond between the reinforcement and concrete transmit enough tensile stresses (i.e. reaching the ultimate concrete tensile strength) until the tensile resistance between two cracks achieved. At this stage, the number of cracks and the distance in between does not change. This stage called stabilized cracking.

Masmoudi *et al.* [1996] showed that the effect of the reinforcement ratio on crack spacing was negligible, but depended on the type of reinforcement used. Greater bond quality leads inevitably to smaller crack spacing and thus smaller crack width. In fact, they stated that the obtained results demonstrate a good bond performance of FRP reinforcing bars relative to the steel rods used in the same environment. However, they found that the residual crack width decreases as the reinforcement ratio increases and the residual crack width is not influenced much by the concrete strength.

Theriault et Benmokrane [1998] deduced that the effect of the concrete strength and the reinforcement ratio on the crack spacing is negligible, and the crack spacing slightly decreases as the load increases. The higher the concrete strength, the wider is the crack for the same applied moment. However, opposite observations were made by GangaRao et Faza [1991], suggesting that the beam's geometry also plays a significant role in the crack formation. Moreover, Theriault et Benmokrane [1998] explained that those wider cracks are due to the release of greater stress at crack initiation, followed by a sudden crack formation. However, a greater reinforcement ratio decreases this effect. Thus, the higher the reinforcement ratio, the bigger the stress at cracking that will be transferred which in turns decreases the crack initiation.

El-Salakawy *et al.* [2002] through their experimental investigation found that, at service load levels, increasing the CFRP reinforcement ratio by 50% and 100% decreased the maximum crack width by approximately 37% and 55%, respectively. They concluded that for beams reinforced with approximately the same reinforcement ratio of CFRP bars and that of steel, the crack width at service load level of beam increased by 44% compared to the control.

Ospina et Bakis [2007] developed a procedure to control flexural cracks in structural concrete beams. They have stated that the flexural cracks are dependent on the value of bond quality between FRP bars and concrete. Wider cracks could be explained by the release of a greater stress at crack initiation, which leads to a sudden high crack formation. However, a greater reinforcement ratio tempers that effect [GangaRao et Faza, 1991]. The reinforcement ratio shows a strong influence on the crack width: A smaller crack width is obtained by means of a higher reinforcement ratio. In fact, a higher reinforcement ratio can resist a bigger stress at cracking tempering the crack initiation.

In conclusion, the crack widths along with crack spacing were influenced by many factors. Bond quality, reinforcement type and ratio, and concrete strength are the most considered parameters in investigating the crack widths of the FRP- reinforced concrete elements.

2.6 Deflection and the Affecting Parameters

Concrete beams reinforced with FRP exhibit larger deflection than that reinforced with the same amount of steel due to its low modulus of elasticity. The serviceability of FRP reinforced concrete structures has been investigated both theoretically and experimentally through many studies [Theriault et Benmokrane, 1998; GangaRao et Faza, 1992]. Moreover, most of the studies have investigated the behaviour of simply supported concrete beams reinforced with different types of FRP reinforcing bars [Theriault et Benmokrane, 1998; Grace *et al.*, 1998; Alsayed, 1998; Pecce *et al.*, 2000; Toutanji et Saafi, 2000; Yost et Gross, 2002; Rasheed *et al.*, 2004].

Few studies attempted to provide design equations for predicting the deflection of FRP reinforced concrete beams [Yost et Gross, 2002; Aiello et Ombres, 2000; Abdalla, 2002]. In such studies, the deformability of the whole element defined by the relations arises from a linear analysis, where a concept of the transformed cross-section moment of inertia was introduced as in Figure 2.7. This concept was stated by the moment–curvature diagram. The moment-curvature diagram can be approximated by two linear regions: one before the concrete cracks, and the second one after the concrete cracks [Razaqpur *et al.*, 2000]. Therefore, there is no need for calculating curvature at different sections along the length of the beam as for steel reinforced concrete. There are only three pairs of moments with

corresponding curvature that define the entire moment–curvature diagram: at cracking, immediately after cracking, and at ultimate.

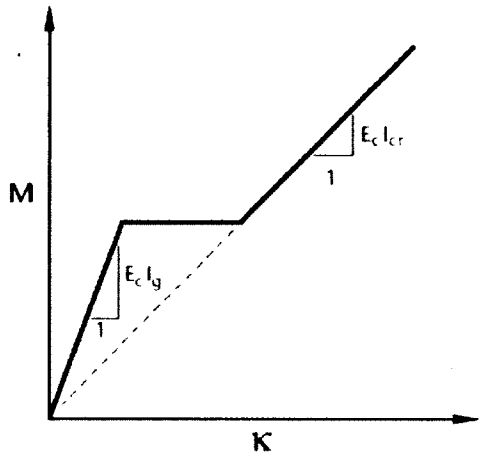

Figure 2.7 Moment-curvature relation of FRP- reinforced concrete [CAN/CSA-S806, 2012]

Accordingly, the influence of service load level on member deflection requires more evaluation [Bischoff, 2005]. Moreover, the suitability of using an averaged effective moment of inertia that is constant along the length of beam compared with integration of curvature along the beam span to compute deflection still needs to be resolved.

The following section summarizes the main factors affecting the deflection of FRP-reinforced concrete members.

2.6.1 Tension stiffening

In practical design, the contribution of concrete in the tensile zone is neglected as the concrete cannot resist tensile stresses. With more investigations, researchers have deduced the term "tension stiffening". Tension stiffening can be defined as the ability of concrete to carry

tension between cracks. At a crack, all the tensile force is transferred from the reinforcement through bond to the surrounding concrete. Hence, between cracks, the concrete stiffens the reinforcement causing reduction in reinforcement strain that is less than strain at cracks or of the bars. Therefore, the reinforcement appears to have a higher effective stiffness [Bischoff et Paixao 2004].

The proper evaluation of tension stiffening will lead to accurate predictions of deflection and crack width for concrete element reinforced with FRP bars. Accordingly, researchers investigated the tension stiffening term taking into account the flexural element properties, concrete strength and reinforcement ratio. Hence, several investigators realized the importance of tension stiffening effects on concrete member.

Bischoff et Paixao [2004] conducted experimental tests using concrete prism to study tension stiffening and cracking. They concluded that concrete prisms reinforced with GFRP exhibit greater tension stiffening than those reinforced with steel at any level of axial strain. On the other hand, Al-Sunna [2006] has investigated the influence of the reinforcement ratio on tension stiffening by testing FRP reinforced concrete beams. These beams were under-reinforced close to balance and over-reinforced with crack inducer to ensure initiation of cracks at mid-span. They concluded that the concrete reinforced with GFRP provide much lower tension stiffening than that provided by steel, which gradually reduces with the increase of stresses in the GFRP bar. This is due to the high strain level developed in the GFRP bar.

Bischoff [2007] stated that the tension stiffening increases for a higher cracking moment and lower value of the cracked moment of inertia (this occurs with low reinforcement ratios). FRP reinforced concrete beams should, in general, exhibit a greater amount of tension stiffening than conventional steel reinforced concrete beams yet still have lower member stiffness and exhibit greater deflection because of the lower value of moment of inertia.

Thus, using the same equation of the steel reinforced concrete elements for predicting the deflection of the FRP reinforced concrete element is underestimated as the tension stiffening is not accurately predicted (i.e. overestimated). Hence, a reduction factor was proposed to reduce the tension stiffening for FRP reinforced concrete element to a more reasonable level. Consequently, the tension stiffening parameter has a great impact on determining the effective moment of inertia. Without considering the tension stiffening in the concrete member reinforced with FRP bars, the deflection and crack width will be underestimated.

2.6.2 Bond action

Bentz [2005] noted that the evaluation of tension stiffening requires a certain parameter which is a function of the bond between the reinforcement and concrete. In general, the maximum bond strength of the FRP bar is lower than the bond strength values compared to steel bars.

For steel bars, the bearing component is the main source of the bond while the FRP bar's surface does not offer the steel bar's characteristics (i.e. high shear strength, high rigidity, and geometry deformation) that provide enough interlocking through the rib. However, for FRP bars, it is the adhesion, mechanical bearing and the friction that control the bond strength [Tighiouart *et al.*, 1998].

Tepfers *et al.* [1998] through an experimental investigation on pullout specimens concluded that smaller bar diameters developed higher bond strength than larger bar diameters. However, the larger the diameter of the bar, the higher the quantity of bleeding water trapped beneath the bar, creating a greater void that reduces the contact surface between the bar and the concrete and hence the bond.

On the other hand, Rafi *et al.* [2007] stated, based on beam testing, that CFRP bars showed a good bond with the concrete. Also, they did not find any signs of premature bond failure. They recorded that the maximum tensile stresses on the CFRP bars have reached 80 to 90% of their ultimate strength. They indicated that the CFRP bars developed bond strengths more than 85% of that of the steel bars.

2.6.3 Concrete strength

It is well known that concrete is a brittle material and raising its strength makes concrete even more brittle [fib., 2007]. In fact, the brittleness of concrete is considered one of the main concerns when high strength concrete (HSC) is used in conventional steel reinforced concrete structures.

Theriault et Benmokrane [1998] tested 12 concrete beams reinforced with FRP bars. The main parameters investigated in this study were the reinforcement ratio and the concrete strength. Through this investigation they concluded that the stiffness of the beam did not change much ($\geq$ 10%) with the concrete strength, which means a slight reduction in deflection will occur. In addition, they found that as the concrete strength and the reinforcement ratio increase, the ultimate moment resistance increases, but this increase is limited by the concrete compressive failure strain.

Rashid *et al.* [2005] have investigated the deflection and crack width behaviour of AFRP (aramid FRP) reinforced high strength concrete beams. They concluded that the load-deflection response of these beams significantly differs from that of steel-reinforced beams in terms of cracking behaviour, post-cracking stiffness, magnitudes of deflections and crack widths, and mode of failure. They deduced that at any particular load level, the maximum surface crack width and maximum deflections are several times larger than those of steel

reinforced beams. Moreover, the ductility of the over-reinforced AFRP beams made with HSC increases as the reinforcement ratio increases. Furthermore, according to cracking moment equations, they noticed that the higher concrete strength leads to a higher cracking moment which probably influences the deflection equation.

2.6.4 Reinforcement ratio

The reinforcement amount controls the bar spacing and the number of layers of reinforcing bars. Theriault et Benmokrane, [1998] conducted an experimental study to investigate the deflection of FRP- reinforced concrete beams. The concrete strength and the reinforcement ratio parameters were considered. Through this investigation, it was concluded that higher reinforced concrete beams showed greater stiffness than less reinforced beams. Moreover, the stiffness of the beam is inversely proportional to the deflection behaviour of the FRP reinforced concrete beam, the reduction in deflection will occur when the reinforcement ratio increases.

El-Salakawy *et al.* [2002] investigated the deflection of FRP- reinforced concrete beams reinforced with different types and ratios of CFRP bars. They observed that increasing the reinforcement ratio decreases the deflection at service load due to higher stiffness and lower FRP bar stresses. Moreover, at the service load level, the measured deflection reduced by approximately 31% and 43% due to the increase of reinforcement ratio by 50% and 100%, respectively. In addition, very similar behaviour of beams reinforced with both sand-coated and ribbed deformed carbon FRP bars was obtained.

Ashour et Family [2006] carried out tests on rectangular and T-beams reinforced with CFRP bars, and concluded that the type and amount of the reinforcement had a considerable

effect on the beam stiffness and the deflection after the first crack initiation. This was later confirmed by Barris *et al.* [2009] through his study on GFRP- reinforced concrete beams.

2.7 Design and codes provision for flexural and serviceability of FRP- reinforced concrete

The flexural capacity can be calculated through well-known methods: strain compatibility or strength state method. The design philosophy is based on the reinforcement type in which the member was reinforced with. FRP- reinforced concrete members, the strain compatibility method should be adopted for design. The design philosophy of such a method relies on the following assumptions:-

- Plane section remain plain under bending forces
- Reinforcement stress-strain relationship is known
- Tensile concrete strength is negligible
- Ultimate concrete stain is well known according to each code and guidelines assignment; for ACI 440.1R-06 [2006], the ultimate concrete strain is 3000 microstrains; while, for CAN/CSA-S806 [2012], the ultimate strain is 3500 microstrains.

By this hypothesis, it is possible to evaluate the flexural capacity of beam. Different modes of failure are available for concrete section reinforced with FRP bars:-

- Balanced failure: simultaneous rupture of FRP and crushing of concrete
- Compression failure: concrete crushing while FRP remains in the elastic range with a strain level smaller than the ultimate strain. On the other hand, concrete reaches its

ultimate strain level which assumed to be equal 3000 or 3500 microstrains according to ACI 440.1R-06 [2006] and CAN/CSA-S806 [2012], respectively.

- Tension failure: rupture of FRP in which FRP reaches its ultimate strain level before concrete crushing.

The behaviour simply can be described by defining the mode of failure. The mode of failure as mentioned earlier can be defined by two main factors flexural stresses and reinforced with only tensile reinforcement depending on which material achieves its ultimate capacity first. When the concrete strain reaches its ultimate strain (3000 or 3500 microstrains), the section fails in a quasi-brittle manner by compression of the concrete block which known as concrete crushing failure. On the contrary, when the reinforcement reaches its ultimate strength before concrete strain achieves its ultimate, the section fails by the rupture of reinforcement. This failure differs in behaviour between steel and FRP reinforced concrete members.

As the steel reinforcement reaches yielding strength, the member is considered to fail by yielding of steel. Thus, the steel propagate its ductile behaviour which relies on their bi-linear stress-strain relationship in approximately (Figure 2.8). However, as the FRP is brittle in nature and the stress-strain relationship is linear. Then, the member fail in ductile manner for steel reinforced member as the steel yields and in brittle manner for FRP reinforced concrete member as the FRP bar reaches its ultimate strain which means rupture of FRP bars.

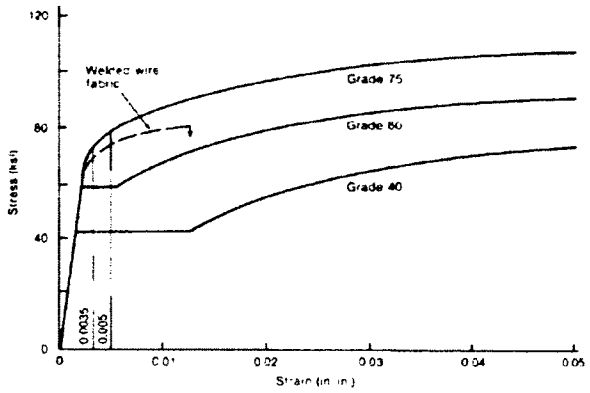

Figure 2.8 Stress-Strain curves for reinforcement [MacGregor 1997]

Such a failure considered being catastrophic and unfavorable when using FRP bars as reinforcement in reinforced concrete member. Thus, it is desirable for elements reinforced with steel reinforcement to fail in tension-controlled failure in which ductility behaviour would be captured. While for elements reinforced with FRP bars should fail in concrete crushing were the brittle catastrophic failures of the FRP reinforced concrete elements would be avoided. It should be noticed that philosophy of failure is based on safety margins and warning time that can be provided by reinforced concrete members before its complete deterioration or destruction. Many approaches are available to calculate the failure mode and the ultimate capacity of FRP reinforced concrete elements.

Here in, the literature presents two unique approaches in which they were adopted later in the analysis. These approaches ACI 440.1R-06 [2006] and CAN/CSA-S806 [2012] are similar in procedure but differ in their stress block factor evaluation. In general some design codes, ACI 440.1R-06 [2006] and JSCE [1997] provides higher safety margins than steel reinforced concrete design to compensate the lack of ductility. Thus, many details with safety

consideration and modified ductility concept that reflect FRP reinforced concrete deformability were developed [Pilakoutas *et al.*, 2002; Newhook *et al.*, 2002].

$$\rho_f = \frac{A}{bd} \qquad 2.1$$

A reinforcement ratio defined in Eq. [2.1] shall be compared to the balanced reinforcement ratio to control the failure mode. If the reinforcement ratio exceeds the balanced reinforcement then the member shall fail in concrete crushing. While if the reinforcement ratio was lower than the balanced reinforcement then the member shall fail in steel yielding in case of steel reinforced concrete member or rupture of FRP in case of FRP reinforced concrete member. The balanced reinforcement ratio relies its deflection on the mechanical properties of FRP and concrete and its equation is derived by considering internal forces equilibrium. ACI 440.1R-06 [2006] proposes to calculate as follows Eq. [2.2]:

$$\rho_{fb} = \alpha_1 \beta_1 \frac{f_c'}{f_{fu}} \frac{E_f \varepsilon_{cu}}{E_f \varepsilon_{cu} + f_{fu}} \qquad 2.2$$

2.7.1 Moment resistance of FRP Reinforced concrete elements:

The flexural capacities of a cross section is determined by assuming the constitutive relationship of concrete in compression is known, the stress-strain curve of the FRP is linear up to failure and the is perfect bond between concrete and the FRP reinforcement. The ultimate moment resistance of an FRP reinforced concrete section that fails by concrete crushing can be calculated assuming different equivalent stress-strain distributions of concrete under compression until failure. The equivalent rectangular stress block is defined by ACI 440.1R-06 [2006] as shown in the illustration diagram (Figure 2.9).

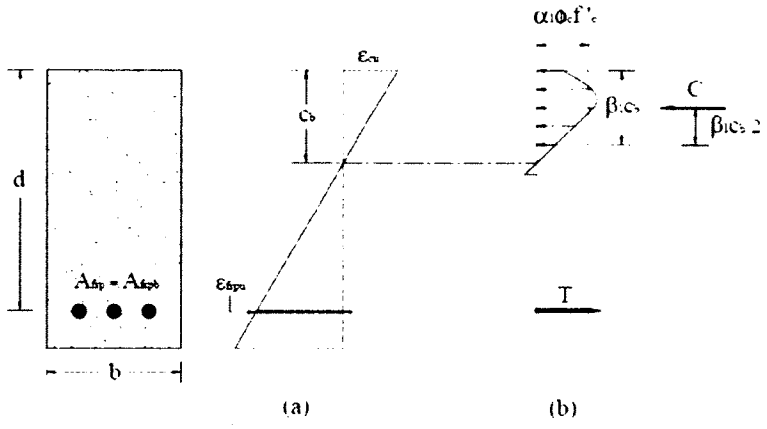

Figure 2.9 Stress-Strain curves for reinforcement

Thus, the ACI 440.1R-06 [2006] proposes the moment of resistance to be calculated on the basis of the equivalent stress block of concrete in compression and based on the equilibrium of forces and strain compatibility, the following (Eq. [2.5]) formulation is obtained:

$$M_n = \rho_f f_f \left(1 - 0.59 \frac{\rho_f f_f}{f_c'}\right) bd^2 \qquad 2.3$$

The stress block defined as mentioned earlier differently in CAN/CSA-S806 [2012], while ACI 440.1R-06 [2006] as α, β as seen in Eq. [2.4]. The CAN/CSA-S806 [2012] defines α, β as following (Eq. [2.5]):-

$$\alpha_1 = 0.85\,;\ \beta_1 = 0.85 - 0.05\left(f_c' - 27.6\right)/6.9 \qquad 2.4$$

$$\alpha_1 = 0.85 - 0.0015(f_c') \geq 0.67\ ;\ \beta_1 = 0.97 - 0.0025(f_c') \geq 0.67 \qquad 2.5$$

With regards to the avaiable experimental results on FRP reinforced concrete elements, [Theriault et Benmokrane,. 1998; Benmokrane, Chaallal et Masmoudi, 1996a; Masmoudi *et al.*, 1998] reporeted that the ultimate moemnt was 15% underestimated by ACI formula when the section failed by concrete compression, but it was 5% overestimated in the case that the section failed by FRP tension. This difference was attributed to the variability of the compressive strength of concrete and tensile strength of the FRP reinforcing bars. Rafi *et al.* [2008] found out that ACI formualtions underestimated the moemnt capacity of their four tested FRP beams to about 33%, probably because the actual srain in concrete exceeded the maximum concrete strain of 0.3% as result of the confiment provided especially by the stirrups.

2.7.2 Shear capacity of FRP reinforced concrete beams:

The shear resistance of reinforced concrete elements is generally determined by the contribution of the un-cracked compression zone, aggregate interlock, dowel action and when provided, shear reinforcement. Due to the lower modulus of elasticity of the FRPs, wider cracks and higher deflections occurs leading to less contribution of the un-cracked compression zone in shear and less shear-load carrying by aggregate interlock and dowel action [Pilakoutas *et al.*, 2002].

Shear failure of the reinforced concrete element is usually proceeded by the formation of cracks inclined to the main axis of the element. Similar to the steel reinforced concrete elements, shear failure can occur in two ways: most commonly diagonal tension failure and shear-compression failure. As the shear is not the thesis concern, the reinforced concrete elements discussed here in; are reinforced with steel stirrups just to avoid shear failure before

the flexural. However, these stirrups will not prevent the shear deformation which may slightly affect the deflection of the beam member. In addition, the thesis concern is about serviceability state of the FRP reinforced concrete member. Thus, the shear deformation will not influence the serviceability state. Furthermore, the mid-span of the member was reinforced with 3 stirrups at 300 mm distance ensuring lower confinement possible that could encountered by stirrups.

2.8 Deflection and Cracking Provisions

2.8.1 The Canadian Building Code (CSA/CAN S806)

CAN/CSA-S806 [2012] has recommended the integration of curvature along the span to determine deflections. The virtual work method was used to calculate deflection of concrete members under any load level with the integral being for all members of the structure. See Eq. [2.6].

$$\delta = \int m\psi dx \qquad 2.6$$

Accordingly, the CAN/CSA-S806 [2012] provided a deflection equation derived by assuming that the moment of inertia between the load points was the cracked moment of inertia, and the moment of inertia elsewhere was the effective moment of inertia as seen in Eq. [2.7]. Figure 2.10 represents four-bending diagram according to the suggested deflection equation.

$$\delta_{max} = \frac{PL^3}{24E_cI_{cr}}\left[3(\frac{a}{L}) - 4(\frac{a}{L})^3 - 8\eta(\frac{L_g}{L})^3\right]$$

$$where, \eta = (1 - \frac{I_{cr}}{I_g}), \qquad 2.7$$

$$L_g = length\ of\ beam\ still\ uncracked$$

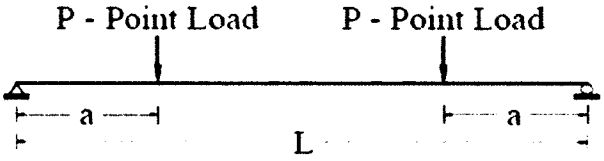

Figure 2.10 The four-point bending loading diagram

According to the CAN/CSA-S806 [2012], a tri-linear moment-curvature relation, as shown in Figure 2.7, is assumed with the flexural stiffness being E_cI_g for the first segment, zero for the second, and $E_{cr}I_{cr}$ for the third. Alternatively, simple deflection equations, clearly derived from the assumed moment-curvature relation, are provided.

For cracking, the CAN/CSA-S806 [2012] adopted the z-equation for the FRP bars introducing the bond property of the FRP bars as a modification:

$$z = k_b \frac{E_s}{E_f} f_f \sqrt[3]{d_c A} \qquad 2.8$$

The CAN/CSA-S806 [2012] noted that if the maximum strain of FRP bars in the tension zone under full service loads exceeds 0.0015, cross-sections of maximum positive and negative moment shall directly proportional with the quantity, z, that must not exceed 45,000 N/mm for interior exposure and 38,000 N/mm for exterior exposure. In fact, the stresses in the reinforcement at the specified load, f_f, is calculated as the internal moment divided by the

product of the reinforcement area and the internal moment arm. For practicality, f_f could be 60% of the design ultimate reinforcement stress in the closest layer to the extreme tension fiber. The value of k_b shall be determined experimentally, but in the absence of data, k_b will be equal to 1.2 for deformed rods. Finally, the CAN/CSA-S806 [2012] recommended that the effective clear cover, d_c, should not be greater than 50 mm.

2.8.2 The Canadian Highway Bridge Design Code (CSA/CAN S6S1-10)

The Canadian Highway Bridge Design Code [CAN/CSA-S6.1S1, 2010] introduces a simplified method to calculate the deflections and rotations using the effective moment of inertia, I_e, as follows:

$$I_e = \left(\frac{M_{cr}}{M_a}\right)^3 I_g + \left[1 - \left(\frac{M_{cr}}{M_a}\right)^3\right] I_{cr} \leq I_g \qquad 2.9$$

While in cracking, CHBDC 2006 [CAN/CSA-S6.1S1, 2010] recommended the modifications proposed by Frosch, [1999] as follows:

$$w = 2\frac{f_{frp}}{E_{frp}}\frac{h_2}{h_1}k_b\sqrt{d_c^{\,2} + \left(\frac{s}{2}\right)^2} \qquad 2.10$$

The value of k_b shall be determined experimentally, but in the absence of data, values of 0.8 for sand-coated and 1.0 for deformed FRP bars is used. In addition, the calculation of clear cover, d_c, shall not be greater than 50 mm.

2.8.3 ACI Guidelines (ACI 440.1R-06)

In North American codes, deflection calculations of flexural members are mainly based on equations derived from linear elastic analysis, using the effective moment of inertia,

I_e. The ACI 440.1R-04 [2004] has also proposed revisions to the design equation in ACI 440.1R-03 [2003]. Consequently, the moment of inertia equation retained the same form of ACI 440.1R-03 [2003]. However, the form of the reduction factor β has changed the variable key in the equation from the modulus of elasticity to the relative reinforcement ratio as shown in Eq. [2.11].

$$I_e = (\frac{M_{cr}}{M_a})^3 \beta I_g + [1 - (\frac{M_{cr}}{M_a})^3] I_{cr} \leq I_g$$
$$where, \beta = \frac{1}{5}(\frac{\rho_{FRP}}{\rho_{bal}}) \leq 1.0 \qquad 2.11$$

Finally, the ACI 440.1R-06, [2006] provided the following equation for the crack width estimation:

$$w = 2\frac{f_{frp}}{E_{frp}}\frac{h_2}{h_1}k_b\sqrt{d_c^2 + (\frac{s}{2})^2} \qquad 2.12$$

In the ACI 440-H [2010] , Bischoff [2005] and Bischoff et Scanlon [2007a] proposed an alternative expression for the effective moment of inertia I_e that works equally well for both steel and FRP-reinforced concrete members without the need for empirical correction factors. They concluded that this approach provides reasonable estimates of deflection for GFRP, CFRP, AFRP and steel reinforced concrete beams and one-way slabs. The expression is presented by Eq. [2.10].

$$I_e = \frac{I_{cr}}{[1 - \eta(\frac{M_{cr}}{M_a})^2] I_{cr}} \leq I_g$$
$$where, \eta = [1 - (\frac{I_{cr}}{I_g})] \qquad 2.13$$

2.8.4 ISIS Manual No.3 (ISIS M03 2007)

When the service load level is less than the cracking moment, M_{cr}, the immediate deflection can be accurately evaluated using the transformed moment of inertia, I_t which known as gross moment of inertia, I_g. If the service moment exceeds the cracking moment, CAN/CSA-A23.3 [2004] recommends the use of the effective moment of inertia, I_e, to calculate the deflection of cracked steel reinforced concrete members. The procedure entails the calculation of a moment of inertia, which is assumed uniform throughout the beam. This value is used in deflection equations based on linear elastic analysis.

The effective moment of inertia I_e, is based on empirical considerations [ISIS Manual No.3, 2007]. It has yielded satisfactory results in applications when the maximum bending moment at service is greater than $2M_{cr}$, where M_{cr} is the value of the moment just sufficient to cause flexural cracking [Ghali et Azarnejad, 1999].

As all codes and guidelines, investigators initially applied the code-based effective moment of inertia concept, Branson's equation developed for steel, to FRP-reinforced concrete members. The deflection predictions based on this concept were not in good agreement with experimental data.

Consequently, attempts were made to modify the I_e expression in order to make it applicable to FRP-reinforced concrete members. The modified expressions were again based on the assumption that a uniform moment of inertia can be substituted for the actual variable moment of inertia of the beam along its length. Mota *et al.* [2006] examined a number of the suggested formulations for I_e and found that Eq. [2.14] provided the most consistently conservative results over the entire range of test specimens. In lieu of experimental results or

specific expertise of the designer in this field, it is recommended that this equation be used in design.

$$I_e = \frac{I_g I_{cr}}{I_{cr} + \left(1 - 0.5\left(\frac{M_{cr}}{M_a}\right)^2\right)\left(I_g - I_{cr}\right)} \qquad 2.14$$

To calculate the crack width, Gergely-Lutz equation [Gergely et Lutz, 1968], widely used for steel reinforced concrete member, was modified to predict the crack width for FRP reinforced concrete member. These modifications have been developed for a certain type of FRP reinforcement and therefore, their use is limited. Even though, the code based equation, originally developed by [Gergely et Lutz, 1968], reported un-conservative results in the lieu of all available experimental data for steel-reinforced concrete members.

Nevertheless, the Gergely-Lutz equation includes the most important parameters: the effective area of concrete in tension, the number of bars, the reinforcement cover, the strain gradient from the level of the reinforcement to the tensile face, and the stress in the flexural reinforcement [ISIS Manual No.3, 2007]. For FRP-reinforced members, it is necessary to consider the bond properties of the bar when calculating crack width. The following equation can be used when the bond properties of the bar are known:

$$w = 2.2 k_b \frac{f_{frp}}{E_{frp}} \frac{h_2}{h_1} \left(d_c A\right)^{1/3} \qquad 2.15$$

The ISIS Manual No.3, [2007] recommended k_b bond dependent coefficient to account for the bond properties of the FRP bar as its surface textures varied along the available commercial products. Accordingly, the k_b bond dependent coefficient is equal to unity, in case of similar bond behaviour to steel bar. On the other hand, for FRP bars with higher bond

behaviour than steel, the k_b value is greater than 1.0, however, for lower bond behaviour, the k_b value will be smaller than 1.0. ISIS Manual No.3 [2007] recommended a k_b value of 1.2 in the absence of significant test data.

CHAPTER 3

FLEXURAL BEHAVIOUR AND SERVICEABILITY OF NORMAL- AND HIGH-STRENGTH CONCRETE BEAMS REINFORCED WITH GFRP BARS

Authors and affiliation

Amr El-Nemr is a PhD candidate in the Department of Civil Engineering at the University of Sherbrooke, Sherbrooke, Quebec, Canada. He received his BS.c. in civil engineering from Arab Academy for Science and Technology, Cairo, Egypt. His research interests include the serviceability of FRP-reinforced concrete beams.

Ehab A. Ahmed is a postdoctoral fellow in the Department of Civil Engineering at the University of Sherbrooke, Sherbrooke, Quebec, Canada and lecturer at Minoufiya University, Shebin El-Kom, Minoufiya, Egypt. He received his PhD in civil engineering from the University of Sherbrooke, Sherbrooke, QC, Canada. His research interests include structural analysis, design and testing, and structural-health monitoring of FRP-reinforced concrete structures.

Brahim Benmokrane, FACI, is an NSERC Research Chair Professor in FRP Reinforcement for Concrete Infrastructure and Tier-1 Canada Research Chair Professor in Advanced Composite Materials for Civil Structures in the Department of Civil Engineering at the University of Sherbrooke, Sherbrooke, QC, Canada. He is a member of ACI Committee 440 FRP Reinforcement and the Canadian Standard Association (CSA) committees on FRP structural reinforcing materials for buildings (CSA S806), bridges (CSA S6), and specification (CSA S807).

Submittal/Acceptance Date: *submitted 13 October 2011*

Acceptance Status: in Peer Review

Journal Title: ACI Structural Journal

Reference: Not published yet

French Titre: *Comportement en flexion et capacité en service de poutres en béton normal ou à haute performance armées de barres de PRFV*

Contribution in thesis: This paper contributes to the state-of-the-art on the flexural behaviour and serviceability performance of GFRP-reinforced concrete (GFRP- reinforced concrete) beams. In this paper the applicability of the current cracking moment equations were verified on the normal- and high-strength concretes. The paper also introduced a comparative study between the normal- and high-strength GFRP- reinforced concrete beams considering flexural strength, mode of failure, concrete and reinforcement strains, deflection, and crack patterns and widths. The accuracy of the crack-width and deflection provisions were assessed through the comparison with the experimental results and design recommendations were introduced.

French Abstract:

Cet article porte sur l'étude du comportement en flexion et de la capacité en service de poutres en béton armé de barres de polymères renforcés de fibres de verre (PRFV) fabriquées avec du béton normal ou du béton à haute performance (BHP). Les poutres testées ont 4250 mm de longueur, 200 mm de largeur et 400 mm de profondeur (167,0×7,9×15,6 po). Trois différents types de renforts en PRFV, caractérisés par des modules d'Young allant de 48,7 à 69,0 GPa (7063 à 10 008 ksi), ont été utilisés. Ces produits sont caractérisés par des finis de surface sablée ou à enroulement hélicoïdal. Un total de 12 poutres pleine grandeur en béton armé de barres en PRFV ont été testées jusqu'à leur rupture sous chargement en flexion 4 points avec une distance entre appuis de chargement de 3750 mm (147.6 po). Les résultats obtenus ont été comparés à ceux obtenus sur 2 poutres de référence armées de barres d'acier. Les paramètres d'essais utilisés dans le cadre de cette étude sont:1) le type et le ratio de renfort en PRFV, 2) le type de fini de surface des barres de PRFV, 3) la résistance du béton, et 4) le

diamètre des barres d'armature. Les résultats expérimentaux obtenus sont la déflection, la largeur des fissures, les déformations du béton et des barres d'armature, les performances en flexion et le mode de rupture. Les résultats expérimentaux ont aussi été utilisés pour évaluer empiriquement la précision des équations de prédiction de la déflection et de la largeur des fissures actuellement utilisées dans les codes de conception traitant de l'utilisation du béton armé de PRF.

Mots-clés: Poutre; déflection, largeur des fissures, polymère renforcé de fibres (PRF); barre d'armature; flexion; capacité en service; béton normal; béton à haute résistance.

ABSTRACT

This paper investigated the flexural behaviour and serviceability performance of GFRP-reinforced concrete (GFRP- reinforced concrete) beams fabricated with normal- and high-strength concretes. The beam specimens measured 4,250-mm long × 200-mm wide × 400-mm deep [167.0×7.9×15.6 in.]. Three GFRP products with moduli of elasticity ranging from 48.7 GPa to 69.0 GPa [7,063 to 10,008 ksi] with sand-coated and helically-grooved surface textures were employed. A total of 12 full-scale beams reinforced with GFRP bars and 2 reinforced with steel bars, serving as control specimens, were tested to failure in four-point bending over a clear span of 3,750 mm [147.6 in.]. The test parameters were: (i) type and ratio of the GFRP reinforcement, (ii) surface configuration of the GFRP bars, (iii) concrete strength, and (iv) bar diameter. The test results were reported in terms of deflection, crack width, strains in concrete and reinforcement, flexural capacity, and mode of failure. The test results were also employed to assess the accuracy of the current deflection and crack-width prediction equations in the FRP-reinforced concrete codes.

Keywords: beam; deflection; crack width; fiber-reinforce polymer (FRP); rebars; flexure; serviceability; normal-strength concrete; high-strength concrete.

INTRODUCTION

Fiber-reinforced polymer (FRP) has been commercially available as reinforcement for concrete over the last 15 years [fib., 2007]. Due to the lack of well-established standards, a wide variety of FRP bars are currently marketed, ranging from the simple smooth and helically-deformed bars to bars treated with external features such as sand-coating. Nowadays, over 10 million meters of FRP reinforcement are used in construction every year [fib., 2007]. These FRP products have a wide range of mechanical properties as well as different surface configurations. Besides, most of the design codes and guidelines use equations for the steel-reinforced members with some modifications to account for the differences in the mechanical properties between FRP and steel bars. Furthermore, serviceability checks such as crack widths and deflections, involve assessing the tension stiffening effect which directly arises from bond behaviour [Pecce *et al.*, 2001]. Thus, employing an equation to predict the performance may yield reasonable predictions with one type of FRP bars but discrepancies with another.

At the ultimate limit state, most of the design codes and guidelines [ACI 440.1R-06, 2006; CAN/CSA-S806, 2002] recommend the over-reinforced section design, where concrete crushing is the dominant mode of failure. This is preferred as it is less catastrophic and yields higher deformability before failure. Some codes, however, permit the under-reinforced section design [CAN/CSA-S6, 2006]. The Distinction between both modes of failure is achieved

through the balanced reinforcement ratio (ρ_{fb}) which is influenced by the mechanical properties of the FRP bars and concrete strength.

Due to the lower modulus of elasticity of the FRP bars compared to that of steel, for the same reinforcement ratio (ρ_f), FRP- reinforced concrete members will exhibit larger deflections and crack widths. Thus, the design of FRP- reinforced concrete members is usually governed by serviceability. For deflection, a number of studies [Masmoudi *et al.*, 1996; Benmokrane, Chaallal et Masmoudi, 1996b; Yost *et al.*, 2003] proposed modifying Branson's original equation [Branson, 1968] for the effective moment of inertia and introduced modification factors for FRP reinforced concrete (FRP- reinforced concrete) members. Other studies [Razaqpur *et al.*, 2000; Bischoff et Scanlon, 2007a; Mota *et al.*, 2006a] proposed an equivalent moment of inertia derived from curvatures. For cracking, modifications were proposed to the original Gergely and Lutz [Gergely et Lutz, 1968] equation or strain limits were introduced to control the crack width [ISIS Manual No.3, 2007]. Furthermore, Feeser et Brown [2005] concluded that sections reinforced with multiple layers of GFRP reinforcement might be more attractive and should be explored. They, also, proposed that multiple layers of reinforcement would enable a GFRP- reinforced concrete section to accommodate larger ρ_f for compression-controlled failure. Besides, using higher concrete strengths to make more efficient use of the GFRP tensile strength is more applicable to designs with multiple layers of reinforcement.

This paper presents the flexural behaviour and serviceability of 12 full-scale, simply supported beams reinforced with three commercially available GFRP bars and 2 full-scale beams reinforced with steel bars fabricated using normal- and high-strength concretes (NSC and HSC). Moreover, the test results were employed to assess the accuracy of the current

design equations in North American FRP codes and guidelines [ACI 440.1R-06, 2006; ISIS Manual No.3, 2007; CAN/CSA-S806, 2002] considering the ultimate and serviceability limit states.

RESEARCH SIGNIFICANCE

Due to lack of standards, a wide variety of FRP products are commercially available. Thus, the need to investigate serviceability-related issues and validate the accuracy of design codes and guidelines are paramount. This paper investigates the flexural behaviour and serviceability performance of normal- and high-strength concrete beams reinforced with different types, diameters, ratios, and configurations of GFRP bars. Moreover, the accuracy of the current deflection and cracking equations in North American FRP codes and guidelines is verified.

EXPERIMENTAL PROGRAM

Materials

Reinforcing bars—Three types of GFRP bars were used. The GFRP products are referred to as GFRP-1 (No. 13; No. 15), GFRP-2 (No. 13; No. 15), and GFRP-3 (No. 15; No. 25). Figure 3.1 shows the GFRP bars. Both GFRP-1 and GFRP-2 have sand-coated surface and are classified according to their modulus of elasticity as Grade I and III [CAN/CSA-S807, 2010], respectively. GFRP-3 has a helically-grooved surface and is classified according to its modulus of elasticity as Grade III [CAN/CSA-S807, 2010]. Grade 400 10M steel bars were used for the reference beams. The tensile properties of the GFRP bars were determined by testing five representative specimens according to *Annex C* in [CAN/CSA-S806, 2002]. Table 3-1 provides the properties of the FRP and steel bars.

Concrete—Ready-mixed normal- and high-strength concretes (NSC and HSC) with 28-day target compressive strengths of 30 and 65 MPa [4.4 and 9.4 ksi], respectively, were used. A cubic meter of the NSC contained 350 kg [770 lbs] of cement, 813 kg [1789 lbs] of sand, and 1032 kg [2270 lbs] of aggregate with a water/cement ratio (*w/c*) of 0.44 and air entrained ratio of 5-6%. On the other hand, a cubic meter of HSC contained 490 kg [1078 lbs] of cement, 813 kg [1789 lbs] of sand, and 1032 kg [2270 lbs] of aggregate with a water/cement ratio (*w/c*) of 0.32 and 0% of air entrained. The maximum aggregate size for the NSC was 20 mm [0.8 in.], compared to 14 mm [0.6 in.] for the HSC. The concrete strengths for each batch were determined by testing three 150×300 mm cylinders on the day of testing. The compressive strengths ranged from 29.0 to 33.5 MPa [4.2 to 4.9 ksi] and from 59.1 to 73.4 MPa [8.6 to 10.6 ksi] for the NSC and HSC, respectively. It should be mentioned that the first batch of the HSC did not achieve the 65 MPa [9.4 ksi] and its concrete strength was 59.1 MPa [8.6 ksi]. The tensile strength determined from split-cylinder testing ranged from 2.5 to 3.6 MPa [0.4 to 0.5 ksi] and from 3.7 to 4.6 MPa [0.5 to 0.7 ksi] for the NSC and HSC, respectively. Table 3-2 lists the concrete strengths for each beam.

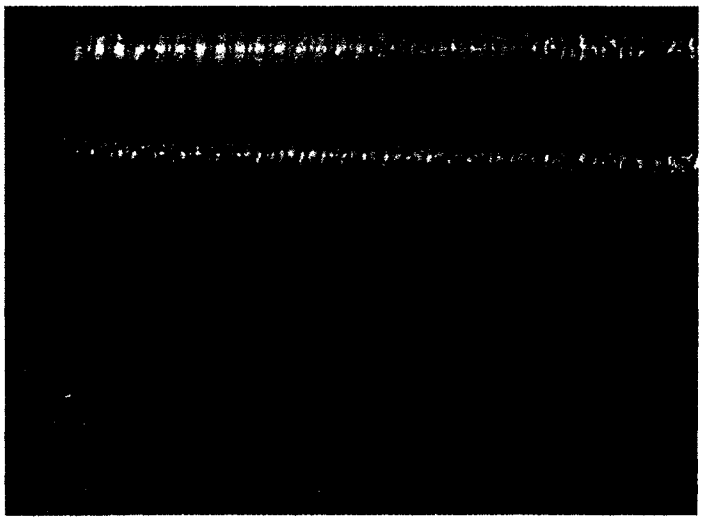

Figure 3.1 GFRP reinforcing bars

Table 3-1 Properties of the Reinforcing Bars

Bar type	Designated diameter of FRP bar[1]	Nominal cross-sectional area[1] (mm^2)	Surface configuration	Tensile strength, f_{fu}, (MPa)	Modulus of elasticity, E_f, (GPa)	Ultimate strain (%)	Guaranteed strength and strain[2]		E/f_{fu}
							f_G MPa	ε_G (%)	
GFRP-1 (G1)	13	129	Sand-coated	817±9	48.7±0.6	1.7	790	1.6	59.6
	15 (16)[3]	199	Sand-coated	762±10	50.0±1.0	1.5	732	1.4	65.6
GFRP-2 (G2)	13	129	Sand-coated	1639±61	67.0±1.0	2.5	1456	2.2	40.9
	15 (16)[3]	199	Sand-coated	1362±33	69.3±3.2	2.0	1263	1.8	50.9
GFRP-3 (G3)	15 (16)[3]	199	Helically-grooved	1245±45	59.5±1.1	2.1	1110	1.9	47.8
	25	510	Helically-grooved	906±29	60.3±2.9	1.5	819	1.3	66.6
Steel (ST)	10M	100	Ribbed-deformed	f_y= 450	200	0.2	N/A	N/A	N/A
	15M	199	Ribbed-deformed	f_y= 450	200	0.2	N/A	N/A	N/A

Notes – 1 mm = 0.0394 in., 1 kN = 0.225 kips, 1 MPa = 0.145 ksi

[1] FRP bars designated according to [CAN/CSA-S807, 2010] and [ACI 440.6M-08, 2008]

[2] Guaranteed tensile strength and elongation according to [ACI 440.1R-06, 2006] = average – 3 × standard deviation

[3] FRP bars of 199 mm^2 cross-sectional area designated as No. 15 according to [CAN/CSA-S807, 2010] and as No. 16 according to [ACI 440.6M-08, 2008].

Table 3-2 Details of the Test Specimens

Series	Beam[1]	f_c'[2] (MPa)	f_t[2] (MPa)	ρ_f (%)	ρ_{fb}[3] (%)	ρ/ρ_{fb}	A_fE_f (kN)	Reinforcement configuration
I	N2#13G2	33.5	3.6	0.38	0.15	2.45	17286	2 No. 13 - 1 row
	N3#13G1	33.5	3.6	0.56	0.43	1.31	18347	3 No. 13 - 1 row
	H2#13G2	59.1	4.6	0.38	0.22	1.67	17286	2 No. 13 - 1 row
	H3#13G1	59.1	4.5	0.56	0.63	0.9	18347	3 No. 13 - 1 row
II	N5#15G2	29.0	2.5	1.52	0.2	7.58	68954	5 No. 15 - 2 rows
	N6#15G1	33.5	3.6	1.82	0.5	3.67	59700	6 No. 15 - 2 rows
	H5#15G2	73.4	3.7	1.52	0.4	3.75	68954	5 No. 15 - 2 rows
	H6#15G1	73.4	3.7	1.82	0.9	2.02	59700	6 No. 15 - 2 rows
III	N5#15G3	33.8	3.1	1.52	0.23	6.47	59203	5 No. 15 - 2 rows
	N2#25G3	33.8	3.1	1.51	0.42	3.57	61506	2 No. 25 - 1 row
	H5#15G3	73.4	3.7	1.52	0.42	3.58	59203	5 No. 15 - 2 rows
	H2#25G3	73.4	3.7	1.51	0.76	1.98	61506	2 No. 25 - 1 row
V	N3#10ST	33.5	3.6	0.44	2.92	0.15	60000	3 10M - 1 row
	H3#10ST	59.1	4.6	0.44	4.79	0.09	60000	3 10M - 1 row

Note – 1 mm=0.0394 in., 1 kN=0.225 kips

[1] Concrete type (N: Normal-strength, H: High-strength) followed by the number and diameter of the reinforcing bars, ending by the reinforcement type (G1: GFRP-1, G2: GFRP-2, G3: GFRP-3, ST: Steel).

[2] Average of three cylinders (150×300 mm) on the day of testing.

[3] Calculated according to [ACI 440.1R-06, 2006].

Test specimens

A total of 14 full-scale simply supported beams were constructed and tested. The beams measured 4,250 mm long, 200 wide, and 400 mm deep [167.0×7.9×15.6 in.]. The test parameters were the type of GFRP bars, reinforcement ratio (ρ_f), concrete strength (f'_c), and bar diameter (d_b). The beams were categorized into four series as shown in Table 3-2. Two of the four beams in each series were fabricated using NSC, while the other two were fabricated using HSC. Beams in Series I were reinforced with sand-coated No. 13 GFRP bars, while those in Series II were reinforced with sand-coated No. 15 GFRP bars. Beams in Series III were reinforced with helically-grooved No. 15 and No. 25 GFRP bars. The control beams in Series IV were reinforced with deformed 10M steel bars. It should be mentioned that the beams in Series II and III had approximately the same axial-reinforcement stiffness ($A_f E_f$) to assess the effect of surface configuration and bar diameter. All of the NSC and HSC beams were designed as over-reinforced with a ρ_f/ρ_{fb} ratio greater than 1.0, so that the failure occurs due to concrete compression. The H3#13G1 beam, however, had a ρ_f/ρ_{fb} of 0.9 (under-reinforced) when the actual material properties were considered. The entire beams were reinforced in compression with two 10M steel bars. The beams were provided with closely spaced steel stirrups (10 mm @ 100 mm [0.4 in @ 3.9 in.]) in the shear spans to avoid specimen shear failure and to minimize the effect of the shear induced deformation on the mid-span deflection. On the other hand, the constant moment zone included only two stirrups spaced at 300 mm [11.8 in.] to maintain the locations of the longitudinal bars and minimize stirrup confinement action, which may affect cracking behaviour. Figure 3.2 shows the geometry and reinforcement details of the beams, while Table 3-2 lists the complete specifications for each beam.

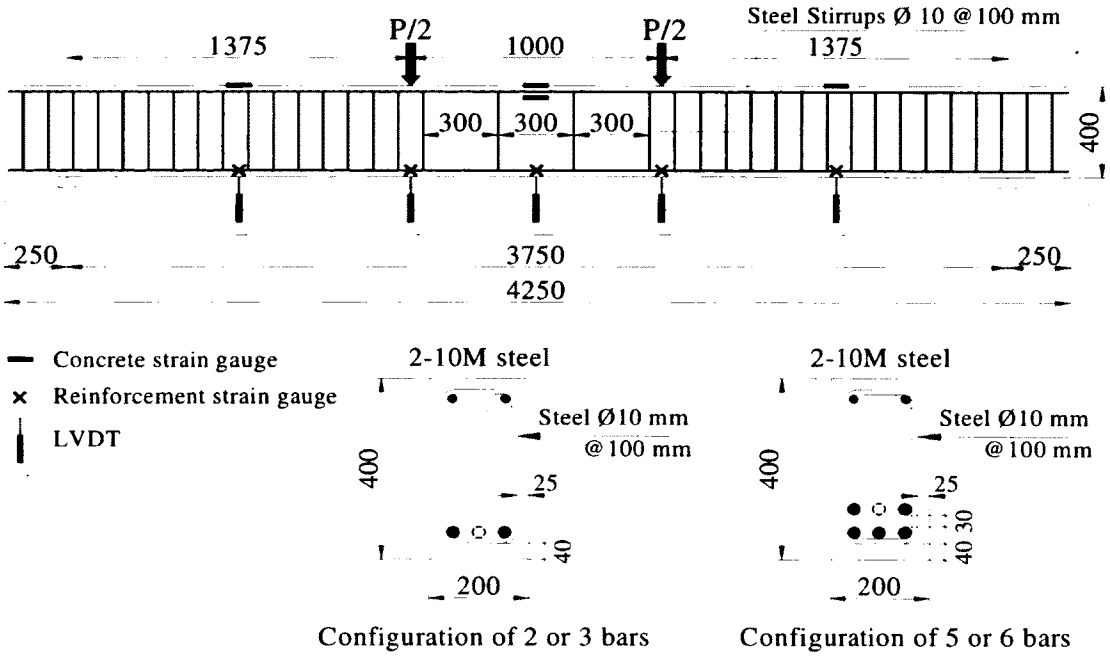

Configuration of 2 or 3 bars Configuration of 5 or 6 bars

Figure 3.2 Dimensions, reinforcement details, and instrumentation
Note – 1 mm=0.0394 in.

Instrumentation and testing

The reinforcing bars as well as the compression-concrete zone of the beams were instrumented with electrical resistance strain gauges to capture the strains at the desired locations. Besides, five linear variable displacement transducers (LVDTs) were installed on each beam to measure deflection at different locations during testing. In addition, one LVDT was installed at the position of the first flexural crack after measuring its initial width with a hand-held microscope with 50X magnifying power. Figure 3.2 also shows the instrumentation of the beams.

All beam specimens were tested under four-point bending over a clear span of 3,750 mm [147.6 in.] (Figure 3.2). The load was monotonically applied using a 500-kN hydraulic actuator with a stroke-controlled rate of 0.6 mm/min [0.02 in./min]. During the test, crack formation on one side of each beam was marked and the corresponding loads were recorded.

The actuator, strain gauges, and LVDTs were connected to a data-acquisition unit to continuously record their readings.

TEST RESULTS AND DISCUSSION

First cracking moment

During the test, the beams were observed visually until the first crack appeared and the corresponding load was recorded. The cracking load was also verified from the load-deflection and load-strain relationships. Table 3-3 provides the cracking moments of the tested beams. The cracking moment of the NSC beams, excluding the self-weight of the beams, ranged from 12.20 to 14.15 kN.m [9.0 to 10.4 kips.ft] with an average of 13.27 kN.m [9.8 kips.ft]. Since the cracking moment is directly related to concrete tensile strength, which, in turn, is a function of compressive strength, increasing the concrete compressive strength is expected to yield higher cracking moments. The cracking moment of the HSC beams ranged from 17.49 to 23.87 kN.m [12.9 to 17.6 kips.ft], excluding the self-weight of the beams, with an average of 21.61 kN.m [15.9 kips.ft]. The ratio of the average cracking moment of the HSC beams to that of the NSC beams was 1.63. This ratio is close to the ratio between the square root of the average compressive strength of the HSC beams (66.2 MPa [9.6 ksi]) and that of the NSC beams (32.5 MPa [4.7 ksi]), which was 1.43. The cracking moments were predicted using Eq. [3.1]:

$$M_{cr} = f_r / y_t I_g \qquad 3.1$$

where: $f_r = 0.62\lambda\sqrt{f_c'}$ for [ACI 440.1R-06, 2006] 3.2

$f_r = 0.6\lambda\sqrt{f_c'}$ for [ISIS Manual No.3, 2007; CAN/CSA-S806, 2002; CAN/CSA-S6, 2006] 3.3

Table 3-3 Experimental and Predicted Cracking and Ultimate Moments

Beam	Experimental moments			M_a/M_{cr} [4]		ACI 440.1R-06			CAN/CSA S806-02		
	M_{cr}	M_n	Failure mode [2]	$0.3M_n$	$0.67M_n$	M_{cr} [1]	M_n	Failure mode [2]	M_{cr} [1]	M_n	Failure mode [2]
	kN.m	kN.m				Exp/Pred	Exp/Pred		Exp/Pred	Exp/Pred	
N2#13G2	13.75	82.78	C.C.	1.8	4.0	0.87	0.94	C.C.	0.90	0.87	C.C.
N3#13G1	13.46	81.34	C.C.	1.8	4.0	0.85	0.89	C.C.	0.88	0.82	C.C.
H2#13G2	17.49	101.59	C.C.	1.7	3.9	0.79	0.91	C.C.	0.82	0.82	C.C.
H3#13G1	19.94	82.58	FRP-R	1.2	2.8	0.90	0.77	FRP-R	0.94	0.77	FRP-R
N5#15G2	12.20	129.32	C.C.	3.2	7.1	0.84	0.98	C.C.	0.88	0.93	C.C.
N6#15G1	11.98	118.34	C.C.	3.0	6.6	0.76	0.89	C.C.	0.79	0.84	C.C.
H5#15G2	23.38	178.54	C.C.	2.3	5.1	0.93	0.85	C.C.	0.97	0.80	C.C.
H6#15G1	24.06	181.73	C.C.	2.3	5.1	0.96	0.93	C.C.	1.00	0.88	C.C.
N5#15G3	12.61	110.58	C.C.	2.6	5.9	0.79	0.82	C.C.	0.82	0.77	C.C.
N2#25G3	13.20	115.93	C.C.	2.6	5.9	0.83	0.81	C.C.	0.86	0.76	C.C.
H5#15G3	23.78	188.37	C.C.	2.4	5.3	0.95	0.95	C.C.	0.99	0.90	C.C.
H2#25G3	21.04	189.06	C.C.	2.7	6.0	0.84	0.90	C.C.	0.87	0.85	C.C.
N3#10ST[3]	14.15	45.88	S-Y	1.0	2.2	1.09	0.99	S-Y	0.89	1.01	S-Y
H3#10ST[3]	21.24	48.57	S-Y	0.7	1.5	1.03	1.13	S-Y	0.94	0.89	S-Y
Average						0.89	0.91	---	0.90	0.85	---
Standard deviation						0.10	0.09	---	0.06	0.07	---
Coefficient of variation %						11%	10%	---	7%	8%	---

Notes – 1 kN.m=23730 lb.ft

[1] Beam self-weight subtracted from the predicted values

[2] FRP-R: rupture of FRP bar; C.C.: Concrete crushing.

[3] Values calculated at 1200 με, 0.67 M_y, and M_y, respectively.

[4] M_a is defined as the applied moment at certain load level (0.30 M_n and 0.67 M_n).

Eq. [3.2] and [3.3] were employed for both NSC and HSC. Table 3-3 provides a comparison between the experimental and predicted values for the cracking moments. As can be seen, the cracking moment of the GFRP- reinforced concrete beams was generally lower than those predicted with CAN/CSA-S806 [2002] and ACI 440.1R-06 [2006]. ACI 440.1R-06 [2006] overestimated the cracking moment for the GFRP- reinforced concrete beams by 18 and 10% for NSC and HSC, respectively. CAN/CSA-S806 [2002] overestimated the cracking moment for the GFRP- reinforced concrete beams by 14 and 7% for NSC and HSC, respectively. CAN/CSA-S806 [2002] yielded slightly better predictions of cracking moments than ACI 440.1R-06 [2006] because of the former's smaller modulus of rupture. Thus, Eq.

[3.3] seems applicable for predicting the modulus of rupture of NSC and HSC in the range of tested concrete strengths.

Flexural capacity and mode of failure

The GFRP- reinforced concrete beams were designed to fail by concrete crushing when the concrete reaches its maximum compressive strain, $\varepsilon_{cu} \approx 0.003$, (over-reinforced). This is the common design concept for FRP- reinforced concrete sections according to CAN/CSA-S806 [2002] and ACI 440.1R-06 [2006]. The ρ_{fb} is calculated from Eq. [3.3]. The terms α_1 and β_1 are calculated from Eq. [3.5] for ACI 440.1R-06 [2006] and Eq. [3.6] for CAN/CSA-S806 [2002] and ISIS Manual No.3 [2007].

$$\rho_{fb} = \alpha_1 \beta_1 \frac{f_c'}{f_{fu}} \frac{E_f \varepsilon_{cu}}{E_f \varepsilon_{cu} + f_{fu}} \qquad 3.4$$

where: $\alpha_1 = 0.85$; $\beta_1 = 0.85 - 0.05\left(f_c' - 27.6\right)/6.9$ 3.5

$$\alpha_1 = 0.85 - 0.0015(f_c') \geq 0.67 \;\; ; \;\; \beta_1 = 0.97 - 0.0025(f_c') \geq 0.67 \qquad 3.6$$

The GFRP- reinforced concrete beams failed by concrete crushing, except for specimen H3#13G1. The actual properties of the materials yielded under-reinforced section, and the failure mode was rupture of the GFRP bars. On the other hand, the steel-RC beams failed due to yielding of the steel bars because they were designed as under-reinforced, which is the common case of steel-RC members. At failure, the concrete strain of all the tested beams was very low compared to the 0.003 or 0.0035 values provided by the design codes and guidelines. This relates to the absence of lateral ties (stirrups) in the critical flexural zone of the beams. This, in turn, led to premature buckling of compression bars before yielding and the consequent disintegration of the confined concrete. The premature buckling was due to a large unsupported length of compression bars (300 mm [11.8 in.]).

In the case of the NSC beams, increasing ρ_f from 0.36 to 1.47% (N2#13G2; N5#15G2) increased the load-carrying capacity from 82.78 to 118.34 kN.m [61.0 to 87.3 kips.ft] (143%). Increasing ρ_f from 0.55 to 1.78% (N3#13G1; N6#15G1), however, increased the capacity from 81.34 to 181.73 kN.m [60.0 to 134 kips.ft] (224%). Increasing ρ_f by 3 to 4 times resulted in an average increase of 83.5% in the load-carrying capacity. Kassem *et al.*, [2011] reported concrete crushing in FRP- reinforced concrete beams, whereas the increased ρ_f did not significantly increase the flexural capacity. The increases were 4 and 16% when ρ_f was increased by 50 and 100%, respectively. The difference between those small increase ratios in the flexural capacity and that obtained herein may be related to the smaller ρ_f increase (2 times) and confinement with closely spaced stirrups in the critical flexural zone (10M steel stirrups every 80 mm [3.15 in.]).

Similarly, for the HSC beams, increasing ρ_f from 0.36 to 1.47% (H2#13G2; H5#15G2) and from 0.55 to 1.78% (H3#13G1; H6#15G1) increased the ultimate load-carrying capacity by 28 and 116%, respectively. The very high increase in case of H3#13G1 and H6#15G1 is due to the difference in their modes of failure. Similar behaviour was observed for the steel-reinforced beams.

Yost et Gross [2002] reported that using higher concrete strength resulted in more efficient use of the FRP. For some of the tested beams, increasing the concrete strength increased the ultimate load-carrying capacity. The increased ratio was not consistent because of the lower-than-expected concrete strains at failure. Furthermore, this did not make it possible to quantify the effect of bar diameter and surface texture on the ultimate load-carrying capacity of the GFRP- reinforced concrete beams.

The load-carrying capacity of the test specimens was calculated and compared to the measured values. Table 3-3 shows the prediction of the ultimate load-carrying capacity of the tested beams as well as the mode of failure. The prediction shows that ACI 440.1R-06 [2006] and CAN/CSA-S806 [2002] were un-conservative for the NSC and HSC beams. Due to the lower-than-expected concrete strains at failure in the beams; the experimental-to-predicted load-carrying capacity was less than 1.0. The difference between ACI 440.1R-06 [2006] and CAN/CSA-S806 [2002] predictions, however, were related to the β_1 factor and the assumed strain at the ultimate which is 0.003 for ACI 440.1R-06 [2006] and 0.0035 for CAN/CSA-S806 [2002].

Table 3-4 Strains, Neutral Axis-to-Depth Ratio, and Curvature of Test Specimens

Beam	Strain in concrete (με)			Strain in reinf. (με)		*c/d*				Curvature, ψ		
	at 2000 $\mu\varepsilon^2$	0.30M_n	M_n	0.30M_n	M_n	at 2000 $\mu\varepsilon^2$	0.30M_n	M_n	Theo.[3]	at 2000 $\mu\varepsilon^2$	0.30M_n	M_n
N2#13G2	-173	-690	-2541	5349	16359	0.05	0.11	0.13	0.12	0.003	0.006	0.019
N3#13G1	-203	-314	-1561	4378	13726	0.09	0.07	0.10	0.13	0.002	0.005	0.015
H2#13G2	-201	-391	-2344	3981	17316	0.25	0.08	0.10	0.11	0.001	0.005	0.023
H3#13G1	-200	-165	-1675	2174	10563	0.07	0.07	0.14	0.11	0.003	0.002	0.012
N5#15G2	-729	-745	-2959	2053	7550	0.28	0.28	0.29	0.24	0.003	0.003	0.010
N6#15G1	-488	-562	-1976	2367	7693	0.19	0.19	0.20	0.22	0.003	0.003	0.010
H5#15G2	-461	-642	-2230	2616	10111	0.19	0.18	0.19	0.20	0.002	0.003	0.012
H6#15G1	-302	-400	-1891	2915	10251	0.13	0.12	0.16	0.19	0.002	0.003	0.012
N5#15G3	-521	-412	-1839	1571	6430	0.21	0.21	0.22	0.22	0.003	0.002	0.008
N2#25G3	-575	-459	-1627	1666	6429	0.22	0.22	0.20	0.22	0.003	0.002	0.008
H5#15G3	-317	-455	-2313	2440	11035	0.19	0.14	0.16	0.19	0.002	0.003	0.014
H2#25G3	-313	-494	-1726	3077	9578	0.14	0.14	0.15	0.19	0.002	0.004	0.011
N3#10ST[1]	-221	-304	-611	1655	3490	0.16	0.16	0.15	0.23	0.001	0.002	0.004
H3#10ST[1]	-219	-283	-452	2225	4281	0.13	0.11	0.10	0.20	0.002	0.003	0.005

[1] Values calculated at 1200 με, 0.67 M_y, and M_y, respectively.
[2] Values calculated at 2000 με.
[3] Values calculated at ultimate.

Table 3-4 reveals a slight increase in the *c/d* ratio at M_n compared to that at 0.30M_n, where M_n is nominal moment capacity. Moreover, the neutral axis depth increased with ρ_f since the equilibrium of forces requires a larger compression block for the greater force. Increasing the concrete strengths for the beams with the same longitudinal

reinforcement type and amount yielded smaller *c/d* ratio because the higher concrete strengths resulted in a smaller compression block for the same force. The theoretical positions for the neutral axis were calculated assuming a cracked-section analysis. Table 3-4 showed good agreement between the theoretical predictions and experimental results.

Strain in reinforcement and concrete

Figure 3.3 shows the mid-span strains in the compression-concrete zone and the tensile reinforcing bars versus the applied moment. Table 3-4 shows the strains in the reinforcement and concrete at $0.3M_n$ and at failure. All the GFRP- reinforced concrete beams failed in compression by concrete crushing except H3#4G1, because the actual material properties yielded an under-reinforced section in this beam. This mode of failure could be seen from the lower-than-ultimate strains in the GFRP bars and relatively high compressive strains in the concrete. As mentioned earlier, the concrete's compression failure was trigged by the buckling of the compression steel reinforcement.

Generally, the GFRP- reinforced concrete beams showed typical bi-linear moment-strain relationship. The difference between the NSC and HSC could be seen in the cracking moment, since the HSC beams exhibited higher cracking moments. Figure 3.3 shows that increasing ρ_f decreased the strain in the GFRP bars at the same load level for either concrete type. For beams with the same reinforcement type and amount, increasing the concrete strength from NSC to HSC slightly reduced the strains in the GFRP bars after cracking at the same load level. In addition, GFRP- reinforced concrete beams with close $E_f A_f$ are expected to yield the same moment-strain relationship. The GFRP- reinforced concrete beams in Series III had the $E_f A_f$ as the steel-reinforced ones. After cracking, however, they

showed lower strains in the GFRP bars than in the steel bars. This may be related to the good bond behaviour of the GFRP bars, which yielded more cracks, leading to smaller stains at the same load level.

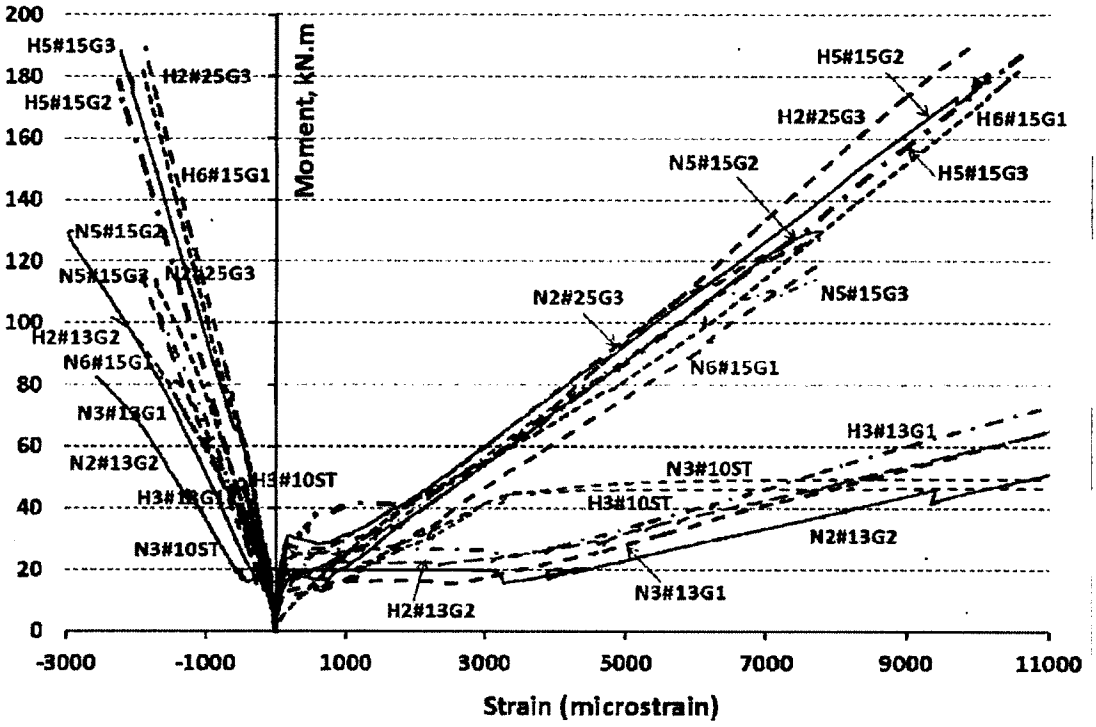

Figure 3.3 Moment-to-maximum concrete and reinforcement strain relationship

Figure 3.3 also shows that Series I beams with low ρ_f (0.38 and 0.56%) experienced very high strain increases at cracking. The sharp increase at the cracking was more than 3,000 με in the NSC and HSC beams. While three of these beams were designed as over-reinforced sections that did not prevent the large increase due to poor energy absorption at cracking. Maintaining minimum practical reinforcement (i.e. 1%) may be of interest to ensure that the section behaves reasonably after cracking.

Table 3-4 provides the calculated curvature at failure as a function of $1/d$. The calculated values ranged from $0.008/d$ to $0.015/d$ for compression-controlled failure (excluding N2#13G2), which agrees with the range of $0.0089/d$ to $0.012/d$ [Gulbrandsen, 2005] and the range of $0.009/d$ to $0.014/d$ [Kassem *et al.*, 2011]. On the other hand, the tension-controlled failure of the H3#13G1 beam yielded a very high curvature of $0.023/d$. Based on the moment-curvature diagrams of 50 GFRP- reinforced concrete beams [Vijay et GangaRao, 1996], the maximum unified curvature at a service load that satisfies both deflection and crack-width serviceability limits should be limited to $0.005/d$. A curvature limit exceeding $0.005/d$ generally failed to satisfy either the deflection or the crack width criteria for beams with span-to-depth ratios of 8 to 13 [Vijay et GangaRao, 1996]. The service load level for the FRP- reinforced concrete members, however, has no fixed definition in the design codes and guidelines. ISIS Manual 03-07 recommended a value of 2,000 με as a limit for the strain in the FRP bars under service load. Other researchers assume that the service load of the FRP- reinforced concrete members is about 30% of their nominal flexural capacity, $0.3M_n$ [Bischoff *et al.*, 2009]. The former often satisfies the serviceability requirements, but, in some cases, the $0.30M_n$ yields very high strain levels. These cannot be considered as service strain, such as in case of N2#13G2 and N3#13G1, which were 5,349 and 4,378 microstrains, respectively. Kassem *et al.* [2011] also reported strain values as high as 4,119 microstrains in the GFRP bars and 3,850 microstrains in the CFRP bars at $0.3M_n$, which is also high and could not be considered as strains at service. Furthermore, at a curvature limit of $0.005/d$, strains in FRP bars were typically as high as 4,500 microstrains [Vijay et GangaRao, 1996]. Thus, in this study, the key results were presented at 2,000 microstrains in the GFRP bars, at $0.3M_n$, and at $0.67M_n$.

Deflection Behaviour

Figure 3.4 provides typical bi-linear load-deflection relationships for the tested GFRP- reinforced concrete beams. Each curve represents the average deflection obtained from 2 LVDTs mounted at beam mid-span. The load-deflection relationships (Figure 3.4) revealed that ρ_f had a direct impact on the stiffness of the beam specimens, hence, on the load-deflection behaviour.

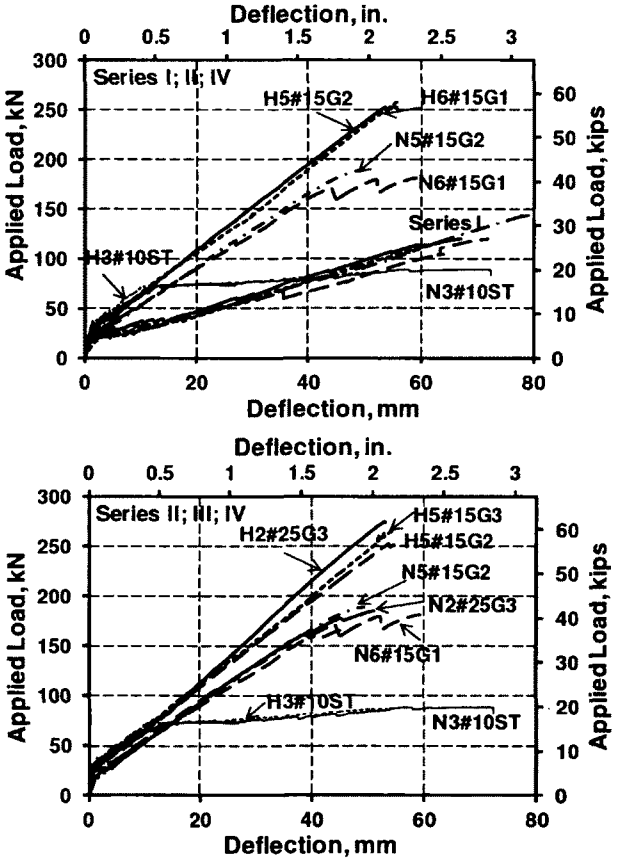

(a) Series I, II, IV (b) Series II, III, IV

Figure 3.4 Load-to-mid-span deflection relationships: (a) Series I, II, IV; (b) Series II, III, IV

The Series I GFRP- reinforced concrete beams (with the lowest ρ_f) showed the highest deflection compared to Series II and III. Due to the difference in the modulus of elasticity of the GFRP bars employed herein, $E_f A_f$ was used as reference. Series I beams had $E_f A_f$ around 18 MN [4,047 kips], while Series II and III beams had $E_f A_f$ of about 60 MN [13,488 kips]. Thus, Series I beams exhibited the largest deflection compared to Series II and III at the same load level. Figure 3.4 indicates that using HSC while maintaining the same $E_f A_f$ contributed to enhancing the deflection of the GFRP- reinforced concrete beams, in addition to enhancing the load-carrying capacity of Series II and III beams. Series I beams with low ρ_f and the same $E_f A_f$, however, did not show significant differences in load-deflection relationships.

Comparing beams N2#25G3, N5#15G3, N5#15G2, and N6#15G1 (which had the same $E_f A_f$) showed the same load-deflection relationships. This was confirmed by comparing H5#15G2 and H6#15G1. The NSC and HSC beams with the same $E_f A_f$ yielded the same load-deflection relationships. Furthermore, comparing the load-deflection relationships of N2#25G3 and N5#15G3 reveals that increasing the GFRP bar diameter from 15 to 25 mm [0.6 to 1.0 in.] while maintaining the same $E_f A_f$ did not affect the load-deflection relationships. In addition, comparing N5#15G3, N5#15G2 and N6#15G1 showed that the load-deflection relationships were not affected by GFRP-bar properties or surface configuration when the same $E_f A_f$ was achieved. This was confirmed by comparing the load-deflection relationships of Series II and III GFRP- reinforced concrete beams against Series IV steel-RC beams, which were almost the same. Providing the same $E_f A_f$ with GFRP and steel bars yielded the same load-deflection relationships up to yielding of the steel bars. Table 3-5 summarizes the deflection of the tested beams at $0.3M_n$ and $0.67M_n$.

The deflection values from Table 3-5 were plotted against the $E_f A_f$ as well as the ρ_f/ρ_{fb}, as shown in Figure 3.5. This figure shows that the deflection values at $0.3M_n$ and $0.67M_n$ followed the same trend. The higher the $E_f A_f$ and the ρ_f/ρ_{fb}, the lower the deflection values. Assuming that beam deflection limit at service load is span/240 (L/240), as provided for by [CAN/CSA-A23.3, 1994]—which yields 15.63 mm [0.6 in.]— all the beams except H2#13G2 exhibited deflections smaller than 15.63 mm [0.6 in.] at $0.30M_n$.

Table 3-5 Experimental-to-Predicted Deflection Ratios

Beam	Measured deflection (mm)		$\delta_{exp}/\delta_{pred}$ ACI 440[4]		$\delta_{exp}/\delta_{pred}$ ACI 440-H		$\delta_{exp}/\delta_{pred}$ CSA S806[3]		$\delta_{exp}/\delta_{pred}$ ISIS[14]	
	$0.30M_n$	$0.67M_n$	$0.30M_n$	$0.67M_n$	$0.30M_n$	$0.67M_n$	$0.30M_n$	$0.67M_n$	$0.30M_n$	$0.67M_n$
N2#13G2	15.07	48.35	1.65	1.17	1.22	1.16	0.70	0.96	0.75	0.99
N3#13G1	15.38	41.31	1.17	0.97	1.29	1.03	0.76	0.85	0.82	0.87
H2#13G2	19.92	54.45	2.14	1.10	1.67	1.10	0.75	0.85	0.82	0.87
H3#13G1	10.75	39.56	0.84	0.83	1.06	0.89	0.54	0.79	0.60	0.81
N5#15G2	10.98	28.95	1.29	1.28	1.28	1.30	1.03	1.18	1.06	1.19
N6#15G1	9.43	27.34	0.95	1.05	0.97	1.07	0.76	0.97	0.79	0.97
H5#15G2	13.15	35.18	1.09	1.05	1.07	1.07	0.81	0.96	0.84	0.96
H6#15G1	13.10	37.19	0.94	1.03	1.03	1.06	0.75	0.94	0.81	0.95
N5#15G3	7.92	23.69	0.87	0.92	0.82	0.94	0.63	0.83	0.66	0.84
N2#25G3	13.15	36.82	1.10	1.03	1.03	1.05	0.76	0.93	0.79	0.94
H5#15G3	9.53	25.13	0.96	1.00	1.01	1.02	0.79	0.92	0.82	0.92
H2#25G3	14.19	33.96	1.01	0.97	1.12	1.01	0.84	0.89	0.88	0.90
Average			1.17	1.03	1.13	1.06	0.76	0.92	0.80	0.93
Standard deviation			0.38	0.12	0.22	0.10	0.12	0.10	0.11	0.10
Coefficient of variation (%)			32%	11%	19%	10%	15%	11%	14%	10%
Overall average			1.10		1.09		0.84		0.87	
Overall standard deviation			0.28		0.17		0.14		0.12	
COV (%)			26%		15%		16%		14%	

Note – 1 mm=0.0394 in.

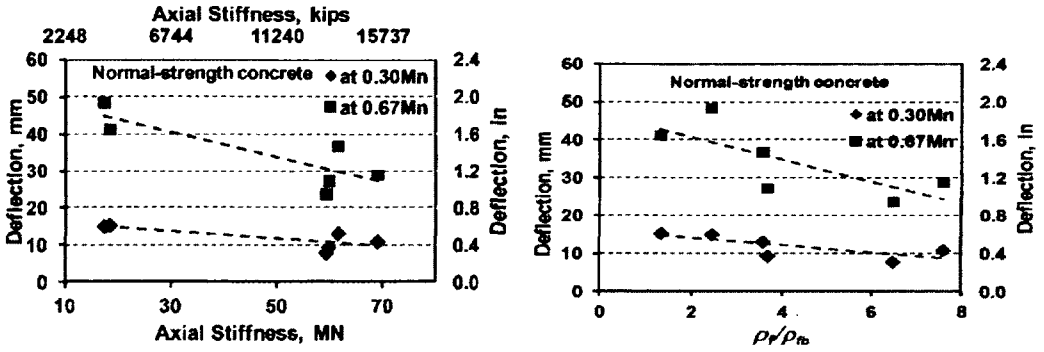

(a) Normal-strength concrete

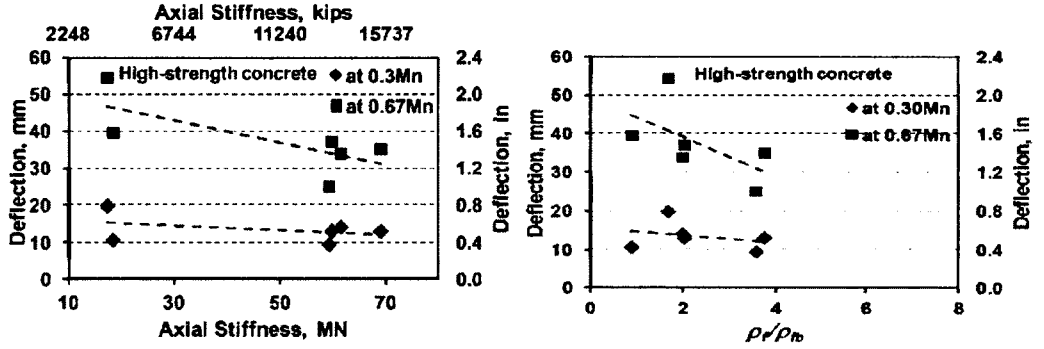

(b) High-strength concrete

Figure 3.5 Deflection versus the axial-reinforcement stiffness and ρ_f/ρ_{fb}: (a) Normal-strength concrete; (b) High-strength concrete

Crack propagation and crack width

All beam specimens were initially un-cracked before testing, except N6#15G1, which had a hair crack in the pure bending zone (this crack was not considered in the analysis). Flexural cracks appeared when the concrete's tensile strength and, consequently, the crack moment were reached in the pure bending zone. Table 3-6 gives the initial crack width of the first crack in each beam. Figure 3.6 shows the crack pattern of the tested GFRP-reinforced concrete beams of Series II and III at two loading levels: $0.3M_n$ and $0.67M_n$. The former corresponds to beam service load as reported by other researches [Bischoff *et al.*, 2009]; the latter presents the threshold at which cracks almost stabilized.

Table 3-6 Experimental-to-Predicted Crack Width (w_{exp}/w_{pred}) and Predicted k_b Value

Beam	Measured crack width, w_{exp} (mm)	w_{exp}/w_{pred}	k_b

					ACI 440[4]			ISIS[14]			ACI 440[4]		ISIS[14]	
	Initial	2000 με	$0.30M_n$	$0.67M_n$	2000 με	$0.30M_n$	$0.67M_n$	2000 με	$0.30M_n$	$0.67M_n$	2000 με	$0.30M_n$	2000 με	$0.30M_n$
N2#13G2	0.20	0.77	1.03	2.38	1.62	0.95	1.01	1.71	0.94	0.99	1.48	1.14	1.35	1.04
N3#13G1	0.10	0.40	0.78	1.82	1.11	1.03	1.08	1.02	0.88	0.90	1.5	1.41	1.17	1.10
H2#13G1	0.10	0.54	0.83	1.44	1.13	0.63	0.49	1.20	0.60	0.46	1.6	1.02	1.45	0.93
H3#13G2	0.20	0.61	0.55	0.72	1.77	0.66	0.38	1.57	0.58	0.34	1.93	2.09	1.46	1.58
N5#15G2	0.09	0.30	0.31	0.70	0.81	0.55	0.55	0.68	0.44	0.44	1.14	1.13	0.83	0.83
N6#15G1	0.05	0.14	0.15	0.44	0.36	0.18	0.25	0.31	0.15	0.20	0.51	0.46	0.38	0.35
H5#15G2	0.08	0.20	0.26	0.57	0.53	0.29	0.28	0.46	0.23	0.23	0.90	0.75	0.66	0.55
H6#15G1	0.16	0.33	0.45	1.06	0.88	0.39	0.41	0.76	0.32	0.33	1.21	1.16	0.90	0.87
N5#15G3	0.12	0.53	0.40	0.69	1.40	0.59	0.46	1.20	0.48	0.37	2.02	1.91	1.48	1.40
N2#25G3	0.13	0.53	0.45	0.93	1.09	0.86	0.80	1.05	0.78	0.72	1.49	1.55	1.24	1.28
H5#15G3	0.09	0.38	0.62	1.19	1.02	0.65	0.55	0.87	0.52	0.44	2.35	1.95	1.72	1.43
H2#25G3	0.11	0.31	0.54	1.34	0.65	0.73	0.80	0.63	0.65	0.73	0.91	1.03	0.75	0.85
Average					1.03	0.63	0.59	1.03	0.63	0.59	0.96	0.55	0.51	1.42
Standard deviation					0.42	0.25	0.27	0.42	0.25	0.27	0.42	0.25	0.26	0.52
Coefficient of variation (%)					41%	41%	47%	41%	41%	46%	44%	45%	51%	37%

Note – 1 mm=0.0394 in.

Looking at Figure 3.6 reveals that increasing ρ_f in the normal- and high-strength GFRP- reinforced concrete beams increased the number of cracks and, consequently, reduced the average crack spacing. Moreover, the crack depth also decreased when ρ_f increased. Comparing Series I and II beams, which had the same reinforcing bars (sand-coated GFRP bars: G1 and G2) it could be noticed that increasing ρ_f or $E_f A_f$ resulted in a higher number of cracks and also yielded smaller initial crack widths except in case of H6#15G1, which seems to be affected by the pre-existing hair crack.

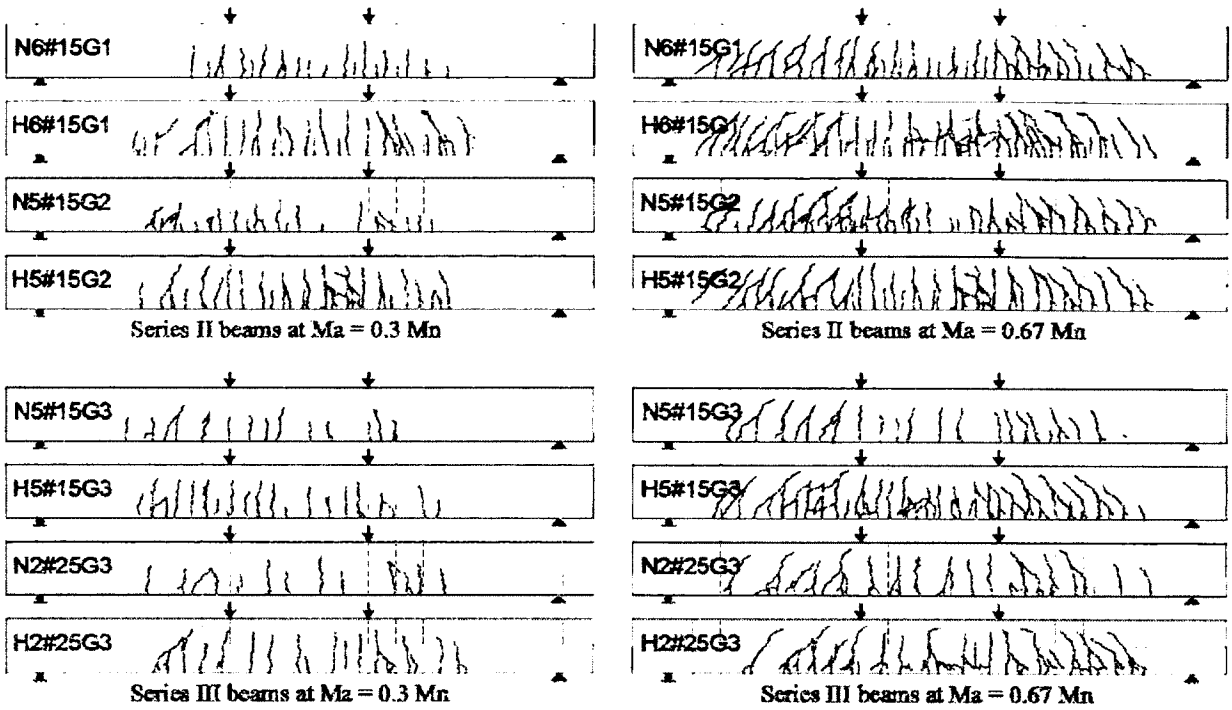

Figure 3.6 Crack patterns of beam specimens of Series II and III at $0.3M_n$ and $0.67M_n$

Comparing Series II and III beams, which have almost the same $E_f A_f$, although different types of GFRP bars (sand-coated: G1; G2 and helically grooved: G3) revealed that fewer cracks in beams reinforced with helically-grooved GFRP bars. This tends to confirm that the sand-coated GFRP bars have better bond characteristics than the helically-grooved ones. Figure 3.6 also pointed out the effect of concrete strength on cracking behaviour. Given the same load level, the higher concrete strength resulted in more cracks with closer spacing and smaller crack width than beams with lower concrete strength. Moreover, HSC produced higher cracking moments which enhance the comparable behaviour. Similar behaviour was also reported [Bouguerra *et al.*, 2011] in FRP- reinforced concrete slabs where using HSC resulted in closer cracks with smaller widths.

Most design codes specify a flexural crack-width limit for steel-reinforced concrete structures to protect the reinforcing bars from corrosion and to maintain the structure's aesthetical appearance. Unlike steel reinforcement, FRP is corrosion resistant. Therefore, the serviceability limits for crack widths in FRP- reinforced concrete elements may be directly related to aesthetic considerations. The FRP design codes and guidelines permit a larger crack width for FRP- reinforced concrete elements compared to their counterparts reinforced with steel. CAN/CSA-S806 [2002] and CAN/CSA-S6 [2006] specify a service-limiting flexural-crack width of 0.5 mm [0.02 in.] for exterior exposure (or aggressive environmental conditions) and 0.7 mm [0.03 in] for interior exposure. In addition, ACI 440.1R-06 [2006] recommends using CAN/CSA-S806 [2002] limits for most cases. On the other hand, since there is a direct relationship between the strain in the reinforcing bars and the crack width, ISIS Manual No.3 [2007] specifies 2,000 microstrains as a strain limit in FRP-reinforcing bars to control crack width.

Figure 3.7 gives the moment-crack width relationships for the tested beams. Table 3-6 lists the crack widths at 2,000 microstrains in the FRP, at $0.3M_n$, and at $0.67M_n$. Series I beams evidenced very high crack widths at service-load levels. Beyond that, the cracks were very wide with a maximum of 2.38 mm [0.09 in.]. High-strength concrete yielded smaller initial crack widths and enhanced the crack widths at both service- and ultimate-load levels (Figure 3.7 a; b). At 2,000 με one beam (N2#13G2) showed a crack width larger than 0.7 mm [0.03 in.] (0.77 mm [0.031 in.]), while, at $0.3M_n$, the three beams exceeded this limit: 1.03, 0.78 and 0.83 mm [0.04, 0.03, and 0.033 in.] for N2#13G2, N3#13G1, and H2#13G1, respectively. As mentioned earlier, the strains in those 3 beams at $0.3M_n$ were very high and not expected to satisfy the crack-width criterion at this load level. Thus, even with over-

reinforced section practical design values for ρ_f/ρ_{fb} might be needed. The ACI 440.1R-06, [2006] ratio of ρ_f/ρ_{fb}=1.4 might be adequate for some cases.

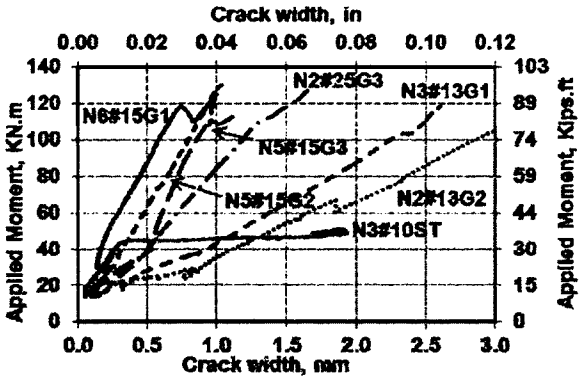

(a) Series I and II

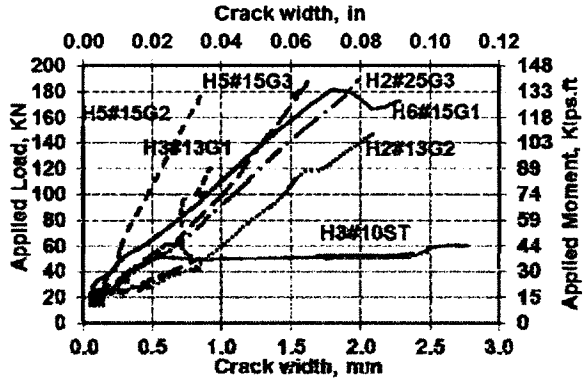

(b) Series II and III

Figure 3.7 Moment-to-maximum crack-width relationships: (a) Series I and II; (b) Series II and III

Increasing the $E_f A_f$ from about 18 MN [4,047 kips] (Series I) to about 60 MN [13,489 kips] (Series II) with the same sand-coated GFRP bars greatly enhanced the crack widths at all load levels. The average crack width in Series II beams was 0.42 and 0.36 that of Series I at 2,000 με and $0.3M_n$, respectively. The beams satisfied the severe-exposure crack-width criterion (0.5 mm [0.02 in.]) at both load levels. On the other hand, comparing Series II and III beams reveals that the helically-grooved GFRP bars yielded larger cracks than the sand-coated ones, even when the same $E_f A_f$ was provided. The average crack width of Series

III beams was 1.80 and 1.72 times that of Series II beams at 2,000 microstrains and $0.3M_n$, respectively. Once again, this tends to confirm that the sand-coated GFRP bars have better bond characteristics than the helically-grooved ones.

The effect of bar diameter on crack width can be seen in Figure 3.7b for NSC and HSC. Using 2 No. 25 GFRP bars instead of 5 No. 15 GFRP bars increased the crack width, especially at higher load levels. This effect was greater in the NSC (N5#15G3, N2#25G3) beams than in the HSC (H5#15G3, H2#25G3) ones.

DEFLECTION AND CRACKING PROVISIONS

Deflection provisions

CAN/CSA S806-02

CAN/CSA-S806, [2002] employs curvature integration along the span to determine the deflection of a concrete member at any point, assuming the section is fully cracked with no tension stiffness contribution in the cracked regions of the beam. Thus, the curvature in the cracked zone is given by M/E_cI_g for the un-cracked parts of the beam and M/E_cI_{cr} when the applied moment is higher than the cracking moment. CAN/CSA-S806, [2002] based on the closed form solution, provided deflection equations for simple loading cases such as Eq. [3.7] for a simply supported member subjected to two-point loading:

$$\delta = PL^3/24E_c I_{cr}\left[3(a/L)-4(a/L)^3-8(1-I_{cr}/I_g)(L_g/L)^3\right] \quad 3.7$$

ACI 440.1R-06

ACI 440.1R-06 [2006] specifies the effective moment of inertia formulation (I_e) to be employed in calculating the deflection of cracked FRP- reinforced concrete beams and one-way slabs. The procedure entails calculating a uniform moment of inertia throughout the beam

length and uses deflection equations derived from linear elastic analysis. The effective moment of inertia (I_e) provided by Branson [1968] was modified with a factor (β_d) to account for FRP materials instead of steel. The effective moment of inertia expression used by ACI 440.1R-06 [2006] is given as following where the M_a is the applied moment:

$$I_e = (M_{cr}/M_a)^3 \beta_d I_g + [1-(M_{cr}/M_a)^3] I_{cr} \le I_g \quad 3.8$$

where $\beta_d = 0.2(\rho_f/\rho_{fb}) \le 1.0$ 3.9

ACI 440-H, [2010]

ACI 440-H [2010] proposed an alternative expression for the effective moment of inertia (I_e) that works for both FRP- and steel-RC members without the need for empirical correction factors [Bischoff et Scanlon, 2007b]. The expression included the new factor (γ), which accounts for stiffness variation along the member. ACI 440-H [2010] expression is presented as follows:

$$I_e = I_{cr}/[1-\eta\gamma(M_{cr}/M_a)^2] \le I_g \quad 3.10$$

where $\eta = 1-(I_{cr}/I_g)$; $\gamma = 1.72-0.72(M_{cr}/M_a)$ 3.11

ISIS Manual No. 3-07

ISIS Manual No.3 [2007] presented Eq. [3.12], which was based on the Mota *et al.*, [2006a] proposal for I_e.

$$I_e = I_g I_{cr}/\left[I_{cr} + \left(1-0.5(M_{cr}/M_a)^2\right)(I_g - I_{cr})\right] \quad 3.12$$

Crack width provisions

Current crack-width prediction equations are modified forms of the original Gergely-Lutz equation [Gergely et Lutz, 1968] for steel-RC members. The equation was modified to account for the FRP's differences in bond and mechanical properties compared to those of steel. The currently available equations are:

$$w = 2\frac{f_f}{E_f}\frac{h_2}{h_1}k_b\sqrt{d_c^2+(s/2)^2}$$ [ACI 440.1R-06, 2006; CAN/CSA-S6, 2006; CAN/CSA-S6, 2002] 3.13

$$w = 2.2k_b\frac{f_f}{E_f}\frac{h_2}{h_1}(d_c A)^{1/3}$$ [ISIS Manual No.3, 2007] 3.14

The bond coefficient (k_b), which accounts for the bond between FRP bars and the surrounding concrete, is the key parameter in predicting cracks with using Eq. [3.13] and [3.14]. A conservative value of 1.4 should be used when the experimentally determined values are not available [ACI 440.1R-06, 2006]. ISIS Manual No.3 [2007] recommends a k_b of 1.2 in the absence of significant test data. CAN/CSA-S6 [2002] recommends a k_b of 0.8 for sand-coated bars and 1.0 for deformed bars.

COMPARISON BETWEEN EXPERIMENTAL AND PREDICTED RESULTS

Deflection

The predicted deflections of the tested beams were compared with the experimental deflection values at 0.3 times the beam's load-carrying capacity ($0.3M_n$) and at $0.67M_n$. Table 3-5 provides the experimental-to-predicted deflection ratios ($\delta_{exp}/\delta_{pred}$). The predications showed that the employed deflection provisions are viable for both concrete types (NSC and HSC). Based on the predicted deflections, ACI 440.1R-06 [2006] and ACI 440-H [2010] yielded un-conservative deflections at $0.3M_n$ and $0.67M_n$. At $0.3M_n$ the $\delta_{exp}/\delta_{pred}$ according to ACI 440.1R-06 [2006] and ACI 440-H [2010] was 1.17±0.38 and 1.13±0.22, respectively.

Considering the overall average (average of all predictions at $0.3M_n$ and $0.67M_n$), ACI 440.1R-06 [2006] and ACI 440-H [2010] yielded similar $\delta_{exp}/\delta_{pred}$, although ACI 440-H [2010] showed lower COV (15%) in comparison to that of ACI 440.1R-06, [2006] (26%). On the other hand, both CAN/CSA-S806 [2002] and ISIS Manual No.3 [2007] provided conservative deflection predictions. At $0.3M_n$ the $\delta_{exp}/\delta_{pred}$ ratios according to CAN/CSA-S806 [2002] and ISIS Manual No.3 [2007] were 0.76±0.12 and 0.80±0.11, respectively. In addition, considering the overall average, both CAN/CSA-S806 [2002] and ISIS Manual No.3 [2007] showed conservative deflection predictions of 0.84±0.14 and 0.87±0.12 with corresponding COVs of 16 and 14%, respectively. Furthermore, ISIS Manual No.3 [2007] and ACI 440-H [2010] showed the lowest COVs amongst the equations used, namely 14 and 15%, respectively.

Crack width

Table 3-6 compares the measured crack widths to the predicted values. The comparison was conducted at three different load levels: at 2,000 με in the reinforcing bars, $0.30M_n$ and $0.67M_n$. The predictions were conducted using a k_b value of 1.4 for ACI 440.1R-06 [2006] and 1.2 for ISIS Manual No.3 [2007]. The predictions were very conservative for all the tested beams at $0.30M_n$ and at $0.67M_n$. The average w_{exp}/w_{pred} at $0.30M_n$ calculated according to ACI 440.1R-06 [2006] and ISIS Manual No.3 [2007] were 0.63 and 0.55, respectively. Moreover, there were no significance differences between the w_{exp}/w_{pred} at $0.30M_n$ and at $0.67M_n$. The degree of conservativeness was higher for the GFRP- reinforced concrete beams with multi-layer reinforcement.

The bond factor (k_b) was calculated using the experimental results as shown in Table 3-6. The calculated values indicate that the 1.4 is very conservative value, on average, for the sand-coated GFRP bars when the ACI 440.1R-06 [2006] equation was used. Furthermore, the 1.2 value for ISIS Manual No.3 [2007] predictions looks very conservative. Different k_b values were employed in predicting the crack widths as presented in Table 3-7 using [ACI 440.1R-06, 2006; ISIS Manual No.3, 2007; CAN/CSA-S6, 2006]. There was no clear trend for the difference between the NSC and HSC beams. The 1.4 value proposed by the ACI 440.1R-06, [2006] is very conservative for the sand-coated and helically-grooved GFRP bars in NSC and HSC. A k_b value of 1.2 seems to serve well for ACI 440.1R-06 [2006] and CAN/CSA-S6 [2006] equation for the helically-grooved GFRP bars in NSC and HSC as shown in Error! Reference source not found. and Table 3-7. The average w_{exp}/w_{pred} ratio for the four beams reinforced with the helically-grooved GFRP bars using k_b = 1.2 was 0.83±0.13. The k_b value of 0.8 provided by CAN/CSA-S6 [2006] yielded un-conservative crack width predictions with an average w_{exp}/w_{pred} ratio of 1.10±0.44 for all the tested beams (sand-coated and helically-grooved GFRP bars). This k_b value of 0.8, however, yielded conservative predictions for the sand-coated multi-layer GFRP- reinforced concrete beams (Series II) using NSC and HSC with an average w_{exp}/w_{pred} ratio of 0.62±0.27.

Table 3-7 Experimental-to-Predicted Crack Width (w_{exp}/w_{pred}) Using Different k_b Values

Beam	w_{exp}/w_{pred}						
	ACI 440[4]; CSA S6[5]				ISIS[14]		
	k_b=1.4	k_b=1.2	k_b=1.0	k_b=0.8	k_b=1.2	k_b=1.0	k_b=0.8
N2#13G2	0.95	1.11	1.33	1.66	1.71	2.05	2.57
N3#13G1	1.03	1.20	1.44	1.80	1.02	1.22	1.53
H2#13G1	0.63	0.74	0.88	1.10	1.20	1.44	1.80

H3#13G2	0.66	0.77	0.92	1.16	1.57	1.88	2.36
N5#15G2	0.55	0.64	0.77	0.96	0.68	0.82	1.02
N6#15G1	0.18	0.21	0.25	0.32	0.31	0.37	0.47
H5#15G2	0.29	0.34	0.41	0.51	0.46	0.55	0.69
H6#15G1	0.39	0.46	0.55	0.68	0.76	0.91	1.14
N5#15G3	0.59	0.69	0.83	1.03	1.20	1.44	1.80
N2#25G3	0.86	1.00	1.20	1.51	1.05	1.26	1.58
H5#15G3	0.65	0.76	0.91	1.14	0.87	1.04	1.31
H2#25G3	0.73	0.85	1.02	1.28	0.63	0.76	0.95
Average	0.63	0.73	0.88	1.10	0.96	1.15	1.43
SD	0.25	0.30	0.36	0.44	0.42	0.51	0.63
COV (%)	41%	41%	41%	41%	44%	44%	44%

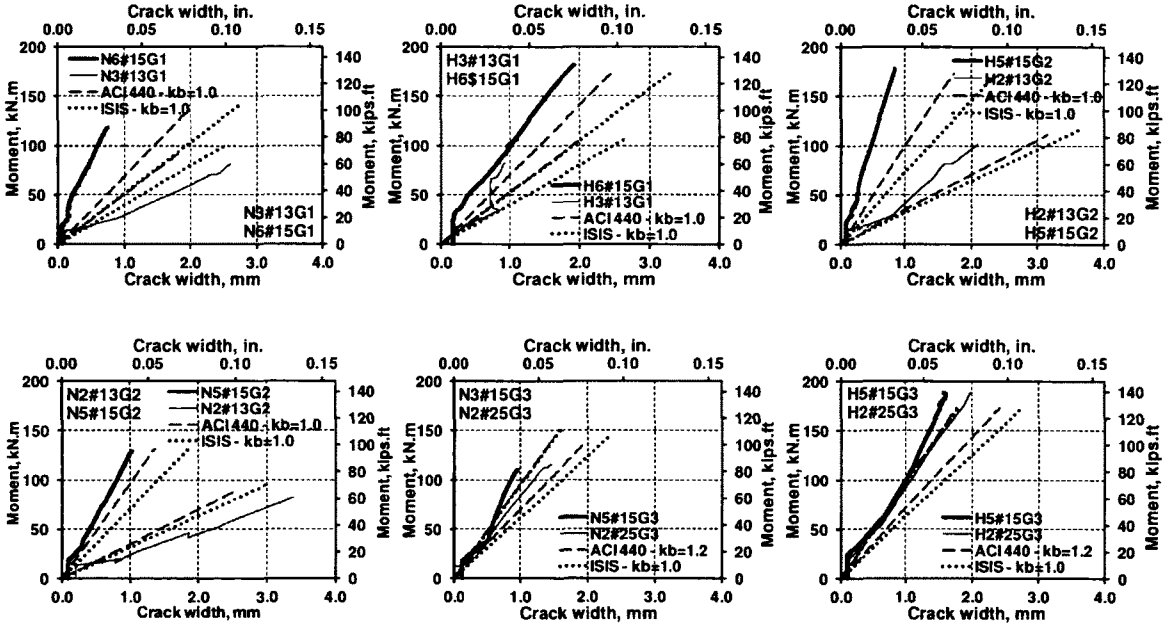

Figure 3.8 Predicted moment-to-crack-width relationships using different k_b values

For ISIS Manual No.3 [2007] predictions using a k_b of 1.2 were not consistently conservative for all the tested beams. The k_b value of 1.2 yielded reasonable yet conservative predictions for the helically-deformed GFRP bars in NSC and HSC with an average w_{exp}/w_{pred} ratio of 0.94±0.25. However, it yielded very conservative prediction for the sand-coated multi-

layer GFRP- reinforced concrete beams (Series II) using NSC and HSC (w_{exp}/w_{pred} = 0.55±0.21).

Employing a k_b of 1.0 yielded un-conservative prediction, on average, with w_{exp}/w_{pred} ratio of 1.15±0.51. This value, however, yielded good and conservative predictions for the sand-coated multi-layer GFRP- reinforced concrete beams (Series II) using NSC and HSC (Table 3-7) with an average w_{exp}/w_{pred} ratio of 0.66±0.25.

CONCLUSIONS

The study reported in this paper investigated the flexural behaviour and serviceability performance of GFRP- reinforced concrete beams with NSC and HSC. Within the scope of this investigation and considering the materials used, the following conclusions can be drawn:

1- All the GFRP- reinforced concrete beams showed typical bi-linear behaviour until failure. Both NSC and HSC evidenced reduced stiffness after cracking. The NSC and HSC beams showed similar behaviour until failure. The post-cracking flexural stiffness of the HSC was higher than that of the NSC when the same axial-reinforcement stiffness ($E_f A_f$) was provided.

2- Using HSC increased the cracking moment of the GFRP- reinforced concrete beams compared to the NSC beams. The CAN/CSA-S806 [2002] modulus of rupture equation (Eq. [3.3]) seems applicable for both NSC and HSC in the range of the tested concrete strengths.

3- Regardless of differences in load-carrying capacity, the high-strength GFRP-reinforced beams showed slightly lower strains compared to the HSC beams at the same load level.

Beams with the same axial-reinforcement stiffness are expected to exhibit similar load-reinforcement-strain relationships in normal- and high-strength concrete.

4- The NSC and HSC beams with low reinforcement ratios, ρ_f, (0.56% or less) showed very sharp increases in reinforcement strains at cracking of over 3,000 microstrains. While the beams were designed as over-reinforced sections, this did not prevent the large strain increase due to poor energy absorption at cracking. A minimum practical reinforcement amount may have to be maintained.

5- Except Series I beams with low reinforcement ratios, ρ_f, the curvature at $0.30M_n$ was $0.004/d$. The GFRP beams satisfied deflection and crack-width serviceability limits ($L/240$ for deflection and 0.7 mm [0.03 in.] for crack width). This partially confirms Vijay et GangaRao [1996] findings. A minimum reinforcement ratio, however, has to be maintained to generalize this phenomenon.

6- Using HSC while maintaining the axial reinforcement stiffness ($E_f A_f$) constant helped enhance deflection of the GFRP- reinforced concrete beams, crack width, and ultimate load-carrying capacity. The results did not support any effect of bar diameter or surface configuration of the GFRP bars on the deflection of the NSC and HSC beams.

7- Increasing the reinforcement ratio and concrete strength resulted in a larger number of cracks and smaller crack widths. Beams reinforced with sand-coated GFRP bars produced larger numbers of cracks and smaller crack widths than those reinforced with helically-grooved GFRP bars. This tends to confirm the better flexural bond characteristics of the sand-coated bars.

8- Bar diameter had an effect on crack width as evidenced by the NSC and HSC beams reinforced with GFRP bars. Employing the same axial-reinforcement stiffness ($E_f A_f$) with two different diameters of helically-grooved GFRP bars (No. 15 and No. 25) yielded

higher crack widths with the No. 25 than with the No. 15. The effect was higher in NSC than in HSC.

9- ACI 440.1R-06 [2006] and ACI 440-H [2010] yielded un-conservative deflection values at the $0.3M_n$ and $0.67M_n$. At $0.3M_n$ the experimental-to-predicted deflection ($\delta_{exp}/\delta_{pred}$) of ACI 440.1R-06 [2006] and ACI 440-H [2010] were 1.17±0.38 and 1.13±0.22, respectively.

10- Both CAN/CSA-S80 [2002] and ISIS Manual No.3 [2007] yielded conservative deflection predictions. At $0.3M_n$, the experimental-to-predicted deflection of CAN/CSA-S806 [2002] and ISIS Manual No.3 [2007] were 0.76±0.12 and 0.80±0.11, respectively.

11- The bond coefficient (k_b) value of 1.4 is very conservative for both of sand-coated and helically-grooved GFRP bars in NSC and HSC. Reasonable crack-width predictions were obtained from ACI 440.1R-06 [2006] and CAN/CSA-S6 [2006] using a k_b factor of 1.2 for the helically-grooved GFRP bars and 1.0 for the sand-coated bars in NSC and HSC. A k_b of 0.8 provided by CAN/CSA-S6 [2006] yielded very un-conservative predictions, on average, for sand-coated and helically-grooved GFRP bars in NSC and HSC. This value (k_b=0.8), however, yielded good yet conservative crack-width prediction for multi-layer sand-coated GFRP bars in NSC and HSC.

CHAPTER 4

EVALUATION OF THE BOND-DEPENDENT COEFFICIENT OF GLASS AND CARBON FRP BARS IN NORMAL AND HIGH-STRENGTH CONCRETES

Authors and affiliation

Amr El-Nemr Doctorate candidate, Department of Civil Engineering, University of Sherbrooke, Sherbrooke, Quebec, Canada, J1K 2R1, Phone: (819) 821-8000 ext. 62967, Fax: (819) 821-7974, E-mail: Amr.M.El-Nemr@usherbrooke.ca

Ehab A. Ahmed is Postdoctoral fellow, Department of Civil Engineering, University of Sherbrooke, Sherbrooke, Quebec, Canada, J1K 2R1, Phone: (819) 821-8000 ext. 62135, Fax: (819) 821-7974, E-mail: Ehab.Ahmed@USherbrooke.ca

Brahim Benmokrane, Canada and NSERC Chair Professor, Department of Civil Engineering, University of Sherbrooke, Quebec, Canada, J1K 2R1, Phone: (819) 821-7758, Fax: (819) 821-7974, E-mail: Brahim.Benmokrane@USherbrooke.ca (corresponding author).

Submittal/Acceptance Date: *submitted 25/10/2012*

Acceptance Status: Under review with file no. CCENG-789

Journal Title: ASCE Journal of Composites for Construction

Reference: In Peer Review.

French Titre: *Évaluation du Coefficient d'adhérence de Barres d'Armature En Polymères Renforcés de Fibres de Verre (PRFV) et de Carbone (PRFC)*

Contribution in thesis: This paper aimed at investigating the unique values for the bond-dependent coefficient (k_b) provided by the design codes according to surface characteristics of the FRP bars and neglecting bar type and diameter as well as concrete type and strength. The paper presented experimental study to calculate the k_b values of different types of FRP bars with different surface configurations and diameters in normal- and high-strength concretes. Moreover, it compared the current k_b values provided by FRP design codes and guidelines with those calculated from the measured crack widths and strains in the beam specimens. The findings of this study did not support the unique k_b value for FRP bars of different types (carbon and glass) with similar surface configurations. Moreover, k_b was found to be dependent on bar diameter.

French Abstract:

La conception des éléments en béton armé de barres d'armature en polymères renforcés de fibres (PRF) est typiquement gouvernée par l'état de service plutôt que l'état ultime. Par conséquent, il existe un besoin relatif à la vérification de la largeur des fissures dans les membrures en béton armé de PRF soumis à des charges de service et à la confirmation que les limites des codes de conception soient respectées. Des développements récents dans l'industrie des PRF ont mené à la mise en marché de barres d'armature en PRF ayant différentes configurations de fini de surface et différentes propriétés mécaniques. Ces paramètres peuvent affecter les propriétés d'adhérence entre les barres de PRF et le béton et, par conséquent, la largeur des fissures dans les membrures de béton armé de PRF. Toutefois, les codes et les

guidelines de conception ne fournissent qu'une valeur unique pour le coefficient d'adhérence (k_b) considérant les différents finis de surface, mais négligeant le type et le diamètre des barres ainsi que le type et la résistance du béton. Cette étude vise à étudier les recommandations de conception actuelles quant aux valeurs de k_b et à vérifier la dépendance des valeurs de k_b en fonction du type (verre (PRFV) ou carbone (PRFC)) et du diamètre des barres de PRF utilisées, et du type et de la résistance du béton. L'étude inclut 20 poutres de 4250 mm de longueur, 200 mm de largeur et 400 mm de profondeur. Les poutres ont été armées soit avec des barres de PRFV à fini de surface sablé ou à enroulement hélicoïdal, soit avec des barres de PRFC à fini de surface sablé. De plus, les poutres ont été fabriquées avec du béton normal ou du béton à haute performance. Les largeurs de fissures et les déformations mesurées ont été utilisées pour vérifier les valeurs de k_b actuellement suggérés par les codes et guidelines de conception traitant des PRF. Les conclusions de cette étude ne supportent pas l'établissement d'un coefficient d'adhérence (k_b) unique pour tous les types de barres de PRF (PRFV ou PRFC) avec des finis de surface semblables. De plus, les résultats ont démontré que le k_b est dépendant du diamètre des barres de PRF.

Mots-clés: Béton; polymères renforcés de fibres (PRF); poutre; déformation; largeur de fissures; coefficient d'adhérence; capacité en service.

ABSTRACT

The design of concrete members reinforced with fiber-reinforced-polymer (FRP) bars is typically governed by serviceability state rather than ultimate state. Consequently, there is a need to check the crack width in the FRP- reinforced concrete members at service load and verify that

they meet the code limits. Recent developments in the FRP industry led to introducing FRP bars with different surface configurations and mechanical properties, which are expected to affect their bond performance and, consequently, the crack width in FRP- reinforced concrete members. The design codes and guidelines, however, provide a unique value for the bond-dependent coefficient (k_b) considering the surface configurations and neglecting FRP bar type, bar diameter, and concrete type and strength. Thus, this study aimed at investigating the current design recommendations for k_b values and checking the dependency of the k_b values on FRP bar type (glass and carbon), diameter, and concrete type and strength. The investigation included 20 beams measuring 4,250 mm long × 200 mm wide × 400 mm deep. The beams were reinforced with sand-coated GFRP bars, helically-grooved GFRP bars, and sand-coated CFRP bars and were fabricated with normal- and high-strength concretes. The measured crack widths and strains were used to assess the current k_b values provided by the FRP design codes and guidelines. The findings did not support the unique k_b value for FRP bars of different types (carbon and glass) with similar surface configurations. Moreover, k_b was found to be dependent on bar diameter.

CE Database Subject Heading: Concrete; fiber-reinforced polymer (FRP); beam; strain; crack width; bond-dependent coefficient; serviceability.

INTRODUCTION

While steel bars have been traditionally used as main reinforcement in concrete structures, durability issues and corrosion-related problems and costs have driven the urgency for introducing alternative reinforcement. Fiber-reinforced-polymer (FRP) bars are corrosive resistant by nature and have been used for decades in concrete structures and bridges. Due to the lower modulus of elasticity of FRP bars (20%–35% that of steel for GFRP and 60%–70% of

steel for CFRP), the design of FRP-reinforced concrete (FRP- reinforced concrete) members is governed by serviceability state (deflection and crack width) rather than ultimate state.

Crack-width calculations, however, include the effect of bond between FRP bars and surrounding concrete. This is normally included in FRP design codes and guidelines through the so-called bond-dependent coefficient (k_b), while the interpretation of this coefficient remains ambiguous [McCallum et Newhook, 2012].

The wide variety of FRP bars currently marketed and the recent development of the FRP industry led to the introduction of different FRP bars with different surface configurations and mechanical properties (such as sand coated, helically grooved, deformed, indented). These differences influence bar bond performance, which relies mostly on friction and mechanical interlock [Tighiouart *et al.*, 1998]. Baena *et al.* [2009] reported that, in addition to bar mechanical properties, bond behaviour between FRP bars and concrete depends on many factors, including concrete compressive strength, bar diameter, and surface treatment. An increase in bond strength and changes in failure mode and failure surface were observed with changing concrete compressive strengths. Analysis of the influence of surface treatment on bond behaviour confirms the existence of different bond mechanisms for different surface treatments. In addition, there was a tendency for FRP bars of larger diameter to show lower bond strength, especially in higher strength concrete. Thus, the variations in surface configuration, bar diameter, and concrete strength are expected to affect the bond performance of FRP bars and, consequently, the bond-dependent coefficient (k_b). FRP design codes and guidelines, however, provide unique values for the bond-dependent coefficient (k_b), depending on surface characteristics of the bar and neglecting FRP bar type, diameter, and type and strength of surrounding concrete.

While many studies have been conducted on the bond behaviour of FRP bars in different concrete types, there have been no consistent interpretations of the bond-dependent coefficient (k_b), which is required for design purposes. The determination of k_b was introduced in ACI 440.1R-03, [2003] through modifying the Gergely et Lutz [1968] equation to account for FRP instead of steel bars. Some typical k_b values for deformed GFRP bars cited in ACI 440.1R-03 [2003] are between 0.71 and 1.83. In addition, ACI 440.1R-03 [2003] suggested that designers assume a value of 1.2 for deformed GFRP bars unless more specific information is available for a particular bar. Later, ACI Committee 440 (Fiber-Reinforced Polymer Reinforcement) adopted a modified version of the crack-width equation proposed by Frosch [1999] in place of the modified Gergely-Lutz equation and introduced it in ACI 440.1R-06 [2006]. Based on assembled experimental data, Subcommittee 440-H (Reinforced Concrete), reported that the k_b in Frosch's equation was 19% greater than the k_b resulting from the equation attributed to Gergely-Lutz [Bakis *et al.*, 2006]. The k_b values based on Frosch's equation ranged from 0.60 to 1.72 with an average of 1.10±0.31 [Bakis *et al.*, 2006]. The *Canadian Highway Bridge Design Code* (CHBDC) 2010 edition [CAN/CSA-S6.1S1, 2010] adopted the ACI 440.1R-06 [2006] crack-width equation, while the k_b values were not updated to account for the 19% increase in k_b values with Frosch's equation.

This paper presents an investigation to evaluate the bond-dependent coefficient (k_b) of different types of FRP bars with different surface configurations and diameters in normal- and high-strength concretes. Moreover, it compares the current k_b values provided by FRP design codes and guidelines with that calculated from the experimental test results (crack widths and strains) of the beam specimens.

RESEARCH SIGNIFICANCE

A wide variety of FRP bars are currently marketed, ranging from simple smooth and helically deformed bars to bars with exterior treatment such as sand-coating. The design codes, however, provide unique values for the bond-dependent coefficient (k_b) according to surface characteristics of the FRP bars and neglecting bar type and diameter as well as concrete type and strength. This paper presents an investigation to evaluate the bond-dependent coefficient (k_b) of different types of FRP bars with different surface configurations and diameters in normal- and high-strength concretes. Moreover, it compares the current k_b values provided by FRP design codes and guidelines with that calculated from the measured crack widths and strains in the beam specimens tested.

CRACKING PROVISIONS

For cracking, modifications were proposed to the original Gergely et Lutz [1968] equation to estimate the crack width of the FRP- reinforced concrete members. The FRP design codes and guidelines provide crack-width limits according to the degree of exposure. For example, CAN/CSA-S6.1S1 [2010] provides 0.5 mm for severe exposure and 0.7 mm for normal exposure. On the other hand, CAN/CSA-S806 [2012] controls crack width with a crack-control parameter, while ISIS Manual No.3-07 set a strain limit of 2,000 microstrains at service to control crack width. Calculation of crack width involves a common term that was included in the predicting equation—the bond-dependent coefficient (k_b)—to account for the degree of bond between FRP bars and the surrounding concrete. Different values for k_b were introduced by the available FRP design codes and guidelines concerning the different FRP reinforcing bars. The

following are the currently available equations in North American codes and guidelines for predicting the crack width in FRP- reinforced concrete members:

CAN/CSA S806-12

CAN/CSA-S806 [2012] recommends checking the crack width when the maximum strain in FRP tension reinforcement under full service loads exceeds 0.0015 according to Eq. [4.1]

$$z = k_b \frac{E_s}{E_f} f_f \sqrt[3]{d_c A} \qquad 4.1$$

When the crack-control parameter, z, should not exceed 45,000 N/mm for interior exposure and 38,000 N/mm for exterior exposure. CAN/CSA-S806, [2012] states that the k_b value shall be determined, experimentally. In the absence of test data, however, it may be taken as 1.2 for deformed rods. It should be mentioned that, in determining k_b, the effective clear cover, d_c, should not exceed 50 mm.

ACI 440.1R-06

ACI 440.1R-06 [2006] adopts the maximum reinforcement spacing provisions to control cracking, which was proposed by Frosch [1999]. This formula is independent of reinforcement type (steel or FRP), except that it should be modified by a bond-quality coefficient k_b [ACI 440.1R-06, 2006]. Therefore, the maximum probable crack width for FRP-reinforced members may be calculated from Eq. [4.2].

$$w = 2 \frac{f_f}{E_f} \frac{h_2}{h_1} k_b \sqrt{d_c^2 + (s/2)^2} \qquad 4.2$$

For FRP bars having bond behaviour similar to uncoated steel bars, the bond coefficient k_b is assumed to be equal to 1.0. For FRP bars having bond behaviour inferior to steel, k_b is greater than 1.0, and for FRP bars having bond behaviour superior to steel, k_b is less than 1.0. An analysis of crack-width data by members of ACI Committee 440 on a variety of concrete cross sections and FRP bars, fiber types, resin formulations, and surface treatments, yielded average k_b values ranging from 0.60 to 1.72, with a mean of 1.10. Moreover, data for rough sand-coated FRP-bar surface treatments tended toward the lower end of this range. Regardless of the research work conducted in this area, ACI 440.1R-06 [2006] recommends further research before a committee consensus can be reached on k_b for such reinforcement.

CAN/CSA S6.1S1-10

CAN/CSA-S6.1S1 [2010] employs the same equation as ACI 440.1R-06 [2006], as shown in Eq. [4.3]. Similar to CAN/CSA-S806 [2012], the crack width has to be verified when the maximum tensile strain in FRP reinforcement under full service exceeds 0.0015.

$$w = 2\frac{f_f}{E_f}\frac{h_2}{h_1}k_b\sqrt{d_c^2+(s/2)^2} \qquad 4.3$$

The value of k_b should be determined experimentally, but, in the absence of test data, it may be taken as 0.8 for sand-coated and 1.0 for deformed FRP bars. In calculating d_c, the clear cover shall not be taken greater than 50 mm.

ISIS M-03 (2007)

ISIS Manual No.3 [2007] predicts the crack width using Eq. [4.3]:

$$w = 2.2k_b\frac{f_f}{E_f}\frac{h_2}{h_1}\sqrt[3]{d_c A} \qquad 4.4$$

In the absence of significant test data, k_b =1.2 is recommended.

EXPERIMENTAL PROGRAM

Materials

As the bond-dependent coefficient (k_b) is affected by the surface configuration and bond performance, three types of GFRP and one type of CFRP were used. The GFRP bars were referred to as GFRP-1 for sand-coated, normal-modulus bars (Grade I-[CAN/CSA-S807, 2010]), GFRP-2 for sand-coated, high-modulus bars (Grade III- [CAN/CSA-S807, 2010]), and GFRP-3 for helically grooved, high-modulus bars (Grade III- [CAN/CSA-S807, 2010]). Furthermore, the CFRP bars were referred to as CFRP-1 for sand-coated Grade III [CAN/CSA-S807, 2010] bars. The tensile properties of the reinforcing bars were determined by testing five representative specimens according to [ASTM D7205, 2011]. Figure 4.1 shows the used GFRP bars and Table 4-1 provides the properties of the FRP bars.

Commonly used normal- and high-strength concretes were used to fabricate the beam specimens with a targeted compressive strength of 35 and 65 MPa, respectively. The compressive and splitting concrete strengths were determined by testing three 150 × 300 mm cylinders on the day of testing. The measured compressive and splitting concrete strengths of the normal-strength concrete ranged from 33.5 to 48.1 MPa and from 3.1 to 4.0 MPa, respectively. While the measured compressive and splitting concrete strengths of the high-strength concrete ranged from 59.1 to 81.5 MPa and from 4.5 to 5.5 MPa, respectively. It should be mentioned that the first batch of the high-strength concrete did not achieve the desired strength (59.1 compared to 65 MPa) but it was used for calculating k_b and also denoted as high-strength concrete. The concrete compressive and tensile strengths for each beam are presented in Table 4-2.

Table 4-1 Properties of the reinforcing bars

Bar type	Designated diameter of FRP bar[a]	Nominal cross-sectional area[a] (mm^2)	Surface configuration	Tensile strength, f_{fu}, (MPa) (Average±SD)	Modulus of elasticity, E_f, (GPa) (Average±SD)	Ultimate strain (%)	Guaranteed strength and strain[b]		E_f/f_{fu}
							f_G MPa	ε_G (%)	
GFRP-1 (G1)	13	129	Sand-coated	817±9	48.7±0.6	1.7	790	1.6	59.6
	15	199	Sand-coated	751±23	48.2±1.6	1.6	683	1.6	64.1
	20	284	Sand-coated	728±24	47.6±1.7	1.5	656	1.5	65.4
	22	387	Sand-coated	693±23	46.4±1.5	1.5	625	1.5	67.0
	25	510	Sand-coated	666±74	53.2±2.1	1.3	444	1.0	79.9
GFRP-2 (G2)	13	129	Sand-coated	1639±61	67.0±1.0	2.5	1456	2.2	40.9
	20	284	Sand-coated	1082±37	52.5±1.7	2.1	971	2.0	48.5
	25	510	Sand-coated	1132±23	66.3±0.9	1.7	1063	1.7	58.6
GFRP-3 (G3)	15	199	Helically grooved	1245±45	59.5±1.1	2.1	1110	1.9	47.8
	25	510	Helically grooved	906±29	60.3±2.9	1.5	819	1.3	66.6
CFRP-1 (C1)	10	71	Sand-coated	1938±210	147.0±3.0	1.32	1308	1.6	75.9
	13	129	Sand-coated	1470±121	141.0±2.4	1.04	1107	1.6	95.9

[a] According to [CAN/CSA-S807, 2010].
[b] According to [ACI 440.1R-06, 2006] = average - 3 × standard deviation (SD).

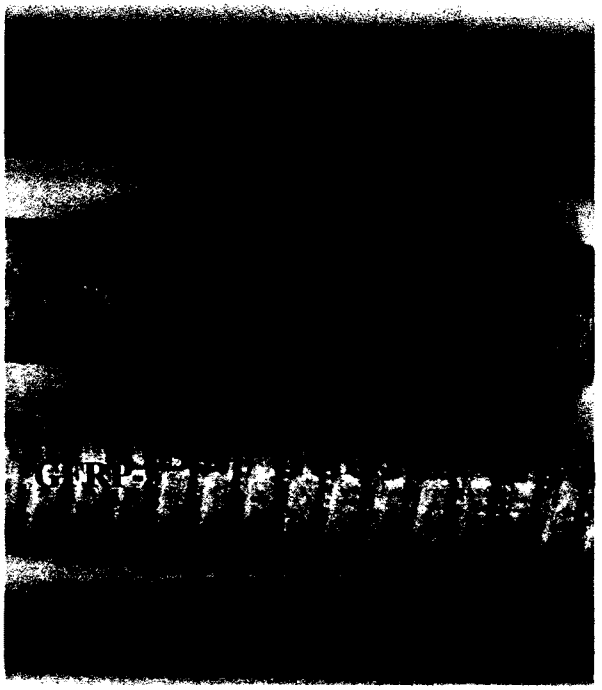

Figure 4.1 Surface configurations of the FRP reinforcing bars

Table 4-2 Details of the test specimens

Series	Beam[a]	f_c'[b] (MPa)	f_t[b] (MPa)	ρ_f (%)	ρ_{fb}[c] (%)	ρ_f/ρ_{fb}	$A_f E_f$ (kN)
I	N3#13G1	33.5	3.60	0.56	0.43	1.31	18347
	N2#13G2	33.5	3.60	0.38	0.15	2.45	17286
II	N2#15G1	38.9	3.81	0.56	0.65	0.87	19144
	N2#15G3	33.8	3.11	0.56	0.21	2.69	23681
III	N3#20G1	42.1	3.18	1.21	0.73	1.67	40555
	N2#22G1	38.9	3.81	1.08	0.61	1.76	35264
	N3#20G2	48.1	3.96	1.21	0.34	3.59	44730
IV	N2#25G1	48.1	3.96	1.46	0.83	1.75	54264
	N2#25G2	48.1	3.96	1.46	0.38	3.85	67626
	N2#25G3	33.8	3.11	1.51	0.42	3.57	61506
V	N3#10C1	44.7	3.24	0.30	0.26	1.13	31311
	N3#13C1	44.7	3.24	0.54	0.42	1.30	54567
VI	H2#13G2	59.1	4.51	0.38	0.22	1.67	17286
	H3#13G1	59.1	4.51	0.56	0.63	0.90	18347
VII	H3#20G2	81.5	5.45	1.21	0.54	2.22	44730
VIII	H2#25G1	81.5	5.45	1.46	1.35	1.08	54264
	H2#25G2	81.5	5.45	1.46	0.61	2.38	67626
	H2#25G3	76.5	4.62	1.51	0.76	1.98	61506
IX	H3#10C1	76.5	4.62	0.30	0.42	0.72	31311
	H3#13C1	76.5	4.62	0.54	0.66	0.82	54567

[a] Concrete type (N: normal strength; H: high strength), number of bars followed by bar diameter, ending with the reinforcement type (G1: GFRP-1, G2: GFRP-2, G3: GFRP-3, C1: CFRP-1).
[b] Average of three cylinders (150×300 mm) on the day of testing.
[c] Calculated according to [CAN/CSA-S806, 2012].

Test specimens

The test parameters of this experimental program were material type (carbon and glass FRP), surface configuration (sand-coated and helically grooved), bar diameter (No. 13 to No. 25), and concrete strength (normal- and high-strength). These parameters were investigated through 20 FRP-reinforced concrete (FRP- reinforced concrete) beams. The FRP- reinforced concrete beams were categorized in nine groups according to the reinforcing bar type and diameter. Groups I to V included No. 13 to No. 25 GFRP bars and No. 10 CFRP bars in normal-strength concrete, while Groups VI to IX included the same FRP bars in high-strength concrete. Table 4-2 shows the details of each group. The beams were reinforced with one layer of FRP

reinforcement comprising two or three bars. The normal-strength FRP- reinforced concrete beams were designed to maintain over-reinforced sections ($\rho_f/\rho_{fb} > 1.0$), except N2#15G1, which was designed as under-reinforced, but the actual material properties yielded an under-reinforced section ($\rho_f/\rho_{fb} < 1.0$). The high-strength FRP- reinforced concrete beams comprised three under-reinforced beams ($\rho_f/\rho_{fb} < 1.0$) when the same cross-sectional areas of FRP reinforcements were used, namely H3#13G1, H3#10C1, and H3#13C1. The significant increase in concrete strength changed those beams from over-reinforced to under-reinforced sections. The entire beams were reinforced in compression with 2 10M steel bars; shear failure was avoided by providing closely spaced steel stirrups (100 mm spacing in the shear span). In addition, two stirrups spaced at 300 mm were placed in the constant moment zone to ensure the positions of longitudinal bars and minimize the confinement provided by the stirrups, which, in turn, influence crack-width results. Figure 4.2 shows the geometry and reinforcement details of the specimens.

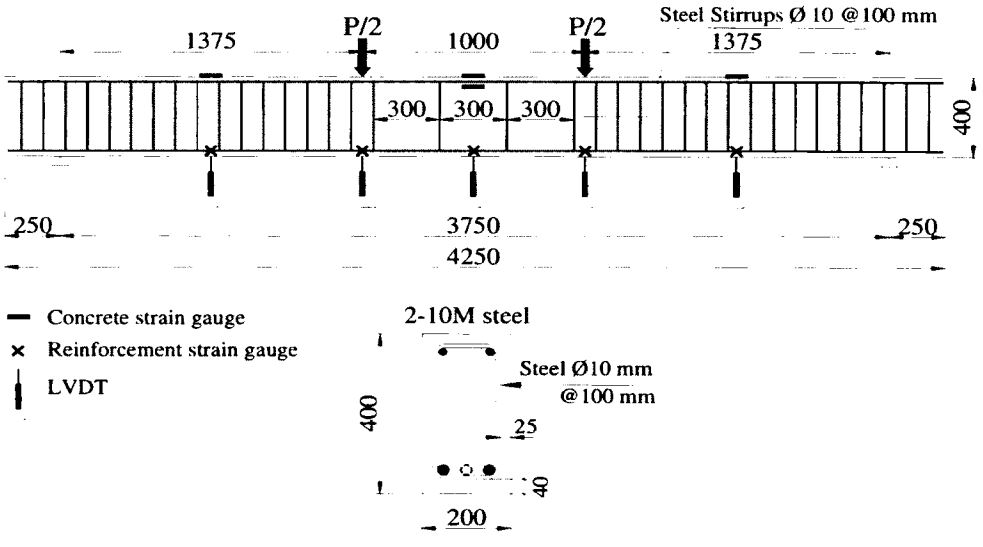

Figure 4.2 Dimensions, reinforcement details, and instrumentation

Instrumentation and testing

The reinforcing bars and compression-concrete zone of the beams were instrumented with electrical resistance strain gauges to capture the strains at the desired locations. Moreover, five linear variable-displacement transducers (LVDTs) were installed on each beam to measure deflection at different locations during testing. In addition, one LVDT was installed at the position of the first flexural crack after measuring its initial width with a handheld microscope with 50X magnifying power. Figure 4.2 also shows beam instrumentation.

All beam specimens were tested under four-point bending over a clear span of 3,750 mm (Figure 4.2). The load was monotonically applied using a 500 kN hydraulic actuator with a stroke-controlled rate of 0.6 mm/min. During the test, crack formation on one side of each beam was marked and the corresponding loads were recorded. The actuator, strain gauges, and LVDTs were connected to a data-acquisition unit to continuously record their readings.

DEFINITION OF SERVICE LOAD

Most design codes specify a flexural-crack-width limit for steel-reinforced concrete structures to protect the reinforcing bars and stirrups from corrosion and to maintain the structure's esthetic shape. Unlike steel reinforcement, FRP is non-corrodible by nature. Therefore, the serviceability limits for the crack width in FRP- reinforced concrete members may be directly related to esthetic considerations. Consequently, larger crack widths are permitted in FRP- reinforced concrete elements compared to their counterparts reinforced with steel. The FRP design provisions specify limiting widths for flexural cracks corresponding to the degree of exposure to the environmental conditions. CAN/CSA-S6.1S1 [2010]; CAN/CSA-S6 [2002] and ACI 440.1R-06 [2006] provide crack width limits of 0.5 mm for exterior exposure and 0.7 mm

for interior exposure. The Japan Society of Civil Engineers [JSCE, 1997] is setting a maximum allowable crack width of 0.5 mm. On the other hand, since there is a direct relationship between strain or stress in reinforcing bars and crack widths, a unified strain limit of 2,000 microstrains for the strain in the GFRP bars was recommended by ISIS Manual No.3 [2007] to keep the crack width less than or equal 0.5 mm under service load. CAN/CSA-S6.1S1 [2010], however, limits the stress in FRP reinforcing bars to $0.25f_{frpu}$ and $0.60f_{frpu}$ for GFRP and CFRP bars, respectively, where f_{frpu} is the characteristic tensile strength (referred to as guaranteed tensile strength, f_G, by ACI 440.1R-06 [2006] of the FRP reinforcing bars (average – 3×standard deviation).

The definition of the term "service load" in laboratory testing is not as direct as provided by loading codes. According to loading codes, the service load is calculated considering the real dead, live, static, and dynamic loads. In a laboratory testing, however, most of the structural elements (especially beams and one-way slabs) are tested under one- or two-point loading schemes. The self-weight of the structural elements is very small compared to the resisting loads/moments and, most probably, there is one load component, which is live load. Many trials were performed to assume a reasonable value for the service load in laboratory testing as a function of the flexural load-carrying capacity of FRP- reinforced concrete elements. Many researchers [Mota *et al.*, 2006a; Kassem *et al.*, 2011; Bischoff *et al.*, 2009; El-Nemr *et al.*, 2011] have assumed that 30% of the nominal flexural capacity ($0.3M_n$) of beams and one-way slabs is a reasonable value for the service load of an FRP- reinforced concrete structural member. The strain in the GFRP reinforcing bars, however, was very high at this load level and, in some specimens, it exceeded 3,500 microstrains. Others recommended load corresponding to the 2,000 microstrains specified by ISIS Manual No.3 [2007]. CAN/CSA-S6.1S1 [2010] limits for the stress in FRP reinforcement under service loads may be also employed where the service loads

are calculated at corresponding stresses of $0.25f_{frpu}$ and $0.60f_{frpu}$ for GFRP and CFRP bars, respectively. Thus, in lieu of a fixed definition for the service-load level, all the aforementioned limits were considered and the bond-dependent coefficient (k_b) was calculated for all those possible service loads. For the calculations, however, an upper crack-width limit of 0.7 mm was maintained, as proposed in *Annex S "Test Method for Determining the Bond-Dependent Coefficient of FRP Rods"* in CAN/CSA-S806 [2012]. In addition, the bond-dependent coefficient was also evaluated at $0.25f_{frpu}$ and $0.125f_{frpu}$, since the authors expected that the service load would fall between those stress limits.

TEST RESULTS AND DISCUSSION

This paper aimed at evaluating the bond-dependent coefficient (k_b) of different FRP bars and diameters in normal- and high-strength concretes. As the calculation of the k_b requires the stresses in the FRP reinforcing bars and the measured crack widths, both of those measurements are presented and briefly discussed in this section. Figure 4.3 shows typical crack patterns of some beams at failure. Figure 4.4 a and b shows the moment-to-reinforcement strain relationships, while Figure 4.5 provides the moment-to-crack-width relationships of the tested beams. Table 4-3, however, summarizes the strains and crack widths at the different loading stages (corresponding to 2,000 microstrains, $0.3M_n$, $0.67M_n$, 0.5 mm crack width, and 0.7 mm crack width, where M_n is the nominal capacity of the beam specimens).

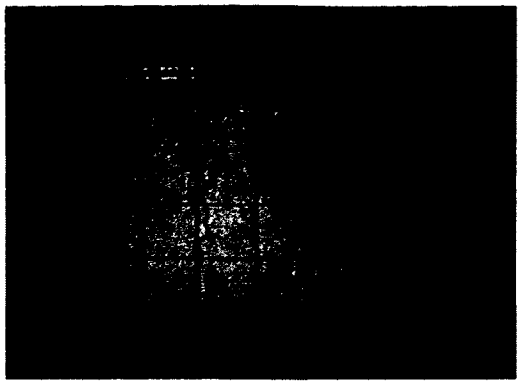

(a) N2#13G2

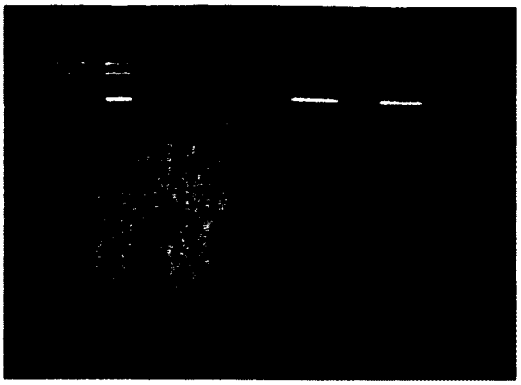

(b) N3#13G1

(c) N2#15G2

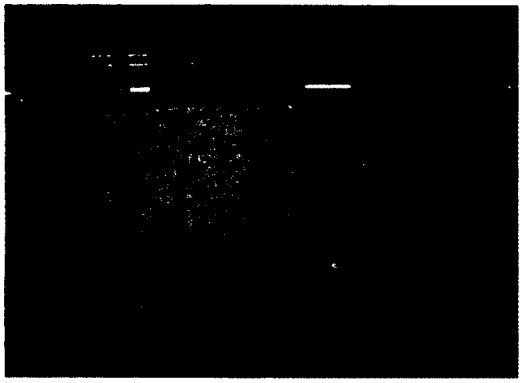

(d) N2#15G3

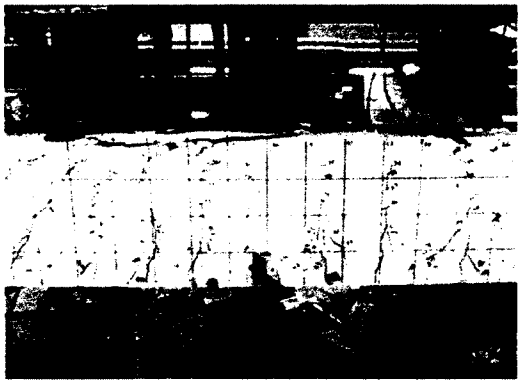

(e) H3#20G2

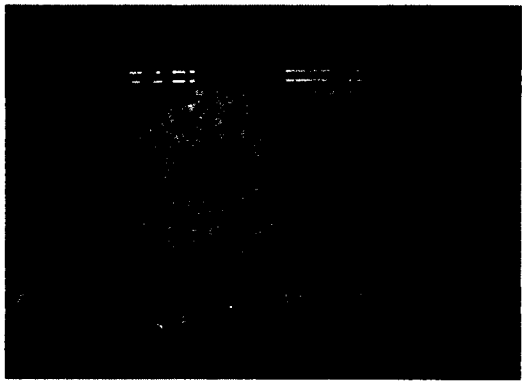

(f) H2#25G3

Figure 4.3 Typical crack pattern of the constant moment zone at failure

Strain in FRP reinforcement

Figure 4.4 shows the strains in the FRP reinforcing bars of the tested beams. According to Figure 4.4, the strains were significantly affected by the axial stiffness of the reinforcing bars ($E_f A_f$). The relationships almost fall into two sets. The first set includes the beams in Groups I, II, and VI, which have $E_f A_f$ ranging from 17,286 to 23,681 kN. The second set, however, consists of the beams in Groups III, IV, VII, VIII, and IX, which have $E_f A_f$ ranging from 35,264 to 67,626 kN. Group V, however, has one beam in each of the two sets.

From Figure 4.4 (a) for normal-strength concrete, it can also be observed that N3#20G2 and N3#13C1 showed almost the same moment-to-strain relationship, regardless of the different $E_f A_f$ (44,730 and 54,567 kN, respectively). Beam N3#20G1 ($E_f A_f$ = 40,555 kN) showed a very close relationship to N3#20G2 and N3#13C1. On the other hand, from the strains in the high-strength concrete (Figure 4.4 (b)), H3#13C1 ($E_f A_f$= 54,567 kN) showed strain values slightly higher than those of H3#20G2 ($E_f A_f$= 44,730 kN) and H2#25G1 ($E_f A_f$= 54,264 kN). This may be related to the smaller ρ_f/ρ_{fb} ratio for the H3#13C1 compared to those of H2#15G1, and H3#20G2. The ρ_f/ρ_{fb} ratios for the three beams were 0.82 (under-reinforced), 1.08, and 2.22 for H3#13C1, H2#15G1, and H3#20G2, respectively. The fact that bars G1, G2, and C1 have the same surface configuration (sand-coated bars) implies that both FRP-bar bond and bar mechanical properties play significant roles in controlling the induced strains. It further implies that the value of the bond-dependent coefficient (k_b) may not necessarily be the same for different FRP bars with the same surface configuration.

In addition, the normal-strength beams with lower reinforcement ratios showed a sharp increase in strain (from 2,000 to 3,000 microstrains) as soon as the first crack appeared.

Even though all those beams were over-reinforced, except N2#15G1, and many of them had ρ_f/ρ_{fb} greater than 1.4, as recommended by ACI 440.1R-06 [2006], this did not prevent them from exhibiting a sharp increase in induced strains after cracking.

Table 4-3 Strains and crack widths of the test specimens

Beam	M_n (kN.m)	Strain in reinforcement (με) at							Crack width (mm) at			
		w= 0.5 mm	w= 0.7 mm	0.30M_n	0.67M_n	0.25f_G	0.125f_G	2000 με	0.30M_n	0.67M_n	0.25f_G	0.125f_G
N3#13G1	81.34	3388	4099	4378	9299	4000	2000	0.4	0.78	1.82	0.67	0.4
N2#13G2	82.78	76	95	5349	11589	5500	2750	0.77	1.03	2.38	1.05	0.84
N2#15G1	64.04	4161	5297	4189	9332	4000	2000	0.96	0.5	1.22	0.96	1.37
N2#15G3	91.31	3009	3802	3448	8122	4750	2375	0.31	0.63	1.68	0.95	0.37
N3#20G1	107.39	3070	4031	3107	3908	3750	1875	0.32	0.51	1.17	0.65	0.3
N2#22G1	132.26	4207	6331	4262	3908	3750	1875	0.47	0.51	1.05	0.45	0.23
N3#20G2	171.43	2768	3983	3755	9132	5000	2500	0.38	0.66	1.35	1.04	0.55
N2#25G1	161.65	2711	3796	2991	6888	2500	1250	0.36	0.55	1.28	0.46	0.31
N2#25G2	167.24	3022	4422	2127	4660	4250	2125	0.33	0.36	0.73	0.68	0.36
N2#25G3	115.93	1929	2958	1666	4016	3250	1625	0.53	0.45	0.93	0.77	0.43
N3#10C1	117.22	4363	9472	6596	offscale	4000[a]	2000[b]	0.32	0.62	1.03	0.46[a]	0.32[b]
N3#13C1	149.92	3777	5434	3052	6458	4000[a]	2000[b]	0.33	0.45	0.96	0.57[a]	0.33[b]
H2#13G2	101.59	252	2759	3984	10204	5500	2750	0.61	0.83	1.44	0.99	0.70
H3#13G1	82.58	571	5756	1000	10408	4000	2000	0.61	0.55	0.72	0.63	0.61
H3#20G2	184.15	3464	5260	3550	7671	5000	2500	0.22	0.51	0.91	0.68	0.35
H2#25G1	173.67	3520	5111	3202	6877	2500	1250	0.23	0.46	0.91	0.30	0.21
H2#25G2	207.20	3806	5688	2601	5904	4250	2125	0.31	0.37	0.73	0.55	0.31
H2#25G3	189.17	2929	3438	3121	6662	3250	1625	0.31	0.54	0.54	0.58	0.28
H3#10C1	146.28	2530	4452	3726	6798	4000[a]	2000[b]	0.43	0.56	0.61	0.57[a]	0.43[b]
H3#13C1	201.44	3905	6392	3482	7171	4000[a]	2000[b]	0.18	0.46	0.76	0.36[a]	0.18[b]

[a] Calculated at 0.60f_G.
[b] Calculated at 0.30f_G.

On the other hand, most of the high-strength beams showed a significant increase in strains at cracking, while the under-reinforced ones (H3#13G1, H2#G2, H3#10C1) showed a sharp increase of more than 3,000 microstrains, similar to the normal-strength beams. This sharp

increase in induced strains might have an impact on the calculations of k_b because it will yield very high stress in the FRP bars after cracking.

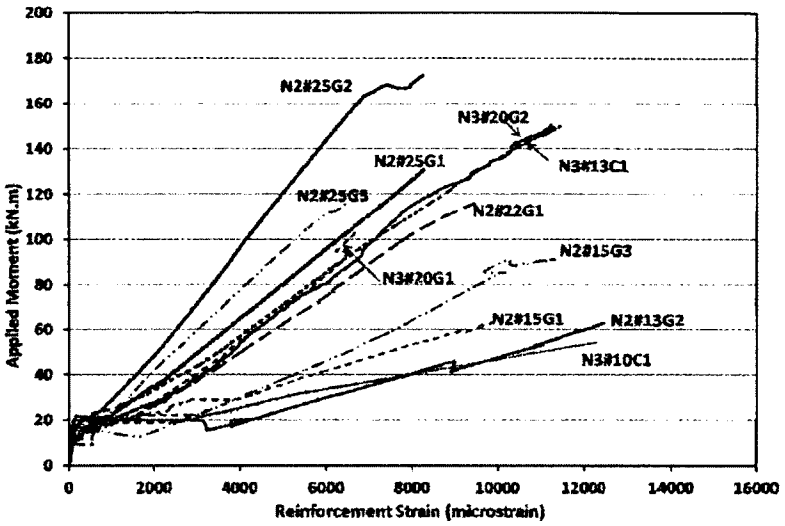

(a) Normal-strength-concrete beams

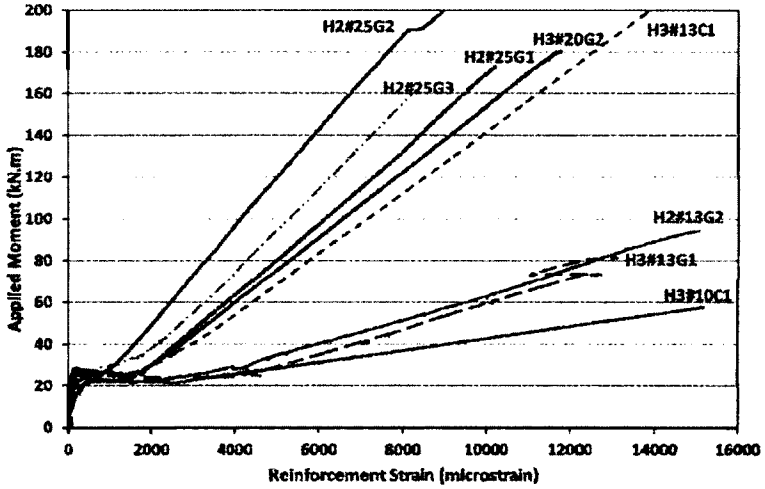

(b) High-strength-concrete beams

Figure 4.4 Moment-to-reinforcement strain relationships (a) Normal-strength-concrete beams; (b) High-strength-concrete beams

Consequently, testing concrete beams reinforced with 2 GFRP bars of very small diameters (9.5 or 12.7 mm), according to *Annex S* of CAN/CSA-S806 [2012] may yield significantly different k_b values compared to the case when more bars are used (i.e. 4 bars). In addition, using 2 bars of large diameter, such as 25 mm, will yield very high reinforcement ratios and consequently prevent the sharp increase in strains after cracking. Thus, there might be a need to maintain a minimum reinforcement ratio when k_b is evaluated according to *Annex S* of CAN/CSA-S806 [2012]. This issue, however, requires more investigation.

Cracking and crack width

All beams were initially un-cracked. When the cracking moment was reached in the pure bending zone, some cracks began to appear. The initial width of the first crack was measured using a handheld microscope with 50X magnifying power. Thereafter, one LVDT was installed to continuously record the variation in the crack width as the applied load varied. Figure 4.3 shows the typical crack pattern for compression failure of normal- and high-strength concrete beams at failure. This figure indicates that the number of cracks appearing in the constant moment zone was affected by the type and diameter of the FRP reinforcing bar as well as concrete strength, which implicitly includes the effect of the bond characteristics of the FRP bars in concrete. Thus, different k_b values based on bar type, surface configuration, and diameter are recommended.

Figure 4.5 presents the moment-to-crack-width relationships of the tested beams. It shows that, regardless the differences in the load-reinforcement strain relationship, N3#20G1, N2#22G1, N2#25G3, N2#25G1, and N3#20G2 had almost the same load-to-crack-width relationships. Moreover, N2#25G2 displayed a crack width smaller than N2#25G3 at the same

load level. Similar results can be observed in the high-strength concrete beams H2#25G1, H2#25G2, H2#25G3, and H3#13C1. Thus, it could be concluded that surface configuration and modulus of elasticity had a direct impact on the load-to-crack-width relationships. Those parameters should be joined to axial reinforcement stiffness as parameters governing crack width and performance of the FRP-reinforced concrete beams. This confirms that a unique bond-dependent coefficient (k_b) value considering only the surface configuration of the FRP bars (regardless of modulus) is not representative of actual behaviour.

The strain-to-crack-width relationships presented in Figure 4.6 show that the relationships are not linear in all cases. The appearance of other cracks during the tests may affect those being measured, and the relationships may become bilinear or even nonlinear. Moreover, they might be transition zone until the stabilization of the crack pattern in the flexural zone. Thus, the reinforcement stress level (determined from measured strains) at which the bond-dependent coefficient (k_b) is calculated can significantly change the determined value.

Consequently, it is very important to fix the point at which k_b should be determined. In this paper, the k_b values were determined at all the possible limits, including strains, crack widths, and ratios of the nominal capacities in order to recommend the most appropriate one.

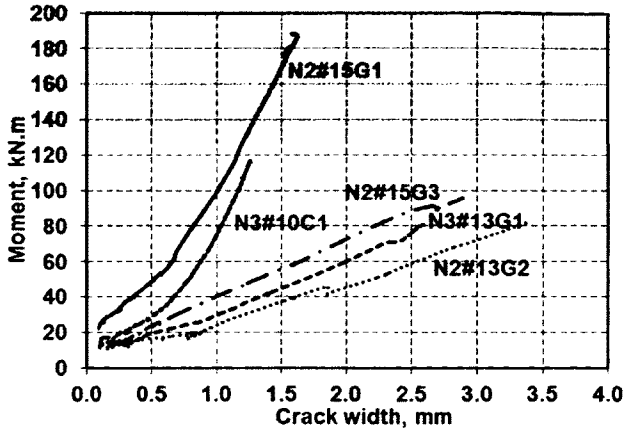

(a) Groups I and II and N3#10C1

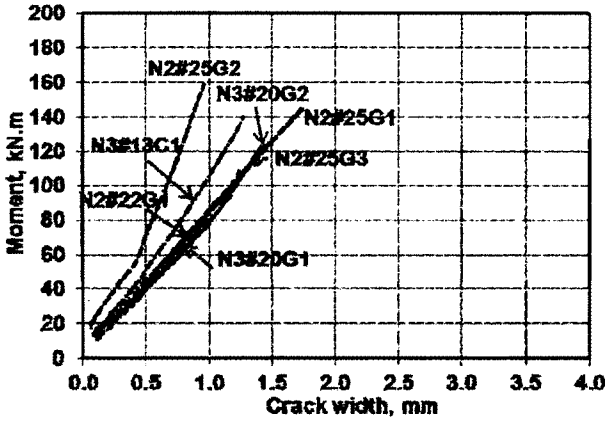

(b) Groups III and IV and N3#13C1

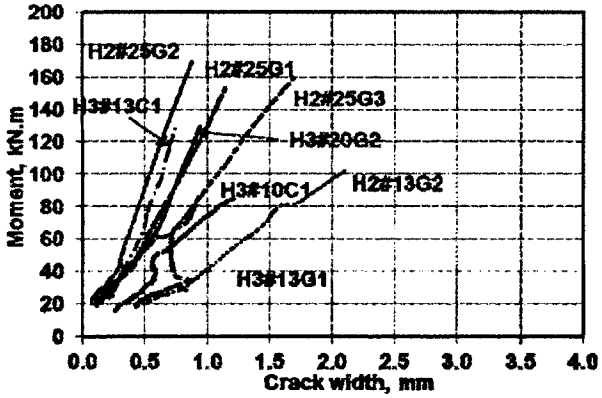

(c) Groups VI to IX

Figure 4.5 Moment-to-maximum crack-width relationships: (a) Groups I and II and 3#10C1; (b) Groups III and IV and 3#13C1; (c) Groups VI to IX

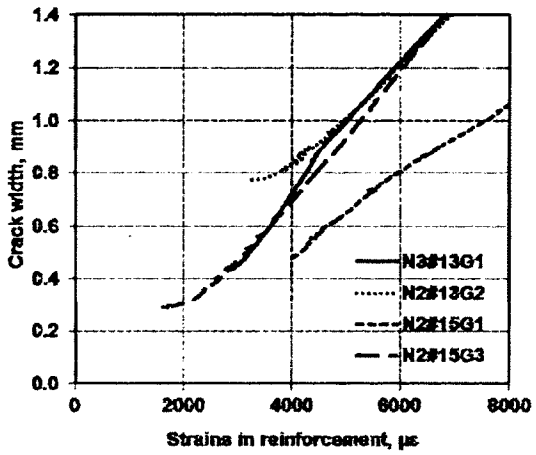

(a) Groups I and II

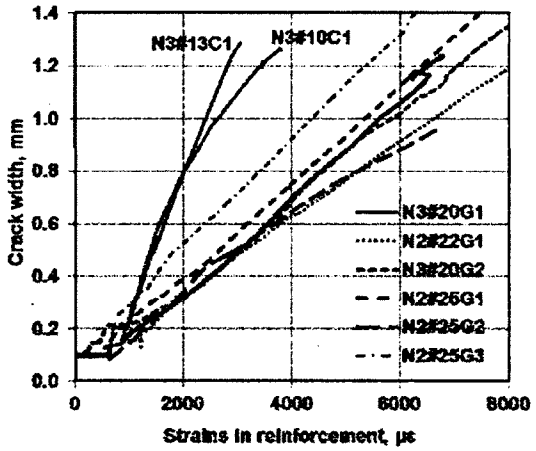

(b) Groups III, IV, and V

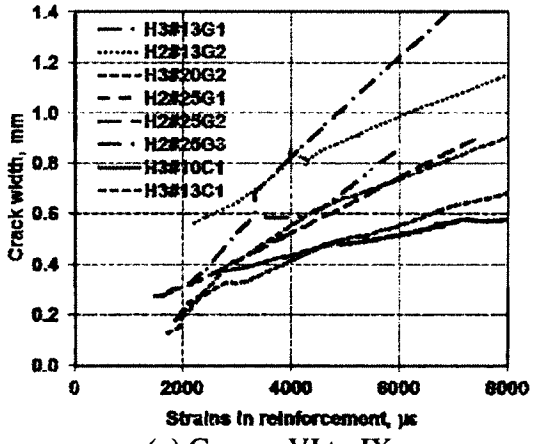

(c) Groups VI to IX

Figure 4.6 Crack width to strain in reinforcement relationships

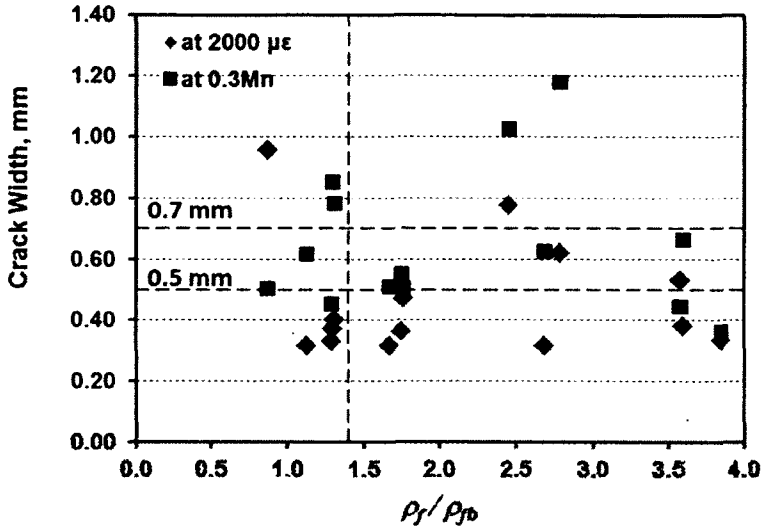

(a) Normal-strength concrete beams

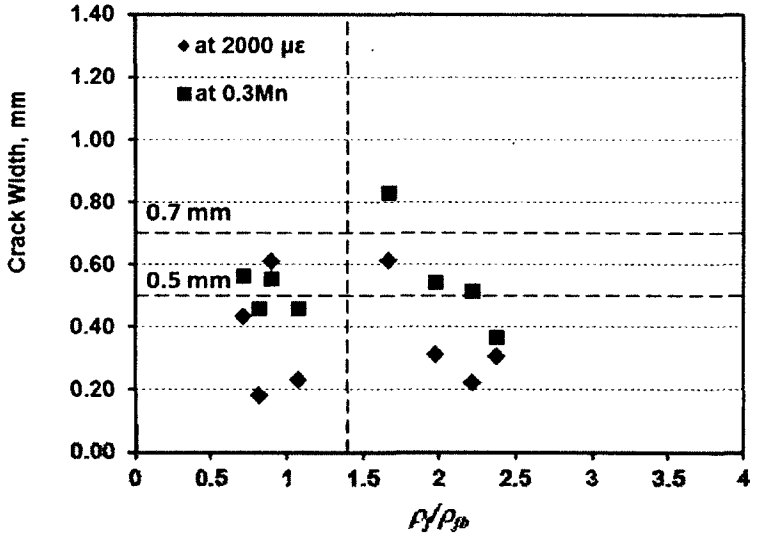

(b) High-strength concrete beams

Figure 4.7 Crack width versus ρ_f/ρ_{fb}: (a) Normal-strength concrete beams; (b) High-strength concrete beams

Furthermore, concerning the relationship between ρ_f/ρ_{fb} and the crack widths measured at 2,000 microstrains and $0.30M_n$ (see Figure 4.7), it can be observed that some beams exhibited crack widths larger than 0.5 mm at the strain level of 2,000 microstrains provided by ISIS Manual

No.3 [2007] to maintain the crack width below 0.5 mm. Moreover, two beams showed crack widths greater than 0.7 mm. This justifies the requirements of CAN/CSA-S6.1S1 [2010] and CAN/CSA-S806 [2012] to check the crack widths when the strains exceed 1,500 microstrains.

On the other hand, many beams showed crack widths larger than 0.7 mm at $0.3M_n$, especially beams with low reinforcement ratios. Thus, if the 0.7 mm limit provided by *Annex S* of CAN/CSA-S806 [2012] as an upper limit for calculating k_b is maintained, the actual strains in the FRP bars in most of the tested beams will be over 2,000 microstrains.

Crack-Width Prediction

ACI 440.1R-06 [2006] recommends using a k_b value of 1.4 when predicting the crack widths for FRP-reinforced concrete members, excluding smooth bars and grids. This value is justified to yield conservative predictions in the absence of experimental data. ISIS Manual No.3 [2007], however, recommends a k_b value of 1.2 in the absence of significant test data. CAN/CSA-S6.1S1 [2010] recommends a k_b value of 0.8 for sand-coated FRP bars and 1.0 for deformed FRP bars. Those values were used in Eq. [4.2] to [4.4], and the measured-to-predicted crack width ratios (w_{exp}/w_{pred}) are listed in Table 4-4 for normal-strength concrete beams and in Table 4-5 for high-strength concrete beams. The crack widths were predicted at the possible service-load levels (2,000 microstrains, $0.30M_n$, $0.25f_G$) as well as at a higher load level ($0.67M_n$) in addition to $0.125f_G$.

In the normal-strength concrete beams (Table 4-4) at 2,000 microstrains, ACI 440.1R-06 [2006], ISIS Manual No.3 [2007], and CAN/CSA-S6.1S1 [2010] yielded non-conservative predictions, on average, with w_{exp}/w_{pred} of 0.98±0.26, 0.92±0.29, and 1.26±0.22, respectively. At a low reinforcement stress level of $0.125f_G$, ACI 440.1R-06 [2006], ISIS Manual No.3 [2007],

and CAN/CSA-S6.1S1 [2010] evidenced very conservative predictions, on average, with w_{exp}/w_{pred} of 0.41±0.27, 0.39±0.29, and 0.69±0.47, respectively. In addition, at $0.25f_G$, the w_{exp}/w_{pred} were very conservative, on average, when predicted with ACI 440.1R-06 [2006] and ISIS Manual No.3 [2007], while CAN/CSA-S6.1S1 [2010] produced non-conservative predictions at this load level.

In high-strength concrete beams (Table 4-5) at 2,000 microstrains, ACI 440.1R-06 [2006] and ISIS Manual No.3 [2007] yielded conservative predictions, on average, with w_{exp}/w_{pred} of 0.91±0.47 and 0.84±0.44, respectively, while CAN/CSA-S6.1S1, [2010] returned non-conservative predictions, on average, with a w_{exp}/w_{pred} of 1.55±0.85. At a low reinforcement stress level of $0.125f_G$, ACI 440.1R-06 [2006] and ISIS Manual No.3 [2007] yielded even better conservative predictions compared to the case of normal-strength concrete with w_{exp}/w_{pred} of 0.93±0.42 and 0.86±0.37, respectively. Similar to the normal-strength concrete beams at $0.25f_G$, the w_{exp}/w_{pred} were very conservative, on average, when predicted using ACI 440.1R-06 [2006] and ISIS Manual No.3 [2007], while CAN/CSA-S6.1S1 [2010] returned non-conservative predictions at this load level.

Concerning the predictions at $0.30M_n$ (the recommended value as a service load by many researchers), ACI 440.1R-06 [2006] and ISIS Manual No.3 [2007] showed reasonably conservative predictions for the normal-strength concrete beams with average w_{exp}/w_{pred} of 0.91±0.17 and 0.77±0.13. With the high-strength concrete beams, the average w_{exp}/w_{pred} were 0.69±0.13 and 0.61±0.11 for ACI 440.1R-06 [2006] and ISIS Manual No.3 [2007], respectively. CAN/CSA-S6.1S1 [2010], however, showed non-conservative predictions with average w_{exp}/w_{pred} of 1.23±0.20 and 1.14±0.26 for normal- and high-strength concretes, respectively. The

small k_b values with CAN/CSA-S6.1S1 [2010] compared to those in ACI 440.1R-06 [2006] and ISIS Manual No.3 [2007] contributed to under estimating the crack widths.

The predicted moment-to-crack-width relationships of the tested beams using the k_b values provided by ACI 440.1R-06 [2006], ISIS Manual No.3 [2007], and CAN/CSA-S6.1S1 [2010] are shown in Figure 4.8 for the normal-strength concrete beams and in Figure 4.9 for the high-strength concrete beams. The relationships were not consistent for the same type of surface configuration, regardless of bar diameter and material type the in normal- and high-strength concrete beams.

In the case of the normal-strength concrete beams shown in Figure 4.8 with the helically grooved GFRP bars (G3: No. 15 and No. 25), employing a k_b of 1.2 in the ISIS Manual No.3 [2007] equation yielded very good agreement with the experimental results. The ACI 440.1R-06 [2006] equation, however, underestimated the crack width of the No. 15 GFRP bars, yet yielded good agreement for the No. 25 GFRP bars.

Table 4-4 Experimental-to-predicted crack width (w_{exp}/w_{pred}) for normal-strength-concrete beams

Beam	ACI 440.1R-06					ISIS Manual No.3-07					CAN/CSA S6-10				
	2000με	$0.30M_n$	$0.67M_n$	$0.25f_G$	$0.125f_G$	2000με	$0.30M_n$	$0.67M_n$	$0.25f_G$	$0.125f_G$	2000με	$0.30M_n$	$0.67M_n$	$0.25f_G$	$0.125f_G$
N3#13G1	1.11	1.03	1.08	0.63	0.41	1.02	0.88	0.90	0.58	0.38	1.26	1.14	1.87	1.10	0.73
N2#13G2	1.62	0.95	1.01	0.79	1.11	1.71	0.94	0.99	0.91	1.18	1.72	0.96	1.11	1.50	1.91
N2#15G3	0.66	0.71	0.84	0.81	0.25	0.69	0.69	0.81	0.83	0.25	0.96	0.88	1.01	1.13	0.34
N3#20G1	0.87	0.94	0.96	0.63	0.27	0.75	0.73	0.76	0.55	0.23	1.19	1.24	1.74	1.12	0.48
N2#22G1	0.98	0.70	0.65	0.23	0.12	0.96	0.63	0.58	0.22	0.12	1.56	1.21	2.95	0.40	0.21
N3#20G2	1.08	1.22	1.11	1.18	0.67	0.93	0.95	0.87	1.04	0.58	1.14	1.40	1.07	2.08	1.17
N2#25G1	0.76	0.87	0.90	0.36	0.33	0.72	0.66	0.70	0.34	0.31	1.15	1.24	2.64	0.62	0.56
N2#25G2	0.70	0.65	0.58	0.45	0.25	0.66	0.56	0.50	0.44	0.24	1.25	1.30	1.33	0.80	0.44
N2#25G3	1.09	0.86	0.80	0.75	0.47	1.05	0.78	0.72	0.73	0.46	1.40	1.19	1.10	1.05	0.66
N3#10C1	0.96	1.02	0.76	0.32[a]	0.31[b]	0.84	0.85	0.63	0.28[a]	0.27[b]	1.13	1.62	2.69	0.55[a]	0.54[b]
N3#13C1	0.94	1.01	0.95	0.48[a]	0.32[b]	0.82	0.81	0.76	0.42[a]	0.28[b]	1.16	1.33	2.28	0.84[a]	0.57[b]
Average	0.98	0.91	0.88	0.60	0.41	0.92	0.77	0.75	0.58	0.39	1.26	1.23	1.80	1.02	0.69
SD	0.26	0.17	0.17	0.27	0.27	0.29	0.13	0.14	0.27	0.29	0.22	0.20	0.74	0.47	0.47
COV (%)	27	19	19	46	66	32	17	19	47	74	17	16	41	46	68

[a] Calculate at $0.60f_G$.
[b] Calculate at $0.30f_G$.

Table 4-5 Experimental-to-predicted crack width (w_{exp}/w_{pred}) for high-strength-concrete beams

Beam	ACI 440.1R-06					ISIS Manual No.3-07					CAN/CSA S6-10				
	2000με	$0.30M_n$	$0.67M_n$	$0.25f_G$	$0.125f_G$	2000με	$0.30M_n$	$0.67M_n$	$0.25f_G$	$0.125f_G$	2000με	$0.30M_n$	$0.67M_n$	$0.25f_G$	$0.125f_G$
H2#13G2	1.29	0.62	0.49	0.76	1.11	1.36	0.60	0.46	0.83	1.11	2.26	0.99	0.76	1.37	1.94
H3#13G1	1.77	0.66	0.38	0.92	1.77	1.57	0.58	0.33	0.82	1.57	3.10	1.15	0.66	1.62	3.10
H3#20G2	0.62	0.73	0.57	0.76	0.77	0.53	0.60	0.47	0.65	0.68	1.08	1.21	0.96	1.32	1.35
H2#25G1	0.48	0.55	0.49	0.50	0.69	0.46	0.50	0.45	0.48	0.68	0.85	0.92	0.82	0.88	1.20
H2#25G2	0.63	0.49	0.43	0.51	0.62	0.60	0.45	0.40	0.49	0.59	1.11	0.83	1.52	0.91	1.09
H2#25G3	0.65	0.73	0.33	0.74	0.71	0.61	0.65	0.29	0.72	0.68	0.89	1.01	0.46	1.03	0.99
H3#10C1	1.26	0.85	0.41	0.85[a]	1.26[b]	1.11	0.76	0.36	0.75[a]	1.11[b]	2.21	1.51	0.73	1.49[a]	2.21[b]
H3#13C1	0.53	0.86	0.65	0.52[a]	0.53[b]	0.46	0.75	0.57	0.46[a]	0.46[b]	0.92	1.50	1.14	0.92[a]	0.92[b]
Average	0.91	0.69	0.47	0.70	0.93	0.84	0.61	0.42	0.65	0.86	1.55	1.14	0.88	1.19	1.60
SD	0.47	0.13	0.10	0.16	0.42	0.44	0.11	0.09	0.15	0.37	0.85	0.26	0.33	0.29	0.76
COV (%)	52	19	22	23	45	53	18	21	24	43	55	22	37	25	48

[a] Calculated at $0.60f_G$.
[b] Calculated at $0.30f_G$.

In the case of the sand-coated CFRP bars (C1: No. 10 and No. 13), ACI 440.1R-06 [2006] and ISIS Manual No.3 [2007] showed reasonably similar predictions using k_b values of 1.4 and 1.2, respectively. On the other hand, in the case of the sand-coated GFRP bars (G1 and G2), the predictions were reasonable with some diameters and evidenced discrepancies for the others. Moreover, the relationships showed that using the same k_b value for the types G1 and G2 sand-coated GFRP bars and type C1 sand-coated CFRP bars did no yield the same agreement between predictions and test results. Furthermore, using a k_b of 0.8 for the sand-coated FRP bars (carbon and glass) according to CAN/CSA-S6.1S1 [2010] underestimated the predicted crack widths in most of the beams tested, except for type G1 No. 22 GFRP bars and type G2 No. 25 GFRP bars. For the high-strength concrete beams shown in Figure 4.9, ACI 440.1R-06 [2006] and ISIS Manual No.3 [2007] showed reasonably similar predictions using k_b values of 1.4 and 1.2, respectively, with helically deformed No. 25 GFRP bars.

On the other hand, CAN/CSA-S6.1S1 [2010] yielded good predictions for the G1 and G2 No. 25 sand-coated GFRP bars. Thus, it could be concluded that FRP bar type, bar diameter, and concrete strength influence k_b values and, consequently, the predicted crack widths.

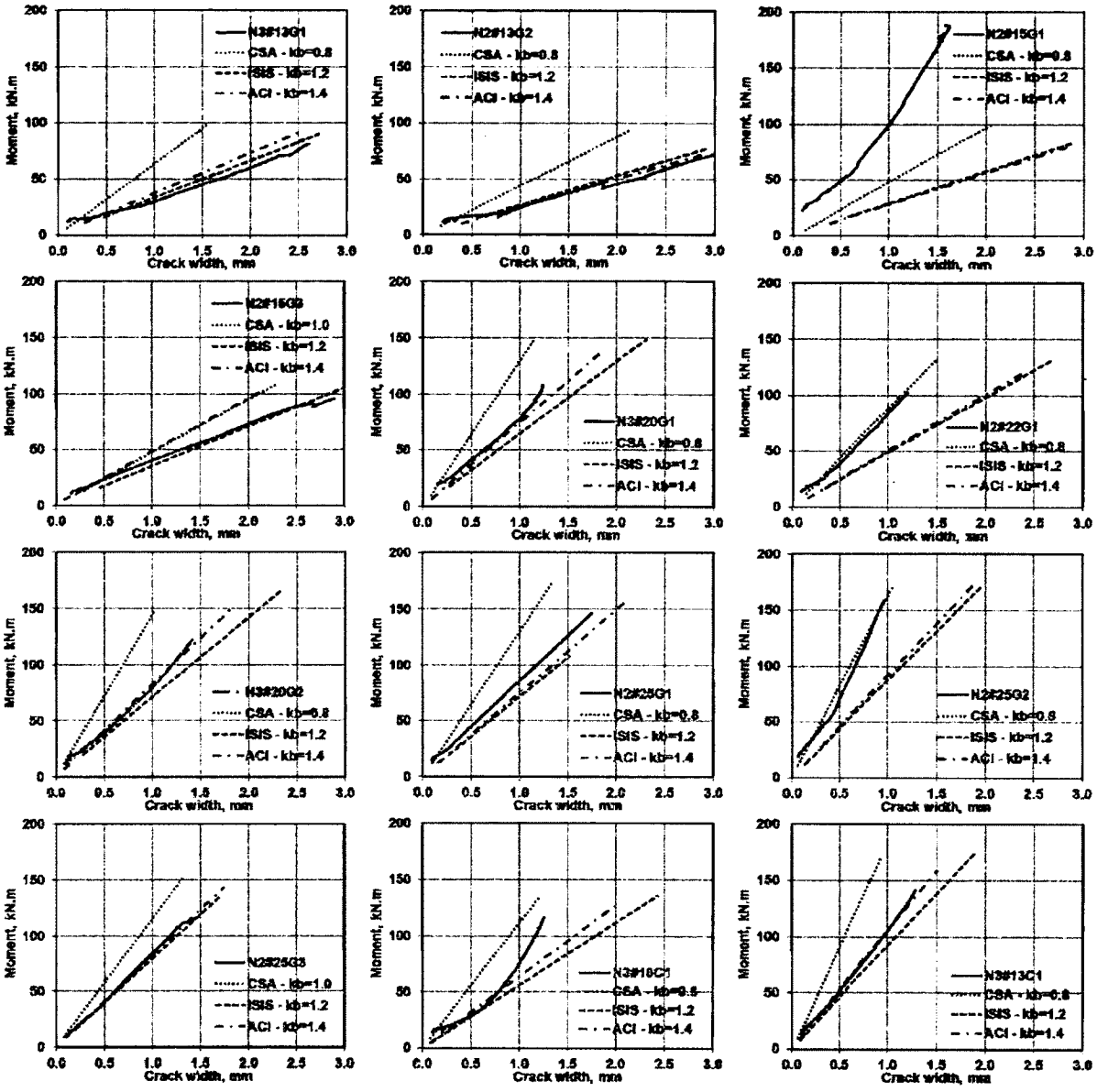

Figure 4.8 Predicted moment-to-crack-width relationships according to ACI 440.1R-06 [2006], ISIS Manual No.3 [2007], and CAN/CSA-S6.1S1 [2010] for normal-strength concrete beams

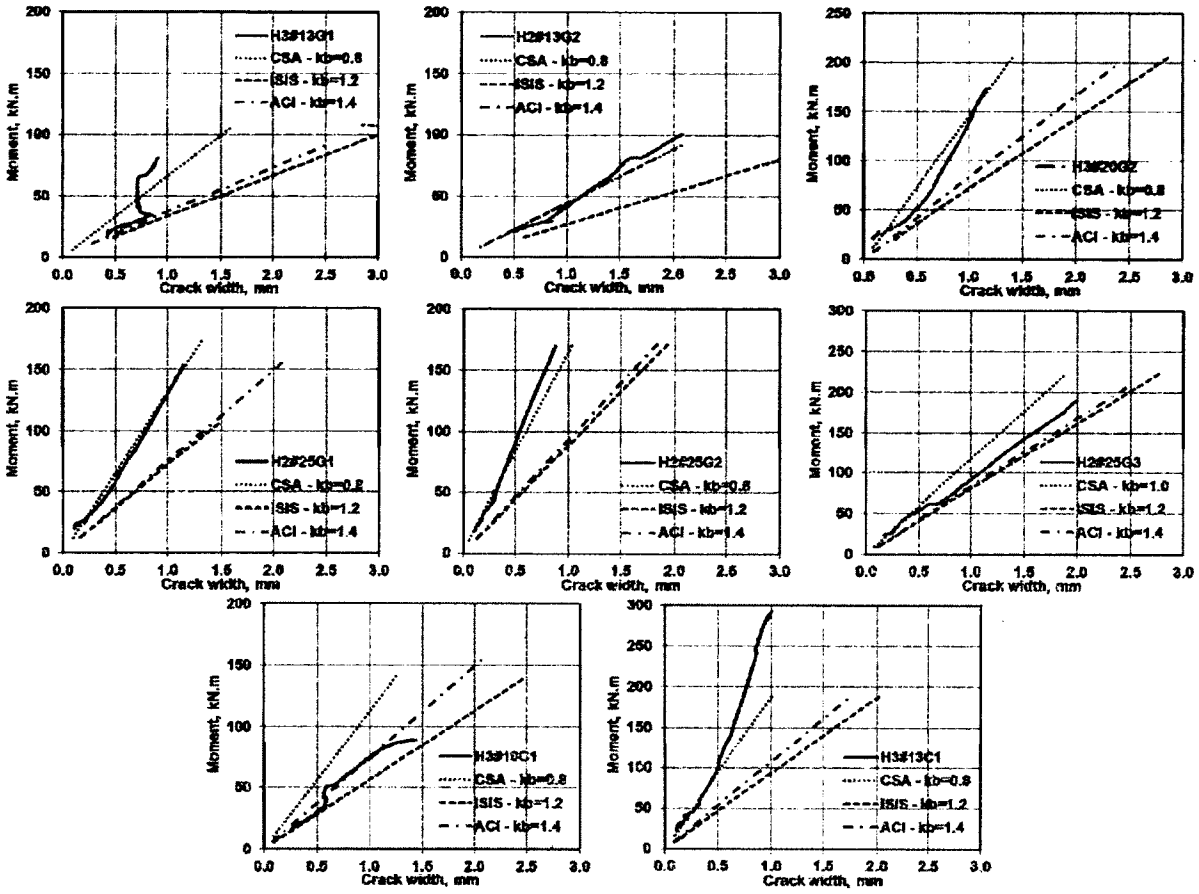

Figure 4.9 Predicted moment-to-crack-width relationships according to ACI 440.1R-06 [2006], ISIS Manual No.3 [2007], and CAN/CSA-S6.1S1 [2010] for high-strength concrete beams

EVALUATION OF THE BOND-DEPENDENT COEFFICIENT (k_b)

As presented in the previous section, predicting the crack widths of FRP- reinforced concrete beams using the k_b values currently recommended in FRP codes and guidelines yielded discrepancies in most cases. In addition, using the same value for different bars with the same surface configuration in the normal- and high-strength concretes was not appropriate. Thus, in

this section, the k_b values were predicted from the experimental results of the tested beams. Table 4-6 shows the k_b values at different limits calculated according to ACI 440.1R-06 [2006], ISIS Manual No.3 [2007], and CAN/CSA-S6.1S1 [2010] provisions and recommendations. The k_b values determined at crack width (w) = 0.7 mm, $0.30M_n$, and $0.25f_G$ were somewhat close. This supports using any of those limits as the recommended levels at which the k_b values should be determined. Nevertheless, the $0.30M_n$ supported by many researchers may still be of interest. Moreover, at $0.30M_n$, the crack width was less than 0.7 mm in all the beams except 3#13G1 and 2#13G2, which implicitly satisfies the requirements of CAN/CSA-S806 [2012], *Annex S*, of keeping 0.7 mm as the maximum crack width that could be used in determining k_b values. In addition, determining k_b values at very low load levels or just after cracking may not be representative because, at this load level, the beam experiences a transition stage until flexural cracks in the flexural moment zone stabilized.

The average k_b value of each beam was determined from the calculated k_b values at a crack width of 0.7 mm, $0.30M_n$, and $0.25f_G$ (see Table 4-7). These values confirm that the bond-dependent coefficient should not be provided as a unique value that takes into consideration surface configuration but not material type. The coefficient also contributes to concrete strength. While the values tend to confirm that k_b is a diameter-dependent parameter, the results did not show a trend or support a consistent relationship to variations in bar diameter.

Table 4-6 Predicted bond-dependent coefficient (k_b) values at different limits

Beam	ACI 440.1R-06; CCAN/CSA S6-10							ISIS Manual No.3-07						
	w= 0.5 mm	w= 0.7 mm	2000 με	0.30M_n	0.67M_n	0.25f_G	0.125f_G	w= 0.5 mm	w= 0.7 mm	2000 με	0.30M_n	0.67M_n	0.25f_G	0.125f_G
N3#13G1	1.2	1.4	1.5	1.4	1.6	1.3	1.5	0.9	1.1	1.2	1.1	1.2	1.0	1.2
N2#13G2	-	-	1.5	1.1	1.2	1.1	1.2	-	-	1.3	1.0	1.1	1.0	1.1
N2#15G1	0.7	0.8	0.8	0.7	0.8	0.8	0.7	0.6	0.7	0.7	0.6	0.7	0.7	0.7
N2#15G3	1.0	1.1	0.9	1.1	1.4	1.2	0.9	0.9	1.0	0.8	1.0	1.2	1.1	0.8
N3#20G1	1.3	1.4	1.2	1.3	1.4	1.3	1.2	0.9	1.0	0.9	0.9	1.0	1.0	0.9
N2#22G1	0.7	0.7	0.8	0.7	0.6	0.7	0.7	0.6	0.5	0.6	0.6	0.5	0.6	0.6
N3#20G2	1.4	1.3	1.4	1.4	1.3	1.3	1.3	1.0	1.0	1.0	1.0	1.0	1.0	1.0
N2#25G1	0.7	0.7	0.8	0.7	0.7	0.7	0.9	0.5	0.5	0.6	0.5	0.6	0.5	0.7
N2#25G2	1.0	0.8	1.1	1.2	0.8	1.2	0.8	0.8	0.7	0.9	1.0	0.6	1.0	0.7
N2#25G3	1.5	1.4	1.5	1.5	1.3	1.4	1.6	1.3	1.1	1.2	1.3	1.1	1.1	1.3
N3#10C1	0.9	0.7	1.2	0.8	-	0.9	1.2	0.7	0.5	0.9	0.6	0.3	0.7	0.9
N3#13C1	1.1	1.1	1.3	1.2	1.1	0.8	1.0	0.9	0.9	0.9	0.9	0.8	0.6	0.7
H2#13G2	-	1.0	1.1	1.0	0.7	0.9	1.0	3.5	0.9	1.0	0.9	0.7	0.8	0.9
H3#13G1	-	1.9	1.9	2.1	0.9	2.0	1.9	2.3	1.5	1.5	1.6	0.7	1.5	1.5
H3#20G2	1.1	1.0	0.8	1.1	0.9	1.0	1.1	0.8	0.7	0.6	0.8	0.7	0.8	0.8
H2#25G1	0.8	0.8	0.6	0.8	0.8	0.8	0.9	0.7	0.6	0.6	0.7	0.6	0.6	0.7
H2#25G2	0.5	0.5	0.6	0.6	0.5	0.6	0.6	0.4	0.4	0.5	0.5	0.4	0.4	0.5
H2#25G3	1.0	1.2	0.9	1.0	1.2	1.0	1.0	0.8	1.0	0.7	0.9	1.0	0.9	0.8
H3#10C1	1.8	1.1	1.8	1.3	1.2	1.2[a]	1.8[b]	1.3	0.8	1.4	0.9	0.9	0.9[a]	1.4[b]
H3#13C1	0.8	0.8	0.5	0.7	0.7	0.8[a]	0.5[b]	0.6	0.6	0.4	0.6	0.5	0.6[a]	0.4[b]

[a] Calculated at 0.60f_G.
[b] Calculated at 0.30f_G.

For the type G1 sand-coated GFRP bars, the k_b values with ACI 440.1R-06, [2006] were 1.4, 0.8, 1.3, 0.7, and 0.7 for N3#13G1, N2#15G1, N3#20G1, N2#22G1, and N2#25G1, respectively, with an average of 1.0, whereas the average of k_b values for the same beams determined with ISIS Manual No.3 [2007] was 0.8. For the type C1 sand-coated CFRP bars, the k_b values according to ACI 440.1R-06 [2006] were 0.8 and 1.0 for N3#10C1, N3#13C1, respectively. ISIS Manual No.3, [2007] yielded k_b values of 0.6 and 0.8 for the same beams. Thus, it could be concluded that k_b also depends on the equation used for the prediction. For type G2 sand-coated bars, the k_b values with ACI 440.1R-06 [2006] were 1.1, 1.3, and 1.1 for

2#13G2, 3#20G2, and 2#25G2, respectively, whereas the k_b values for the same beams determined with ISIS Manual No.3 [2007] were 1.0, 1.0, and 0.9. The k_b values of the type G3 GFRP bars was the closest to recommendations of ACI 440.1R-06 [2006] and ISIS Manual No.3 [2007], while the k_b values for the type C1 sand-coated CFRP bars was close to 1.0.

Table 4-7 Average predicted k_b values in comparison with design provisions

	k_b Average ACI 440.1R-06; CAN/CSA S6-10	k_b Average ISIS Manual No.3-07	Design recommendations		
			ACI 440.1R-06	ISIS Manual No.3-07	CAN/CSA S6-10
N3#13G1	1.4	1.1	Conservative value of k_b = 1.4 (excluding smooth bars and grids)	In the absence of significant test data k_b =1.2	Sand-Coated FRP: k_b = 0.8 Deformed FRP: k_b = 1.0
N2#13G2	1.1	1.0			
N2#15G1	0.8	0.7			
N2#15G3	1.1	1.0			
N3#20G1	1.3	1.0			
N2#22G1	0.7	0.6			
N3#20G2	1.3	1.0			
N2#25G1	0.7	0.5			
N2#25G2	1.1	0.9			
N2#25G3	1.4	1.2			
N3#10C1	0.8	0.6			
N3#13C1	1.0	0.8			
H2#13G2	1.0	0.9			
H3#13G1	2.0	1.5			
H3#20G2	1.0	0.8			
H2#25G1	0.8	0.6			
H2#25G2	0.6	0.4			
H2#25G3	1.1	0.9			
H3#10C1	1.2	0.9			
H3#13C1	0.8	0.6			

The results reported in Table 4-7 also confirm the effect of concrete strength on the calculated k_b values. Among the sand-coated GFRP bars, type G1 returned higher k_b values in high-strength concrete, while type G2 evidenced smaller k_b values in high-strength concrete. The

helically deformed type G2 GFRP bars produced smaller k_b values in high-strength concrete. Type C1 sand-coated CFRP bars, however, showed higher k_b values in high-strength concrete.

CONCLUSIONS

This study aimed at investigating the current design recommendations for k_b values and checking the dependency of k_b values on FRP bar type (glass and carbon), bar diameter, and concrete strength. The investigation included 20 beams measuring 4,250 mm long × 200 mm wide × 400 mm deep fabricated with normal- and high-strength concretes and reinforced with sand-coated GFRP bars, helically-grooved GFRP bars, and sand-coated CFRP bars. The measured crack widths and strains were used to assess the current k_b values. Based on the results and discussions presented herein, the following conclusions were drawn:

1- The bond-dependent coefficient (k_b) is dependent not only on bar surface configuration, but also on bar diameter and material type. Providing one value for k_b based solely on surface configuration was not supported by the test results. The results indicated that concrete strength (normal- and high-strength) had an impact, yet no trend or clear relationship was evidenced.

2- The calculations of k_b values determined at crack width (w) = 0.7 mm, $0.30M_n$, and $0.25f_G$ were somewhat close. This supports using any of those limits as the recommended level at which the k_b values should be determined. The $0.30M_n$ value may be recommended as it has been used by many researchers as a service-load level. Moreover, at $0.30M_n$, the crack width was less than 0.7 mm in all the beams tested, except 3#13G1 and 2#13G2, which implicitly

satisfies the requirements of CAN/CSA-S806 [2012], *Annex S*, of keeping 0.7 mm as the maximum crack width that could be used in determining k_b values.

3- ACI 440.1R-06 [2006] and ISIS Manual No.3 [2007] showed reasonably conservative crack-width predictions (at $0.30M_n$) with average w_{exp}/w_{pred} of 0.91±0.17 and 0.69±0.23 for normal-strength concrete and 0.69±0.13 and 0.61±0.11 for high-strength concrete. CAN/CSA-S6.1S1, [2010], however, showed non-conservative predictions with average w_{exp}/w_{pred} of 1.23±0.20 and 1.14±0.26 for normal- and high-strength concretes, respectively. The small k_b values of CAN/CSA-S6.1S1 [2010] compared to those of ACI 440.1R-06 [2006] and ISIS Manual No.3 [2007] contributed to underestimating crack widths.

4- With the helically-grooved GFRP bars (G3: No. 15 and No. 25), employing a k_b of 1.2 in the ISIS Manual No.3, [2007] equation yielded very good agreement with the experimental results. The ACI 440.1R-06, [2006] equation, however, underestimated the crack width of No. 15 GFRP bars, while yielding good agreement for No. 25 GFRP bars.

5- With the sand-coated CFRP bars (C1: No. 10 and No. 13), ACI 440.1R-06, [2006] and ISIS Manual No.3 [2007] showed reasonably close predictions using k_b values of 1.4 and 1.2, respectively. On the other hand, the predictions were reasonable with some diameters and showed discrepancies for the others with the sand-coated GFRP bars type (G1 and G2). Furthermore, using a k_b of 0.8 for the sand-coated FRP bars (carbon and glass) with the CAN/CSA-S6.1S1 [2010] equation underestimated the predicted crack widths in most of the tested beams fabricated using normal- and high-strength concretes.

6- Maintaining minimum practical reinforcement may be of interest to ensure that the section behaves reasonably after cracking and the sudden increase in the strains is minimized. This

may have an impact on the current test method in CAN/CSA-S806 [2012], *Annex S*, to determine the k_b values when only two bars are recommended.

7- The bond-dependent coefficient (k_b) introduced by FRP design codes and guidelines should be revised to include the effect of bar diameter, FRP material type, and concrete strength, in addition to the surface configuration.

CHAPTER 5

FLEXURAL BEHAVIOUR OF CONCRETE BEAMS REINFORCED WITH DIFFERENT GRADES OF GFRP BARS

Authors and affiliation

Amr El-Nemr Doctorate candidate, Department of Civil Engineering, University of Sherbrooke, Sherbrooke, Quebec, Canada, J1K 2R1, Phone: (819) 821-8000 ext. 62967, Fax: (819) 821-7974, E-mail: Amr.M.El-Nemr@usherbrooke.ca

Ehab A. Ahmed is Postdoctoral fellow, Department of Civil Engineering, University of Sherbrooke, Sherbrooke, Quebec, Canada, J1K 2R1, Phone: (819) 821-8000 ext. 62135, Fax: (819) 821-7974, E-mail: Ehab.Ahmed@USherbrooke.ca

Brahim Benmokrane, Canada and NSERC Chair Professor, Department of Civil Engineering, University of Sherbrooke, Quebec, Canada, J1K 2R1, Phone: (819) 821-7758, Fax: (819) 821-7974, E-mail: Brahim.Benmokrane@USherbrooke.ca (corresponding author).

Submittal/Acceptance Date: *not submitted yet*

Acceptance Status: not yet

Journal Title: Canadian Journal of Civil Engineering

Reference: Not published yet

French Titre: *Étude du comportement en flexion de poutres en béton armé de différents grades de barres en polymères renforcés de fibres de verre*

Contribution in thesis: The paper extends the study presented in Paper 1 where a variety of GFRP bars were used. The test specimens were designed to include the three grades of GFRP bars according to the CSA S807-10 in normal-strength concrete. The paper evaluated the effect of the mechanical properties and surface configurations of the GFRP bars of different grades on the cracking and flexural behaviour. The crack width and deflection equations were also assessed through the experimental results. Design recommendations were also introduced.

French Abstract:

La publication récente du guide de certification CSA S807-10 "*Spécification for fibre-renforcé Polymères*" est un pas en avant pour la standardisation de la fabrication des barres d'armature en polymères renforcés de fibres (PRF) utilisées dans les infrastructures. Ce guide classe les barres de polymères renforcés de fibres de verre (PRFV) dans trois catégories selon leur module d'élasticité (E_{frp}) : catégorie I (E_{frp} < 50 GPa), catégorie II (50 GPa < E_{frp} < 60 GPA) et catégorie III (E_{frp} = 60 GPa). Quant à la configuration de fini de surface des barres de PRF, elle varie en fonction du manufacturier et la surface peut être lisse, sablée, déformée, cannelée ou nervurée. Par conséquent, une variété de barres d'armature de PRFV de différentes catégories de module élastique et de fini de surface est disponible sur le marché. Cette étude porte sur l'évaluation du comportement en flexion et de la capacité en service de poutres en béton armé de barres de PRFV de différents modules élastiques et de différents finis de surface. L'étude inclut la fabrication et la mise à l'essai de 18 poutres pleine grandeur de 4250 mm de longueur, 200 mm de largeur et 400 mm de profondeur, renforcées avec des barres de PRFV caractérisées par différents modules élastiques (catégories I, II et III), différents diamètres (No. 13 à No. 25) et différents finis de surface (sablées et à cannelures hélicoïdales). Les résultats expérimentaux présentés dans cette étude sont la déflection, la largeur de fissures, les déformations dans le béton

et dans les barres de PRF, les performances en flexion et le mode de rupture. Les résultats ont aussi été utilisés pour évaluer empiriquement l'exactitude des équations de prédiction de la déflection et de la largeur de fissures proposées par les codes et guidelines de conception Nord-américains, en vigueur, traitant des composites de PRF en infrastructure.

Mots-clés: Béton; polymères renforcés de fibres (PRF); poutre; déformation; largeur de fissures; coefficient d'adhérence; capacité en service.

ABSTRACT

The recently published CAN/CSA-S807 [2010] "*Specification for fibre-reinforced Polymers*" provided a step forward towards standardizing the fibre-reinforced polymer (FRP) bars. It classifies the glass FRP (GFRP) bars according to their modulus of elasticity (E_f) into three grades, namely: Grade I (E_f <50 GPa), Grade II (50 GPa ≤ E_f < 60 GPa), and Grade III (E_f ≥ 60 GPa). The surface configuration of the FRP bars; however, varies and each manufacturer has his established configuration such as smooth, sand-coated, deformed, grooved, and ribbed. Consequently, a variety of GFRP reinforcing bars with different grades and surface configuration are commercially available. This study presents an investigation to evaluate the flexural behaviour and serviceability performance of concrete beams reinforced with two extensively used GFRP bars in Canada of different grades and surface configurations. The study included fabricating and testing 17 full-scale beams measuring 4,250 mm long × 200 mm wide × 400 mm deep reinforced with GFRP bars of different grades (I, II, III), diameters (No. 13 to No. 25), and surface configurations (sand-coated and helically-grooved). The test results were presented and discussed in terms of deflection, crack width, strains in concrete and FRP reinforcement, flexural

capacity, and mode of failure. The results were also used to assess the accuracy of the current deflection and crack width prediction equations of North American FRP codes and guidelines.

Keywords: Concrete; fiber-reinforced polymer (FRP); beam; strain; crack width; deflection; serviceability.

INTRODUCTION

Fiber reinforced polymer (FRP) reinforcing bars have been used as an alternative reinforcement for conventional steel for the last two decades. Recently, new advancement in FRP technology led to the development different GFRP bars with enhanced physical and mechanical properties. These bars have a variety of surface configurations such as smooth, deformed, sand-coated, and grooved. The recently published CAN/CSA-S807 [2010] "*Specification for fibre-reinforced Polymers*" provided a step forward towards standardizing the fibre-reinforced polymer (FRP) bars. Which, in turn, is expected to increase the fields where the FRP bars are being used as primary reinforcement for concrete structures. In addition, producing GFRP bars with high modulus of elasticity is expected to optimize the reinforcement amount and consequently, yield a cost-effective design.

In general, FRP reinforced section should be over-reinforced to ensure crushing failure in contradicting to under-reinforced section designed for steel reinforced members. Although, this mode of failure yields less catastrophic and higher deformability before failure, some codes allow using the under-reinforced section when employing the FRP reinforcing bars. As seen

from Eq. [5.1, 5.2 and 5.3] the determination of the failure mode is generally related to the mechanical properties of FRP bars and concrete strength. This design concept is common between CAN/CSA-S806 [2012] and ACI 440.1R-06 [2006] when designing FRP reinforced concrete section. The difference between CAN/CSA-S806 [2012] and ACI 440.1R-06 [2006] appears in their assigning for the block factor for α_1 and β_1 as shown in Eq. [5.1, 5.2 and 5.3]

$$\rho_{fb} = \alpha_1 \beta_1 \frac{f_c'}{f_{fu}} \frac{E_f \varepsilon_{cu}}{E_f \varepsilon_{cu} + f_{fu}} \quad 5.1$$

$$\alpha_1 = 0.85 \; ; \; \beta_1 = 0.85 - 0.05\left(f_c' - 27.6\right)/6.9 \quad \text{[ACI 440.1R-06, 2006]} \quad 5.2$$

$$\alpha_1 = 0.85 - 0.0015(f_c') \geq 0.67 \; ; \beta_1 = 0.97 - 0.0025(f_c') \geq 0.67 \quad \text{[ISIS Manual No.3, 2007; CAN/CSA-S806, 2012]} \quad 5.3$$

Due to lower modulus of GFRP bars compared to that of steel bars, the design of GFRP bars normally governed by serviceability (deflection and cracking) rather than ultimate state. Thus, increasing the tensile properties is expected to enhance the serviceability of GFRP-reinforced concrete members. However, the surface configurations may also play a role in the cracking performance and consequently the crack widths. Thus, there is a need for investigating the performance of GFRP bars with different elastic modulus and surface configuration. Furthermore, the deformability of FRP reinforced concrete members should be also evaluated.

In this paper, the flexural behaviour of concrete beam reinforced with different grades of GFRP bars (classified according to CAN/CSA-S807 [2010]) that are being used extensively in Canada [Pultrall, 2012; Schöck, 2012]. A total of 17 full-scale concrete beams reinforced with GFRP bars were tested to failure in four-point bending over a clear span 3,750 mm. The test results were reported in terms of deflection, crack width, strains in concrete and reinforcement,

flexural capacity and mode of failure, and deformability. The test results were compared against the experimentally measured ones.

EXPERIMENTAL PROGRAM

Seventeen full-scale beams reinforced with different types and ratios GFRP bars were fabricated and tested in four bending. The investigated GFRP bars were selected as they are being extensively used in Canada [Pultrall, 2012; Schöck, 2012]. The beams were designed to fail in compression (over-reinforced section). The following sections describe the details of the experimental programs.

Materials

The beams were reinforced with three different commercially-available types of GFRP bars referred to as GFRP-1, GFRP-2, and GFRP-3. The used GFRP products [Pultrall, 2012; Schöck, 2012] were selected as they are extensively used in Canada in many applications. Different diameters from each bar type were used. The tensile properties of the GFRP bars were determined through testing representative specimens in accordance with ASTM D7205, [2011]. Table 5-1 summarizes the properties of these GFRP bars.

According to the CAN/CSA-S807 [2010], the three types of GFRP bars that were utilized herein were classified as Grade I, Grade II for GFRP-1 and Grade III for GFRP-2 and GFRP-3. Figure 5.1 shows the GFRP reinforcing bars. The beam specimens were cast using normal-strength ready-mixed concrete with an average 28-days compressive strength of 35 MPa. Table 5-2 lists the concrete compressive strengths based on average value of tests of three 150x300 mm cylinders on the day of testing. Also, concrete tensile strength was obtained from spilt-cylinder testing and the results are shown in Table 5-2.

Table 5-1 Properties of the GFRP bars

Bar type	Designated diameter of FRP bar*	Nominal cross-sectional area* (mm^2)	Surface configuration	Tensile strength, f_{fu}, (MPa) (Average±SD)	Modulus of elasticity, E_f, (GPa) (Average±SD)	Ultimate strain (%)	Characteristic strength and strain*		E_f/f_{fu}
							f_G MPa	ε_G (%)	
GFRP-1 (G1)	13	129	Sand-coated	817±9	48.7±0.6	1.7	790	1.6	59.6
	15	199	Sand-coated	751±23	48.1±1.6	1.6	683	1.6	64.1
	20	284	Sand-coated	728±24	47.6±1.7	1.5	656	1.5	65.4
	22	387	Sand-coated	693±23	46.4±1.5	1.5	625	1.5	67.0
	25	510	Sand-coated	666±74	53.2±2.1	1.3	444	1.0	79.9
GFRP-2 (G2)	13	129	Sand-coated	1639±61	67.0±1.0	2.5	1456	2.2	40.9
	15	199	Sand-coated	1362±33	69.3±3.2	2.0	1263	1.8	50.9
	20	284	Sand-coated	1082±37	52.5±1.7	2.1	971	2.0	48.5
	25	510	Sand-coated	1132±23	66.3±0.9	1.7	1063	1.7	58.6
GFRP-3 (G3)	15	199	Helically-grooved	1245±45	59.5±1.1	2.1	1110	1.9	47.8
	25	510	Helically-grooved	906±29	60.3±2.9	1.5	819	1.3	66.6

* Designated according to the [CAN/CSA-S807, 2010]

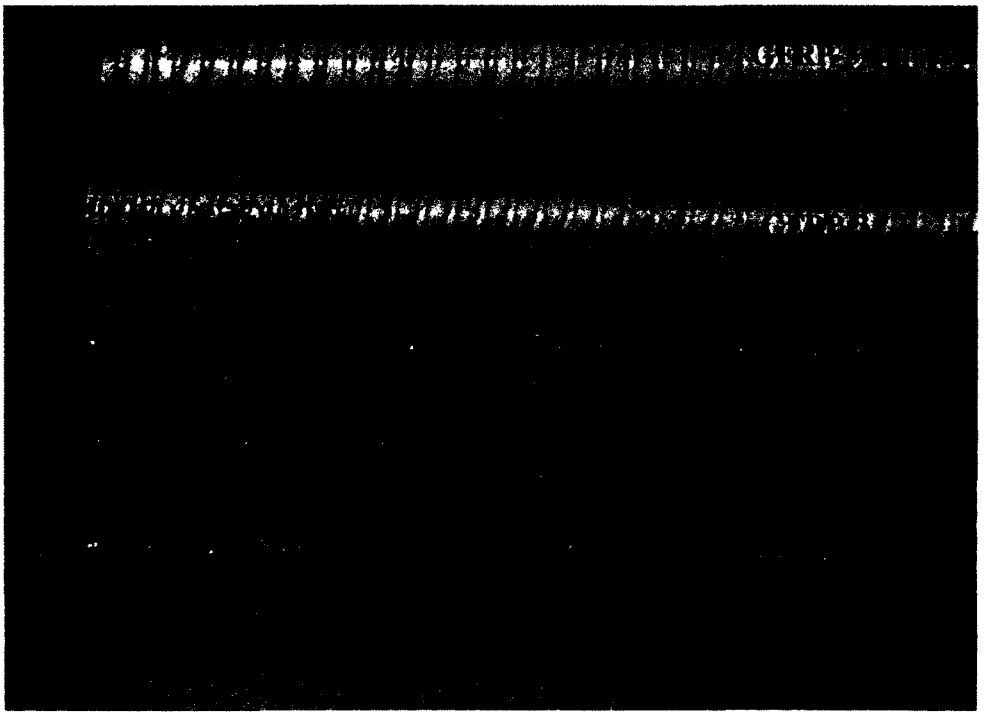

Figure 5.1 GFRP reinforcing bars

Table 5-2 Details of the test specimens

Series	Beam [a]	f_c' (MPa)	f_t (MPa)	ρ_f (%)	ρ_{fb} [b] (%)	ρ_f/ρ_{fb}	A_fE_f (kN)	Reinforcement configuration
I	3#13G1	33.50	3.60	0.56	0.43	1.31	18347	3 No. 13 - 1 row
	5#13G1	38.95	3.81	0.91	0.59	1.54	29864	5 No. 13 - 1 row
	2#13G2	33.50	3.60	0.38	0.15	2.45	17286	2 No. 13 - 1 row
II	3#15G1	38.95	3.81	0.84	0.65	1.30	28716	3 No. 15 - 1 row
	4#15G1	38.95	3.81	1.12	0.65	1.73	38288	4 No. 15 - 1 row
	2#15G2	29.00	2.50	0.56	0.20	2.79	27581	2 No. 15 - 1 row
	2#15G3	33.83	3.11	0.56	0.21	2.69	23681	2 No. 15 - 1 row
III	6#15G1	33.50	3.60	1.82	0.50	3.67	59700	6 No. 15 - 2 rows
	5#15G2	29.00	2.50	1.52	0.20	7.58	68954	5 No. 15 - 2 rows
	5#15G3	33.80	3.10	1.52	0.23	6.47	59203	5 No. 15 - 2 rows
VI	2#20G1	38.95	3.81	0.81	0.69	1.61	27037	2 No. 20 - 1 row
	3#20G1	42.10	3.18	1.21	0.73	1.67	40555	3 No. 20 - 1 row
	2#22G1	38.95	3.81	1.08	0.61	1.76	35264	2 No. 22 - 1 row
	3#20G2	48.13	3.96	1.21	0.34	3.59	44730	3 No. 20 - 1 row
V	2#25G1	48.13	3.96	1.46	0.83	1.75	54264	2 No. 25 - 1 row
	2#25G2	48.13	3.96	1.46	0.38	3.85	67626	2 No. 25 - 1 row
	2#25G3	33.80	3.10	1.51	0.42	3.57	61506	2 No. 25 - 1 row

[a] Beam designation: the number of GFRP bars followed by the diameter of GFRP bars and the last symbol denotes the GFRP bar type (G1: GFRP-1; G2: GFRP-2; G3: GFRP-3)

[b] Calculated according to [ACI 440.1R-06, 2006]

Specimens

Seventeen full-scale concrete beams measuring 4,250 mm long×200 mm wide×400 mm deep were constructed and tested the investigate the performance of the concrete beams reinforced with different grades and ratios of glass FRP bars in single- and two-layer configurations. The beams were divided according to FRP bar diameter into five Series. All beams were reinforced in compression with 2M10 steel bars. M10 mm stirrups at 100 mm spacing were used to avoid shear failure. In addition, the constant moment zone included only two stirrups spaced at 300 mm to maintain the locations of the longitudinal bars and minimize stirrup confinement action, which may affect cracking behaviour. Table 5-2 Details of the test

specimens shows the details of test specimens. Figure 5.2 shows the geometry and reinforcement details of the beams.

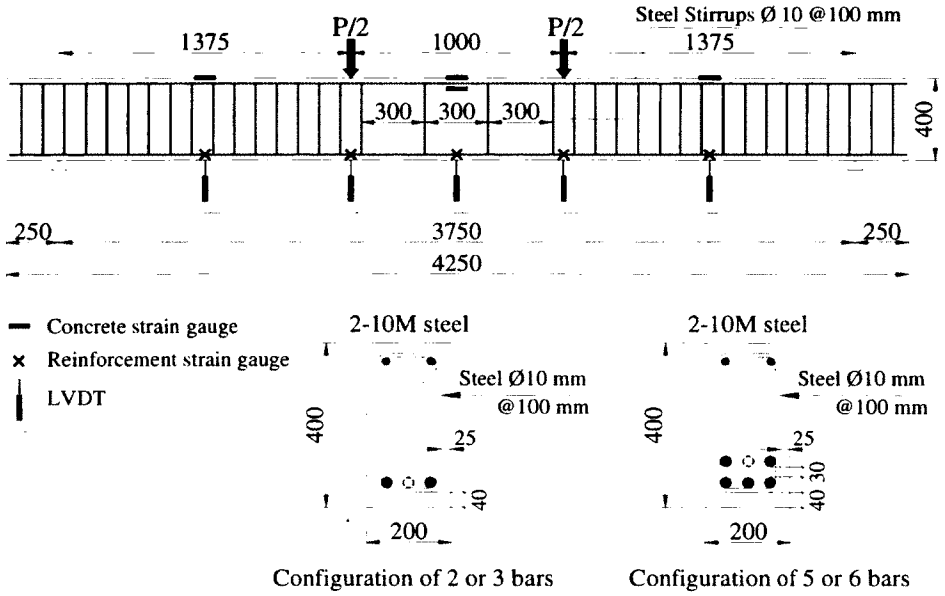

Figure 5.2 Dimensions, reinforcement details, and instrumentation

Instrumentation and Test setup

The reinforcing bars as well as the compressive area of the concrete beams were instrumented with electrical resistance strain gauges to measure the strains in the reinforcing bars as well as the concrete at desired locations. Five linear variable displacement transducers (LVDTs) were installed on each beam to measure the deflections at different locations. In addition, one high-accuracy LVDT was installed at the position of the first flexural crack after measuring its initial width with a hand-held microscope with 50X magnifying power.

The beams were tested under four-point bending over a clear span of 3,750 mm. The load was monotonically applied with a displacement control rate of 0.6 mm/min. During the test,

crack formation on one side of the beam specimen was marked and the corresponding loads were recorded.

Figure 5.3 shows the test setup during a beam testing.

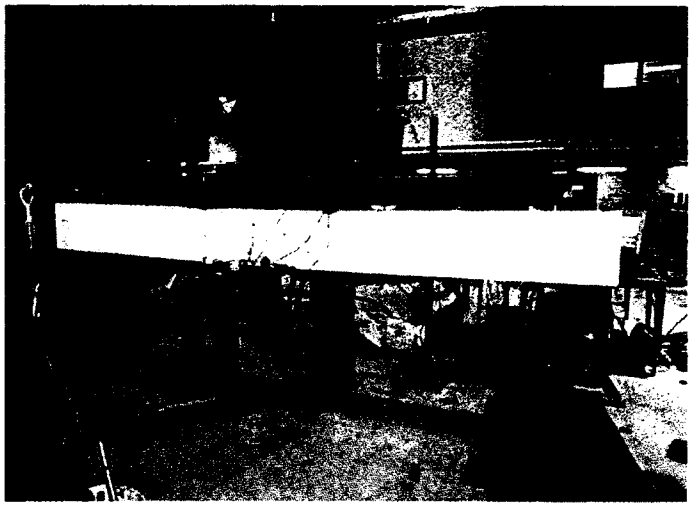

Figure 5.3 Test setup during a beam testing

Test Results and Discussion

Cracking Moment

The beams were observed during the test until the first crack appeared and the corresponding load was recorded. The cracking load was also verified from the load-deflection and load-strain relationships. Table 3 provides the cracking moments of the tested beams excluding beams' self-weight. The cracking moment ranged from 10.09 to 16.32 kN.m. The cracking moment was directly related to concrete tensile strength, which, in turn, is a function of compressive strength. The higher the concrete strength, the higher the cracking moment. The cracking moments were predicted using Eq. [5.4, 5.5, 5.6 and 5.7] and experimental-to-predicted ratios were listed in Table 5-3.

$$M_{cr} = f_r / y_t I_g \qquad 5.4$$

$$f_r = 0.62\lambda\sqrt{f_c'} \quad \text{for [ACI 440.1R-06, 2006]} \quad 5.5$$

$$f_r = 0.6\lambda\sqrt{f_c'} \quad \text{for [ISIS Manual No.3, 2007]and [CAN/CSA-S806, 2012]} \quad 5.6$$

$$f_r = 0.4\sqrt{f_c'} \quad \text{for [CAN/CSA-S6.1S1, 2010] (normal-density concrete)} \quad 5.7$$

Table 5-3 Experimental and predicted cracking and ultimate moments

Beam	Experimental moments			ACI 440 (2006)			CSA S6 (2010)			CSA S806 (2012)		
	M_{cr}	M_n	Failure mode [1]	M_{cr}	M_n	Failure mode [1]	M_{cr}	M_n	Failure mode [2]	M_{cr}	M_n	Failure mode [1]
	kN.m	kN.m		Exp/Pred	Exp/Pred		Exp/Pred	Exp/Pred		Exp/Pred	Exp/Pred	
3#13G1	13.46	81.34	C.C.	0.85	0.89	C.C.	1.49	0.82	C.C.	0.88	0.82	C.C.
5#13G1	15.26	130.63	C.C.	0.88	1.1	C.C.	1.52	1.01	C.C.	0.76	1.01	C.C.
2#13G2	13.75	82.78	C.C.	0.87	0.94	C.C.	1.52	0.87	C.C.	0.9	0.87	C.C.
3#15G1	12.21	101.31	C.C.	0.73	0.89	C.C.	1.26	0.82	C.C.	0.75	0.82	C.C.
4#15G1	15.61	138.19	C.C.	0.88	1.06	C.C.	1.56	0.98	C.C.	0.94	0.98	C.C.
2#15G2	11.22	95.93	C.C.	0.77	0.96	C.C.	1.37	0.9	C.C.	0.81	0.9	C.C.
2#15G3	10.92	91.31	C.C.	0.69	0.9	C.C.	1.2	0.84	C.C.	0.71	0.84	C.C.
6#15G1	11.98	118.34	C.C.	0.76	0.89	C.C.	1.32	0.84	C.C.	0.79	0.84	C.C.
5#15G2	12.2	129.32	C.C.	0.84	0.98	C.C.	1.49	0.93	C.C.	0.88	0.93	C.C.
5#15G3	12.61	110.58	C.C.	0.79	0.82	C.C.	1.38	0.77	C.C.	0.82	0.77	C.C.
2#20G1	15.36	107.39	C.C.	0.89	0.96	C.C.	1.53	0.88	FRP-R	0.92	0.88	FRP-R
3#20G1	16.32	140.35	C.C.	0.9	1.04	C.C.	1.55	0.95	C.C.	0.93	0.95	C.C.
2#22G1	12.88	132.26	C.C.	1	1.08	C.C.	1.33	1	C.C.	0.8	1	C.C.
3#20G2	12.29	171.43	C.C.	0.63	1.15	C.C.	1.07	1.04	C.C.	0.65	1.04	C.C.
2#25G1	11.32	161.65	C.C.	0.58	1.02	C.C.	0.98	0.92	C.C.	0.6	0.92	C.C.
2#25G2	16.77	167.24	C.C.	0.85	0.97	C.C.	1.46	0.88	C.C.	0.89	0.88	C.C.
2#25G3	13.2	115.93	C.C.	0.83	0.81	C.C.	1.45	0.76	C.C.	0.86	0.76	C.C.
Average				0.8	0.95	---	1.36	0.88	---	0.8	0.88	---
Standard deviation				0.12	0.12	---	0.18	0.1	---	0.12	0.1	---
Coefficient of variation %				14%	13%	---	13%	11%	---	15%	11%	---

Note – Measured and predicted moments exclude beams' self-weight.
[1] FRP-R: Rupture of FRP bar; C.C.: Concrete crushing.

Table 5-3 indicated that the experimentally measured cracking moment of the GFRP reinforced concrete beams was generally lower than those predicted using ACI 440.1R-06 [2006] and CAN/CSA-S806 [2012]. The predictions of ACI 440.1R-06 [2006] and CAN/CSA-S806 [2012]; however, were close and the average experimental-to-predicted M_{cr} ratios for both

equations was 0.80±0.12. On the other hand, CAN/CSA-S6.1S1 [2010] underestimated cracking moment and yielded conservative predictions with an average experimental-to-predicted M_{cr} ratio of 1.36±0.18.

Flexural capacity and mode of failure

The beams were designed with a ρ_f/ρ_{fb} ratio greater than 1.0 (over-reinforced), so that the failure was expected to occurs due to concrete crushing. Consequently, all beams failed in compression (concrete crushing). Figure 5.4 shows the typical compression failure of some of the tested beams. At failure, the concrete strain of all the tested beams was lower than the known limits provided by ACI 440.1R-06 [2006] and CAN/CSA-S806 [2012] (3,000 and 3,500 microstrains, respectively) and supported by many studies [Masmoudi *et al.*, 1998; Kassem *et al.*, 2011; Vijay et GangaRao, 1996] where the concrete crushing occurs at about 3,000 microstrains. This is related to the absence of stirrups in the critical flexural zone of the beams which led to premature buckling of compression beams before yielding and the consequent disintegration of the confined concrete. The premature buckling was due to a large unsupported length of compression bars (300 mm). The lower-than-expected concrete strains did not enable evaluating the effect of the bar diameter and surface on the ultimate capacity. But, generally, the higher the E_fA_f, the higher the flexural capacity of the tested beams. In addition, the concrete strength had a contribution to the ultimate capacity as evidenced from beams 2#25G2 and 5#15G2 with the same E_fA_f. Beam 2#25G2 showed an ultimate capacity of 167.24 kN.m compared to 129.32 kN.m of 5#15G2 where the concrete strengths for both beams were 48.13 MPa and 29.00 MPa, respectively.

2#15G3

3#20G2

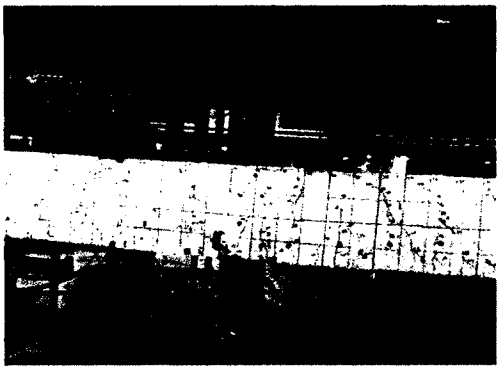

2#25G2

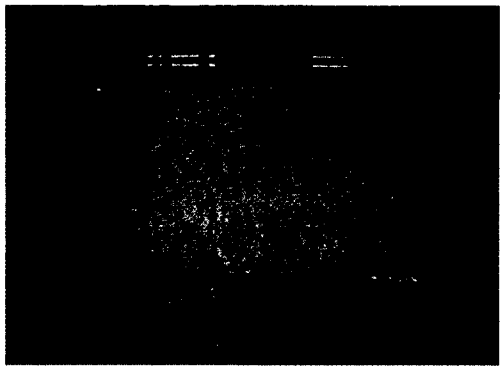

2#25G3

Figure 5.4 Typical compression failure of beams reinforced with GFRP bars Type G2 and G3.

Concerning the load-carrying capacity, the predictions of ACI 440.1R-06 [2006] and CAN/CSA-S6.1S1 [2010], and CAN/CSA-S806 [2012] were close and in good agreement with the experimental results as shown in Table 5-3. The difference between ACI 440.1R-06 [2006]; CAN/CSA-S6.1S1 [2010] and CAN/CSA-S806 [2012] predictions, however, were related to the β_1 factor and the assumed strain at the ultimate which is 0.003 for ACI 440.1R-06 [2006] and 0.0035 for CAN/CSA-S6.1S1 [2010] and CAN/CSA-S806 [2012].

The *c/d* ratios reported in Table 5-4 reveals a slight increase in the *c/d* ratio at M_n compared to that at $0.3M_n$ where M_n is nominal moment capacity. Moreover, the neutral axis

depth increased with ρ_f since the equilibrium of forces requires a larger compression block for the greater force.

Table 5-4 Strains, neutral axis-to-depth ratio, and curvature of test specimens

Beam	Strain in concrete (με)			Strain in FRP (με)		*c/d*				Curvature, ψ		
	at 2000 με	0.30M_n	M_n	0.30M_n	M_n	at 2000 με	0.30M_n	M_n	Theo.	at 2000 με	0.30M_n	M_n
3#13G1	-203	-314	-1561	4378	13726	0.09	0.07	0.10	0.13	0.002	0.005	0.015
5#13G1	-421	-714	-1933	3994	15095	0.17	0.15	0.15	0.15	0.002	0.005	0.011
2#13G2	-173	-690	-2541	5349	16359	0.05	0.11	0.13	0.12	0.003	0.006	0.019
3#15G1	-388	-651	-2341	4434	13345	0.16	0.13	0.15	0.15	0.002	0.005	0.008
4#15G1	-409	-510	-1816	2405	13489	0.14	0.14	0.13	0.17	0.002	0.003	0.014
2#15G2	-586	-346	-1454	4189	14136	0.08	0.08	0.09	0.16	0.008	0.005	0.016
2#15G3	-294	-516	-2129	3448	10277	0.13	0.13	0.17	0.14	0.002	0.004	0.012
6#15G1	-488	-562	-1976	2367	7693	0.19	0.19	0.20	0.22	0.003	0.003	0.010
5#15G2	-729	-745	-2959	2053	7550	0.28	0.28	0.29	0.24	0.003	0.003	0.010
5#15G3	-521	-412	-1839	1571	6430	0.21	0.21	0.22	0.22	0.003	0.002	0.008
2#20G1	-282	-433	-2090	3860	13372	0.11	0.09	0.13	0.15	0.002	0.004	0.015
3#20G1	-439	-657	-3087	3107	6794	0.18	0.18	0.20	0.18	0.002	0.004	0.015
2#22G1	-550	-605	-2646	4262	13651	0.12	0.12	0.16	0.17	0.004	0.005	0.016
3#20G2	-380	-657	-2648	3755	11823	0.16	0.15	0.18	0.18	0.002	0.004	0.014
2#25G1	-371	-542	-2529	2991	10028	0.18	0.15	0.20	0.19	0.002	0.004	0.013
2#25G2	-473	-508	-2045	2127	7573	0.16	0.16	0.18	0.21	0.002	0.003	0.009
2#25G3	-575	-459	-1627	1666	6429	0.22	0.22	0.2	0.22	0.003	0.002	0.008

Strain in reinforcement and concrete

Figure 5.5 shows the mid-span strains in the compression-concrete zone and the tensile reinforcing bars versus the applied moment for the tested beams. Table 5-4 shows the strains in the reinforcement and concrete at 0.3M_n (where M_n is the nominal capacity of the beam specimens) and failure. All the GFRP reinforced concrete beams of reinforcement ratio greater than the balanced ratio ($\rho_f > \rho_{fb}$) failed in compression by concrete crushing. The concrete's compression failure in some beams was triggered by the buckling of the compression steel

reinforcement. This was noticed through the small values for the concrete compressive strain at failure. Thus, the concrete strain values at ultimate (failure) may be affected by the buckling behaviour of compression steel reinforcement.

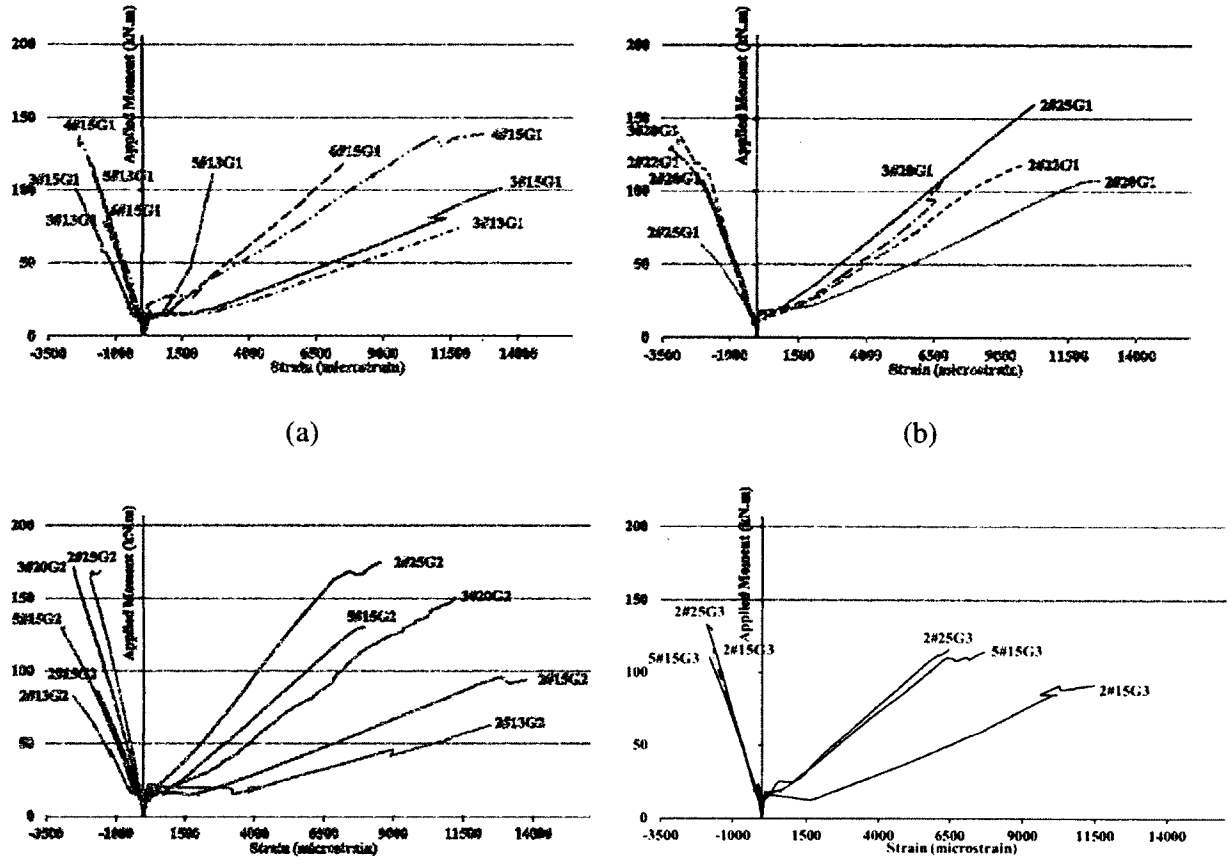

Figure 5.5 Moment-to-maximum concrete and reinforcement strain relationship: (a) and (b) for GFRP-1 (Grade I and II); (c) for GFRP-2 and (d) for GFRP-3 (Grade III).

For the strains in the GFRP reinforcing bars, generally, the GFRP reinforced concrete beams showed typical bi-linear moment-strain relationship. Figure 5.5 shows that increasing the reinforcement ratio ρ_f decreased the strain in the GFRP bars at the same load level. Figure 5.5

also shows that beams with low ρ_f (in Series I and II) experienced very high reinforcement strain increases at cracking. The sharp increase at the cracking was more than 3,000 με. Although beams 2#13G2 and 3#13G1 were designed as over-reinforced sections, large increase in crack width was observed due to poor energy absorption at cracking. Maintaining minimum practical reinforcement may be of interest to ensure that the section behaves reasonably after cracking. ACI 440.1R-06 [2006] specifies a minimum ρ_f / ρ_{fb} ratio of 1.4; however, this limit did not prevent beam 2#13G2 from exhibiting such sharp increase in strains at cracking.

Figure 5.5 also indicated that beams 2#25G3 and 5#15G3 shows the same moment-strain relationship. Beams provided with the same $E_f A_f$ bars with the same bar surface configuration are expected to have the same moment-strain relationships. Similarly were 2#25G2 and 5#15G2 but the lower concrete strength of 5#15G2 (29.0 MPa) than that of 2#25G2 (48.13 MPa) resulted in higher stains for 5#15G2.

The curvature of the tested beams was calculated as a function of $1/d$ and listed also in Table 5-4. Vijay et GangaRao [2001] concluded that at a curvature limit of $0.005/d$, the strains in FRP of are typically as high as 4,500 microstrains. The test results revealed that at a curvature of $0.005/d$ the strains in the GFRP bars were 4,378 με, 3,994 με, 4,434 με, 4,189 με, and 4,262 με for 3#13G1, 5#13G1, 3#15G1, 2#15G2, 2#22G1, respectively. This confirms Vijay et GangaRao [2001] findings for different GFRP bars with different surface configurations.

Deflection behaviour

Figure 5.6 provides typical applied moment to mid-span deflection relationships for the tested GFRP reinforced concrete beams. Each curve represents the average deflection obtained from two LVDTs mounted at beam mid-span. The load-deflection relationships revealed that ρ_f

had direct impact on the stiffness of the beam specimens, hence, on the load-deflection behaviour. The GFRP reinforced concrete beams showed highest deflection corresponding to low ρ_f. Table 5-5 summarizes the deflection of the tested beams at $0.3M_n$ and $0.67M_n$. Assuming that beam deflection limit at service load is span/240 (L/240) as provided for by CAN/CSA-S806 [2012] which yields 15.63 mm all beams except 3#15G1, 2#15G2, 2#20G1 and 2#22G1 exhibited deflection smaller than 15.63 at $0.3M_n$.

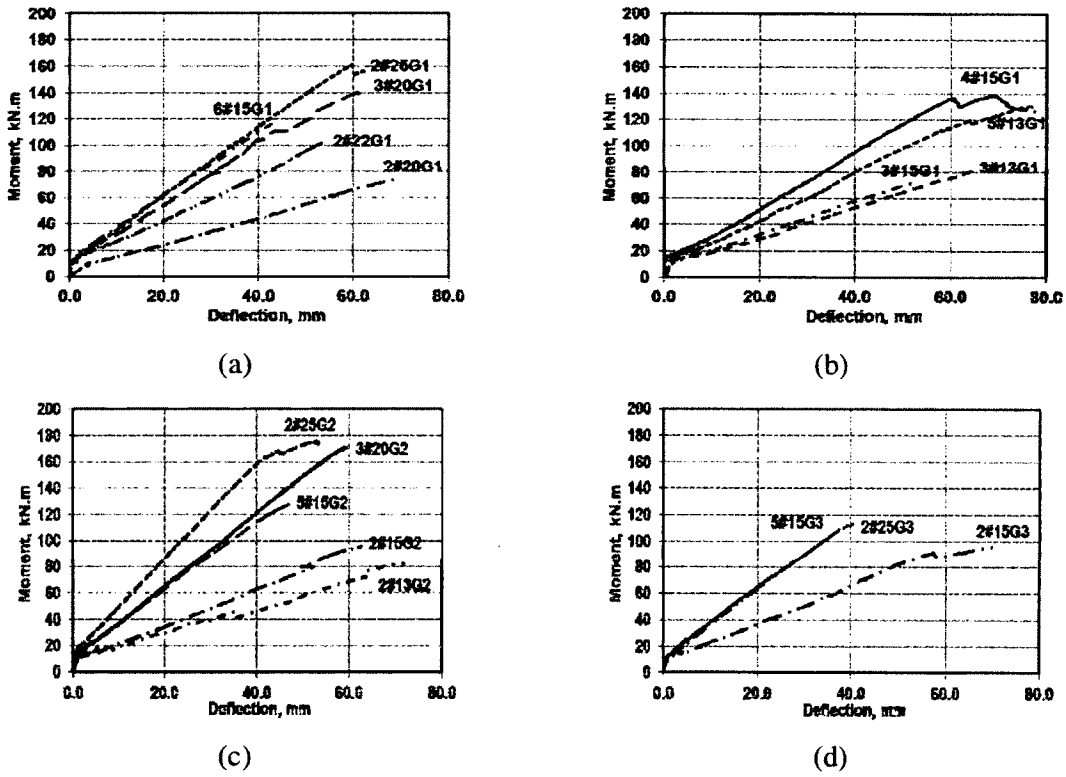

Figure 5.6 Deflection vs. applied moment for beams reinforced with different GFRP Grades: (a) and (b) for GFRP-1, while (c) for GFRP-2 and (d) for GFRP-3

Table 5-5 Experimental-to-predicted deflection ratios

Beam	Measured deflection (mm)		$\delta_{exp}/\delta_{pred}$ CSA S806 (2012)		$\delta_{exp}/\delta_{pred}$ ACI 440-H, [2010]		$\delta_{exp}/\delta_{pred}$ ISIS M-03 (2007)		$\delta_{exp}/\delta_{pred}$ ACI 440 (2006)	
	$0.30M_n$	$0.67M_n$	$0.30M_n$	$0.67M_n$	$0.30M_n$	$0.67M_n$	$0.30M_n$	$0.67M_n$	$0.30M_n$	$0.67M_n$
3#13G1	15.38	41	0.76	0.85	1.29	1.03	0.82	0.87	1.17	0.97
5#13G1	15.45	39	0.85	0.93	1.26	1.10	0.90	0.95	1.12	1.05
2#13G2	15.07	48	0.70	0.96	1.22	1.16	0.75	0.99	1.65	1.17
3#15G1	18.00	48	1.03	1.18	1.52	1.38	1.09	1.19	1.37	1.31
4#15G1	15.45	39	0.97	1.07	1.36	1.22	1.02	1.08	1.20	1.17
2#15G2	16.00	41	0.99	1.09	1.42	1.25	1.05	1.11	1.53	1.22
2#15G3	14.00	37	0.75	0.86	1.18	1.01	0.80	0.87	1.33	0.99
6#15G1	9.43	27	0.76	0.97	0.97	1.07	0.79	0.97	0.95	1.05
5#15G2	10.98	29	1.03	1.18	1.28	1.30	1.06	1.19	1.29	1.28
5#15G3	7.92	24	0.63	0.83	0.82	0.94	0.66	0.84	0.87	0.92
2#20G1	17.99	45	0.96	1.03	1.47	1.23	1.02	1.05	1.22	1.16
3#20G1	15.00	37	0.89	0.99	1.29	1.16	0.93	1.00	1.13	1.11
2#22G1	19.00	46	1.16	1.25	1.66	1.44	1.23	1.26	1.50	1.38
3#20G2	15.00	38	0.93	1.01	1.32	1.18	0.94	1.00	1.42	1.16
2#25G1	15.00	38	1.43	1.29	1.38	1.29	0.93	1.00	1.21	1.24
2#25G2	10.00	27	0.75	0.88	1.00	1.02	0.77	0.89	0.99	1.00
2#25G3	13.15	37	0.76	0.93	1.03	1.05	0.79	0.94	1.10	1.03
Average			0.89	1.01	1.25	1.15	0.90	1.00	1.22	1.12
Standard deviation			0.20	0.14	0.22	0.15	0.15	0.12	0.23	0.14
Coefficient of variation (%)			23%	14%	18%	13%	17%	12%	19%	12%
Overall average			0.95		1.20		0.95		1.17	
Overall standard deviation			0.18		0.19		0.15		0.19	
COV (%)			19%		16%		15%		16%	

The relationships in Figure 5.6 indicated that regardless the small difference in concrete strength between beams; increasing the E_fA_f contributed to enhancing the deflection of the beams. On the other hand, beams with the same E_fA_f reinforced with the same FRP bar type and surface configuration showed the same moment deflection relationships such as in case of 5#15G3 and 2#25G3 and in case of 5#15G2 and 2#25G2. Thus, it could be concluded that using the equivalent E_fA_f of different GFRP bar diameters of the same bar type and surface would not affect the load deflection properties. This is due to maintain both axial and bond properties of the GFRP bars.

The deflection values were plotted against ρ_f/ρ_{fb} and curvature as shown in Figure 5.7a; b. Figure 5.7a shows that the deflection of the beam specimens at $0.3M_n$ was close to the 15.63 mm ($L/240$) except three beams that exhibited larger deflections. Vijay et GangaRao [2001] concluded that a curvature limit of $0.005/d$ may yield beams satisfying deflection and cracking serviceability criteria. The relationships shown in Figure 5.7b indicated that most of the beams with curvatures less than $0.005/d$ yielded deflection values less than 15.63 mm ($L/240$).

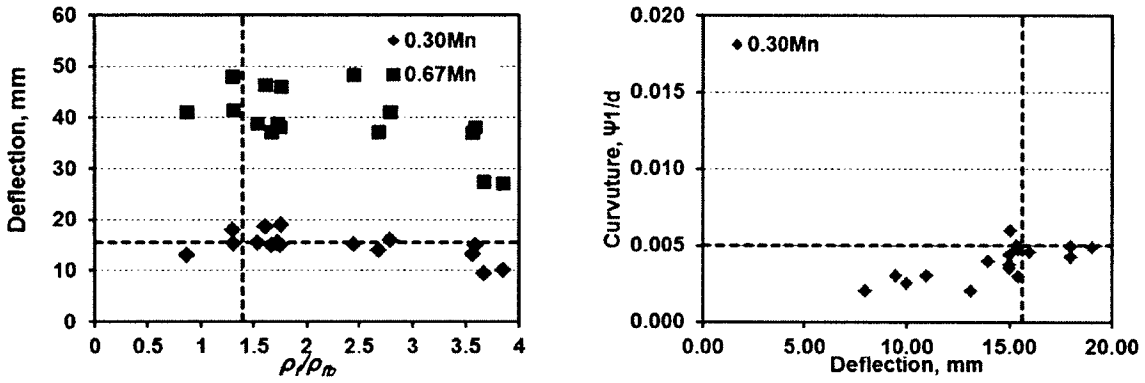

(a) (b)

Figure 5.7 Deflection versus ρ_f/ρ_{fb} and curvature $\Psi 1/d$

Crack pattern and crack width

The beams were initially un-cracked except beam 6#15G1 which showed a hair crack before testing. As the cracking moment was reached, cracks propagated vertically and perpendicularly to the maximum stress induced from the extreme fiber of the beam by the bending moment. More cracks appeared along the beam length as the load increased. The cracks in the bending zone grew vertically; however, the cracks in the shear span were inclined toward the central zone due to shear stresses in this region. After a load level corresponding 0.67 of the nominal moment, no more cracks appeared but the existence cracks widened.

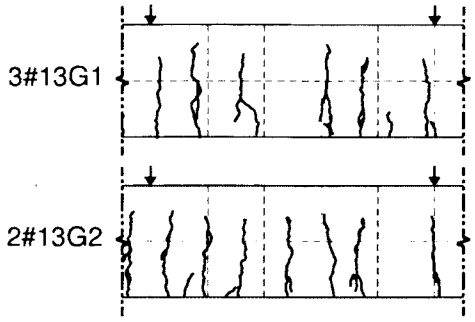

Series I at Ma = 0.30 Mn

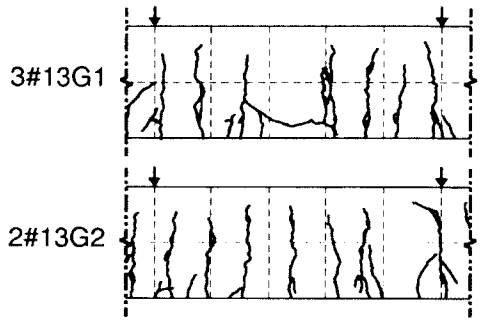

Series I at Ma = 0.67 Mn

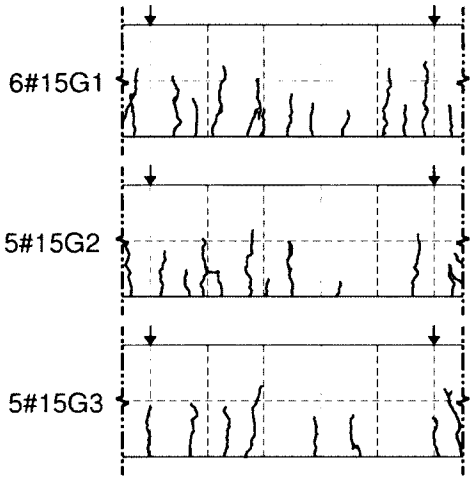

Series III at Ma = 0.3 Mn

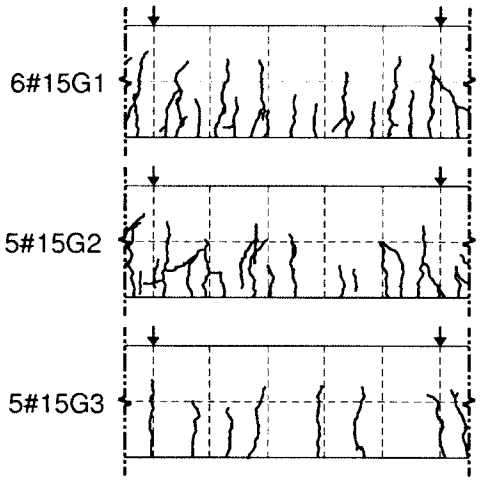

Series III at Ma = 0.67 Mn

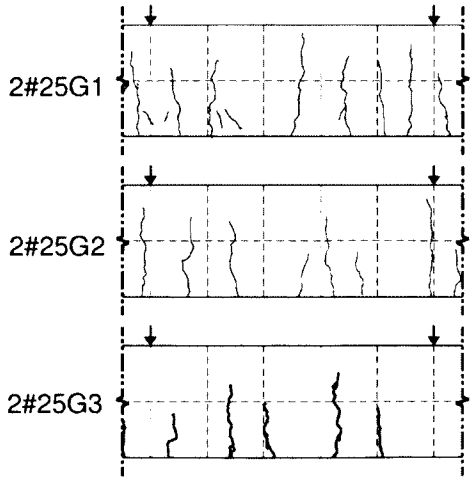

Series V at Ma = 0.3 Mn

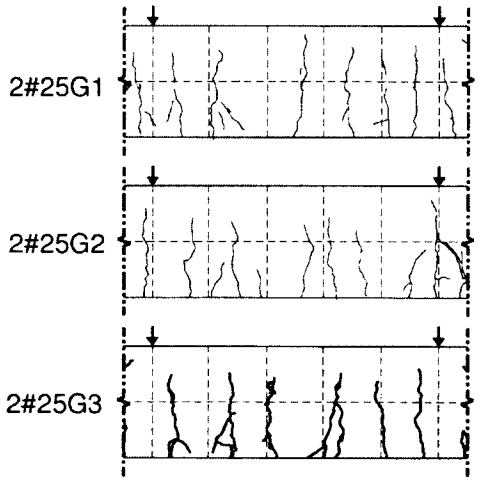

Series V at Ma = 0.67 Mn

Figure 5.8 shows the crack patterns of tested GFRP reinforced concrete beams at load levels

corresponds to $0.3M_n$ and $0.67M_n$.

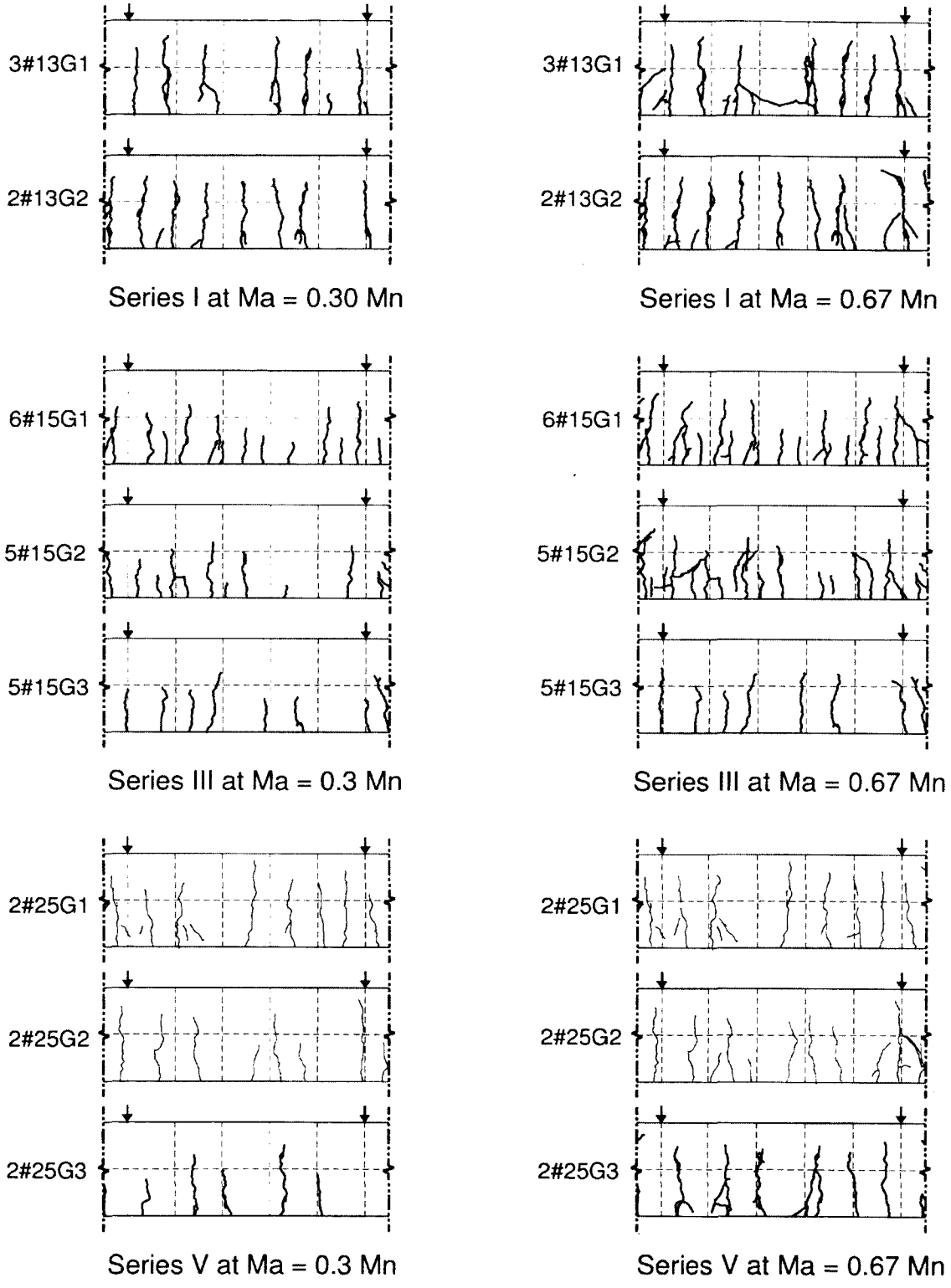

Figure 5.8 reveals that increasing the ρ_f, increases the number of cracks and consequently,

reduces the average crack spacing. Comparing beams in Series III and IV, specifically, beams reinforced with GFRP-1 and GFRP-2 bars, it could be noticed that increasing the bar diameter from No.15 to No. 25 for G2 (sand-coated) and G3 (helically-grooved) bars resulted in fewer number of cracks. In addition, increasing the $E_f A_f$ yielded smaller initial crack widths except in case of 6#15G1 which seems to be affected by pre-exists hair crack. Furthermore, comparing Series III and V, beams revealed fewer cracks in helically-grooved GFRP reinforced concrete beams compared to those reinforced with sand-coated bars. This tends to confirm that the sand-coated GFRP bars have better bond characteristics than the helically-grooved ones.

Figure 5.9 gives the moment crack width relationships for the tested beams. Table 5-6 lists of crack widths at 2,000 microstrains in the FRP bars, $0.3M_n$ and $0.67M_n$. Generally, increasing the $E_f A_f$ decreased the crack widths at all load levels. The average crack width in beams with axial stiffness around 60 MN was 62% and 51%, on average, that of beams with axial stiffness around 18 MN at 2,000 microstrains and $0.3M_n$, respectively. Figure 5.10 also confirms that beams with the same $E_f A_f$ with FRP bars of the same type and surface configurations are expected to exhibit the same moment-crack width relationship as in case of 5#15G3 and 2#25G3 and in case of 5#15G2 and 2#25G2.

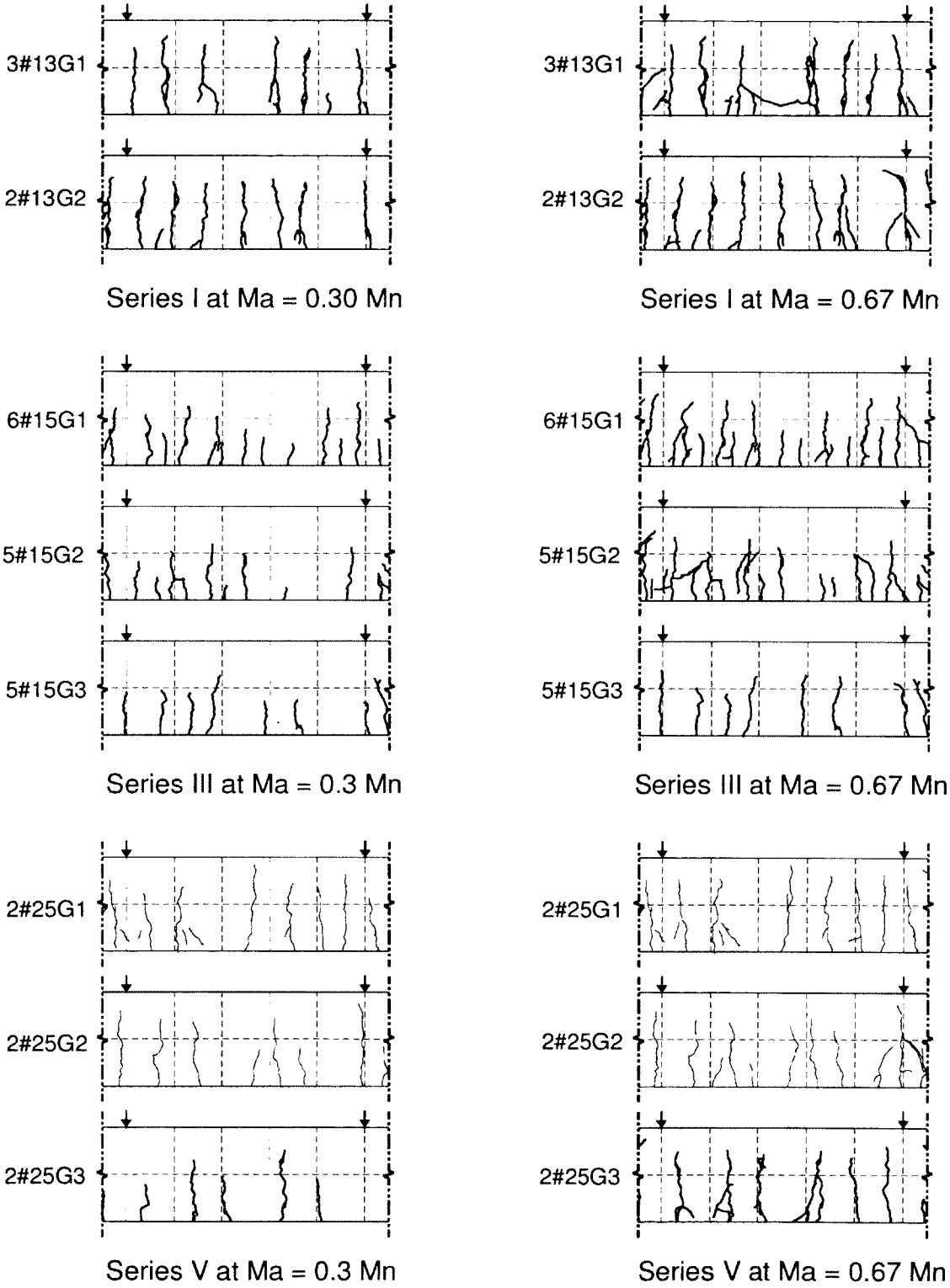

Figure 5.8 Crack patterns of beam specimens of Series I, III and V at $0.3M_n$ and $0.67M_n$

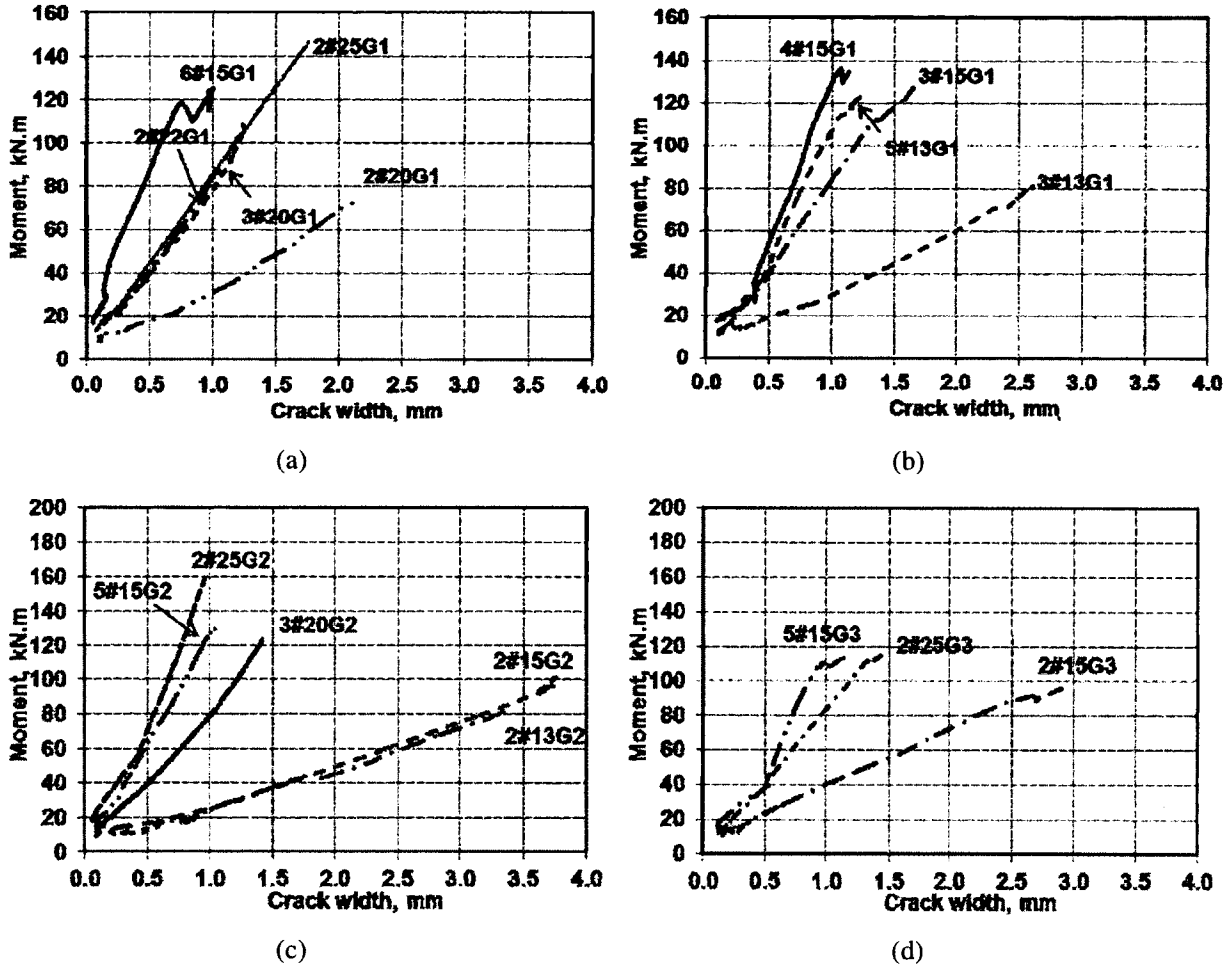

Figure 5.9 Crack width vs. applied moment for beams reinforced with different GFRP bars: (a) and (b) for GFRP-1; (c) for GFRP-2 and (d) for GFRP-3.

Concerning Vijay et GangaRao [2001] conclusion for curvature limit of $0.005/d$ at service to satisfy the cracking serviceability criteria, the relationship between the crack width and the curvature was plotted in Figure 5.10. The figure indicates that limiting the curvature of the FRP-reinforced concrete beams may be a possible solution to satisfy the serviceability. More investigations, however, are needed to verify the limit.

Table 5-6 Experimental-to-predicted crack widths (w_{exp}/w_{pred})

Beam	Measured crack width, w_{exp} (mm)				w_{exp}/w_{pred}								
					ACI 440 (2006)			ISIS M-03 (2007)			CSA S6 (2010)		
	Initial	2000 με	$0.30M_n$	$0.67M_n$	2000 με	$0.30M_n$	$0.67M_n$	2000 με	$0.30M_n$	$0.67M_n$	2000 με	$0.30M_n$	$0.67M_n$
3#13G1	0.10	0.40	0.78	1.82	1.11	1.03	1.08	1.02	0.88	0.90	1.95	1.68	1.73
5#13G1	0.05	0.23	0.46	0.82	0.76	0.86	0.70	0.70	0.75	0.59	1.33	1.39	1.12
2#13G2	0.20	0.77	1.03	2.38	1.62	0.95	1.01	1.71	0.94	0.99	2.81	1.58	1.63
3#15G1	0.10	0.37	0.85	1.44	1.04	1.39	1.07	0.9	1.13	0.85	1.91	2.26	1.71
4#15G1	0.08	0.38	0.41	0.77	1.17	0.85	0.71	1.03	0.69	0.57	2.05	1.38	1.14
2#15G2	0.22	0.62	1.18	2.56	1.35	1.54	1.50	1.40	1.52	1.46	2.23	2.56	2.45
2#15G3	0.16	0.31	0.63	1.68	0.66	0.71	0.84	0.69	0.69	0.81	0.92	0.92	1.10
6#15G1	0.05	0.14	0.15	0.44	0.36	0.18	0.25	0.31	0.15	0.20	0.64	0.31	0.40
5#15G2	0.09	0.30	0.31	0.70	0.81	0.55	0.55	0.68	0.44	0.44	1.40	0.92	0.92
5#15G3	0.12	0.53	0.40	0.69	1.40	0.59	0.46	1.20	0.48	0.37	2.03	0.54	0.61
2#20G1	0.10	0.33	0.73	1.53	0.71	0.83	0.79	0.70	0.76	0.71	1.25	1.33	1.26
3#20G1	0.15	0.32	0.51	1.17	0.87	0.94	0.96	0.75	0.73	0.76	1.54	1.48	1.52
2#22G1	0.09	0.47	0.51	1.05	0.98	0.70	0.65	0.96	0.63	0.58	1.73	1.13	1.04
3#20G2	0.11	0.38	0.66	1.35	1.08	1.22	1.11	0.93	0.95	0.87	1.83	1.92	1.76
2#25G1	0.10	0.36	0.55	1.28	0.76	0.87	0.9	0.72	0.66	0.70	1.31	1.37	1.42
2#25G2	0.06	0.33	0.36	0.73	0.70	0.65	0.58	0.66	0.56	0.50	1.21	1.02	0.92
2#25G3	0.13	0.53	0.45	0.93	1.09	0.86	0.80	1.05	0.78	0.72	1.53	1.14	1.05
Average					1.03	0.84	0.80	0.97	0.73	0.70	1.74	1.32	1.26
Standard deviation					0.40	0.32	0.29	0.43	0.30	0.28	0.69	0.56	0.49
Coefficient of variation (%)					39%	38%	37%	44%	40%	40%	40%	43%	38%

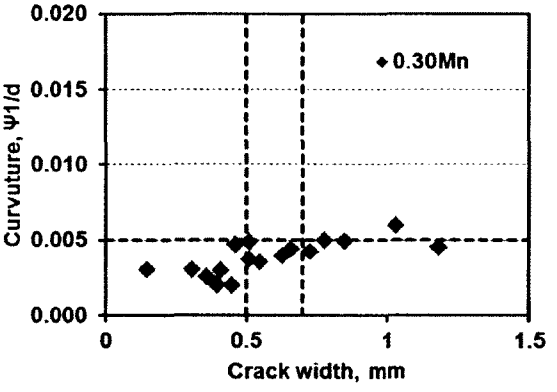

Figure 5.10 Crack width versus curvature Ψ 1/*d* for tested beams

Ductility and deformability

Ductility can be defined as the capacity of a structure to absorb energy without suffering failure, and is generally related to the amount of inelastic deformation that takes place before a complete failure. In other words, it could be represented as the ability to sustain inelastic deformations without loss of its load-carrying capacity prior to failure. For steel-RC members, ductility can be calculated as the ratio of the total deformation at failure divided by the deformation at yielding. This way of estimating ductility, however, cannot be applied to FRP-reinforced concrete structures because of the linear elastic behaviour of the FRP until failure.

An alternative concept based on deformability rather than ductility has been proposed by Jaeger *et al.* [1997] and Newhook *et al.* [2002] to ensure that there is enough deformation of the structural FRP- reinforced concrete element before failure. ISIS Manual No.3 [2007] and CAN/CSA-S6.1S1 [2010] concept is based on computing the deformability factor, *J*, from Eq. [5.8] (where, M is the bending moment, Ψ is the curvature, and the subscripts u and s refer to ultimate state and service limit state) at a corresponding concrete strain of 1,000 microstrains while Newhook *et al.* [2002] is based on calculating the *J* factor at a corresponding strain of 2,000 microstrains in the FRP reinforcement.

$$Deformation\ factor = \frac{\psi_U M_U}{\psi_S M_S} \qquad 5.8$$

ISIS Manual No.3 [2007] and CAN/CSA-S6.1S1 [2010] state that the deformability factor, *J*, should equal to, at least, 4.0 for rectangular sections and 6.0 for T-sections. On the other hand, Newhook *et al.* [2002] suggested that the value $\Psi_s M_s$ should be taken corresponding to 2,000 microstrains in the FRP reinforcement (service state). Table 5-7 presents the deformability factor, *J*, of the tested beams according to CAN/CSA-S6.1S1 [2010] and Newhook *et al.* [2002]. According to CAN/CSA-S6.1S1 [2010], the deformability factor, *J*, ranged from

0.5 to 8 which did not meet the requirements of the CAN/CSA-S6.1S1 [2010] for many beams. The premature buckling and the smaller concrete strains at failure affects the deformability index that may be used to verify the ductility of FRP- reinforced concrete members as provided by CAN/CSA-S6.1S1 [2010]. Thus, due to the limited strain capacity of the concrete in the tested specimens, the deformability factor based on the experimental results may be below the CAN/CSA-S6.1S1 [2010] threshold. Moreover, to satisfy the deformability requirements, special attention should be devoted towards the lateral ties (stirrups) in the critical flexural zone.

Table 5-7 Deformability of the tested beams at ε_c = 1,000 με and ε_{FRP} = 2,000 με

Beam	Curvature at ε_c = 1,000 με	Curvature at ε_{FRP} = 2,000 με	Moment at ε_c = 1,000 με	Moment at ε_{FRP} = 2,000 με	Moment at Ultimate state	curvature at Ultimate state	Deformability at ε_{FRP} = 2,000 με	Deformability at ε_c = 1,000 με
3#13G1	0.0110	0.0012	58.98	16.07	81.34	0.0153	64	1.9
5#13G1	0.0068	0.0024	56.13	22.70	130.37	0.0170	40	5.8
2#13G2	0.0088	0.0033	37.56	19.59	82.78	0.0189	24	4.7
3#15G1	0.0065	0.0026	47.78	16.34	108.78	0.0129	33	4.5
4#15G1	0.0068	0.0024	56.13	22.70	130.41	0.0016	4	0.5
2#15G2	0.0085	0.0023	60.98	17.46	102.73	0.0137	36	2.7
2#15G3	0.0071	0.0023	49.73	15.46	95.66	0.0124	33	3.4
6#15G1	0.0051	0.0012	61.76	16.68	118.34	0.0097	56	3.7
5#15G2	0.0037	0.0026	51.41	37.98	129.32	0.0101	13	6.9
5#15G3	0.0047	0.0025	69.00	39.95	110.58	0.0083	9	2.8
2#20G1	0.0084	0.0031	60.10	25.01	107.39	0.0157	22	3.3
3#20G1	0.0057	0.0024	64.40	27.92	140.35	0.0155	33	5.9
2#22G1	0.0077	0.0023	59.74	20.42	132.26	0.0163	46	4.7
3#20G2	0.0063	0.0024	73.91	31.16	171.29	0.0220	51	8.0
2#25G1	0.0062	0.0020	81.59	32.97	155.36	0.0208	48	6.4
2#25G2	0.0054	0.0024	106.04	47.64	175.34	0.0170	26	5.2
2#25G3	0.0046	0.0026	70.07	41.39	115.93	0.0081	9	2.9

[1] Service state defined as strain corresponds to 1,000 με of compressive strain in concrete
[2] Service state defined as strain corresponds to 2,000 με of FRP strain recommended by [ISIS Manual No.3, 2007]

In this respect, Park et Paulay [1975] suggested that the maximum spacing of closed ties in the plastic hinge zone of a RC member should be *d*/4 for proper moment redistribution.

Rasheed *et al.* [2005] concluded that to ensure realization of full potential with respect to ductility, the maximum spacing of ties in RC flexural members need to be maintained at *d*/4, particularly at critical sections. This will prevent premature disintegration of the confined concrete core in the compression zone due to buckling of compression reinforcement.

Vijay et GangaRao [2001], based on experimental results, reported that *c/d* ratio in range of 0.15 to 0.30 appears to be a reasonable design choice for concrete beams and slabs to achieve a deformability factor of 6 or higher. Furthermore, the increase of deformability factor more than 6 were attributed to several factors such as plastic hinge formation, confinement, significant concrete cracking in compression zone and stress distribution [Vijay et GangaRao, 1996]. The *c/d* ratio reported in Table 5-4 revealed that beams with *c/d* ratios greater than or equal to 0.15 showed deformability factors, *J*, equal to 4 or above except two beams.

The deformability index calculated according to Newhook *et al.* [2002] (2,000 microstrains in the FRP reinforcement) ranged from 4 to 64; however, there is no limit to compare with. Further investigation is needed to define limits when this definition is employed.

Deflection Provisions

ACI-440.1R-06 (ACI 440, 2006)

ACI 440.1R-06 [2006] specifies the effective moment of inertia formulation, I_e, to be employed in calculating the deflection of the cracked FRP-reinforced concrete beams and one-way slabs. The procedure entails calculating a uniform moment of inertia throughout the beam length and uses deflection equations derived from linear elastic analysis. The current ACI 440.1R-06 [2006] deflection equation is shown in Eq. [5.9 and 5.10]:

$$I_e = (M_{cr}/M_a)^3 \beta_d I_g + [1-(M_{cr}/M_a)^3] I_{cr} \le I_g \quad 5.9$$

$$\beta_d = 0.2(\rho_f/\rho_{fb}) \le 1.0 \quad 5.10$$

ISIS Manual No. 3 (ISIS M-03, 2007)

ISIS Manual No.3 [2007] presented Eq. [5.11] which was based on Mota *et al.* [2006a] proposal for the effective moment of inertia reported that Eq. [5.11] provides consistently conservative predictions over the entire range of the test specimens they used.

$$I_e = \frac{I_g I_{cr}}{I_{cr} + \left(1 - 0.5\left(\frac{M_{cr}}{M_a}\right)^2\right)(I_g - I_{cr})} \quad 5.11$$

ACI-440-H (2010)

ACI 440-H [2010] proposed an alternative expression for the effective moment of inertia, I_e, that works equally well for both steel and FRP-reinforced concrete members without the need for empirical correction factors [Bischoff, 2005; Bischoff et Scanlon, 2007c]. The ACI 440-H [2010] equation was provided to estimate the deflection for GFRP-, CFRP-, AFRP- and steel-reinforced concrete beams and one-way slabs. The expression is presented in Eq. [5.12].

$$I_e = \frac{I_{cr}}{[1-\eta\left(\frac{M_{cr}}{M_a}\right)^2]} \le I_g; \quad where\ \eta = [1-\left(\frac{I_{cr}}{I_g}\right)] \quad 5.12$$

CAN/CSA S806-02 (CSA S806, 2012)

CAN/CSA-S806 [2012] employs curvature integration along the span to determine the deflection of a concrete member at any point, assuming the section is fully cracked with no

tension stiffness contribution in the cracked regions of the beam. Thus, CAN/CSA-S806 [2012] provided deflection equation such as Eq. [5.13] for a simply supported member subjected to two-point loading:

$$\delta_{\max} = \frac{PL^3}{24E_c I_{cr}}\left[3\left(\frac{a}{L}\right) - 4\left(\frac{a}{L}\right)^3 - 8\eta\left(\frac{L_g}{L}\right)^3\right]; \quad where\ \eta = (1 - \frac{I_{cr}}{I_g}) \qquad 5.13$$

Crack Width Provisions

The FRP design codes and guidelines permit a larger crack width for FRP- reinforced concrete elements compared to their counter parts reinforced with steel. CAN/CSA-S806 [2012] and CAN/CSA-S6.1S1 [2010] specify on service-limiting flexural-crack width of 0.50 mm for exterior exposure (or aggressive environmental conditions) and 0.70 mm for interior exposure. In addition, ACI 440.1R-06 [2006] recommends using CAN/CSA-S6.1S1 [2010] limits for most cases. On other hand, since there is a direct relationship between the strain in the reinforcing bars and the crack width, ISIS Manual No.3 [2007] specifies 2,000 microstrains as a strain limit in FRP reinforcing bars to central crack width.

ACI 440.1R-06 (ACI 440, 2006)

Frosch [1999] observed that Gergely-lutz equation [Gergely et Lutz, 1968] was developed on the basis of limited range of concrete cover distance. Thus, an alternative expression was provided to best first the experimental results over a large range concrete cover. This was developed by replacing part of the equation, (A_c) tension zone area, by spacing between bars. The current ACI 440.1R-06 [2006] and CAN/CSA-S6.1S1 [2010] adopted the Frosch's

equation [Frosch, 1999] by introducing k_b bond-coefficient to the equation as following (Eq. [5.14]):

$$w = 2\frac{f_f}{E_f}\frac{h_2}{h_1}k_b\sqrt{d_c^{\,2}+\left(\frac{s}{2}\right)^2} \qquad 5.14$$

ISIS Manual No. 3 (ISIS M-03, 2007)

Historically, the most common used crack width equation was Gergely-lutz equation [Gergely et Lutz, 1968] which was developed using a data base of nearly 1000 crack width measurements from several studies [Gross *et al.*, 2009]. The equation was proposed for the steel reinforced concrete members. The equation was, then, generalized to other types of reinforcement such as FRP. This equation, as shown in Eq. [5.15] was modified by replacement the steel reinforcement stress with reinforcing strain and introducing bond-dependent coefficient to account for different surface configuration available in the current reinforcement used (GFRP bars).

$$w = 2\frac{f_f}{E_f}\frac{h_2}{h_1}k_b\sqrt{d_c^{\,2}+\left(\frac{s}{2}\right)^2} \qquad 5.15$$

The ISIS Manual No.3 [2007] set a k_b value of 1.2 for all types of reinforcement bars in absence of significant test data.

CAN/CSA S6.1S1-10 (CSA S6, 2010)

The CAN/CSA-S6.1S1 [2010] employs the same equation as the ACI 440.1R-06 [2006] as shown in Eq. [5.16]. Similar to CAN/CSA-S806 [2012], the crack width has to be verified when maximum tensile strain in FRP reinforcement under full service exceeds 0.0015.

$$w = 2\frac{f_f}{E_f}\frac{h_2}{h_1}k_b\sqrt{d_c^2 + (s/2)^2} \quad 5.16$$

The value of k_b shall be determined experimentally, but in the absence of test data may be taken as 0.8 for sand-coated and 1.0 for deformed FRP bars. In calculating d_c, the clear cover shall not be taken greater than 50 mm.

Comparison between Experimental and Predicted Results

Deflection

Assuming that beam deflection limit at service load is span/240 (L/240) as provided for by CAN/CSA-S806 [2012] which yields 15.63 mm all beams except 3#15G1, 2#15G2, 2#20G1 and 2#22G1 exhibited deflection smaller than 15.63 at $0.3M_n$. The predicted deflections of the tested beams were compared with the experimental deflection values at $0.3M_n$ and $0.67M_n$. Table 5-5 provides the experimental-to-predicted deflection ratios ($\delta_{exp}/\delta_{pred}$). Based on the predicted deflections, the ACI 440.1R-06 [2006] and ACI 440-H [2010] underestimated the deflection at $0.3M_n$ load level with an overall average $\delta_{exp}/\delta_{pred}$ value of 1.22±0.23 and 1.25±0.14, respectively. However, both CAN/CSA-S806 [2012] and ISIS Manual No.3 [2007] equations slightly underestimated the deflection for all beams at $0.67M_n$ load level with an average $\delta_{exp}/\delta_{pred}$ value of 1.01±0.14 and 1.00±0.12, respectively. On the other hand, CAN/CSA-S806 [2012] and ISIS Manual No.3 [2007] equations slightly overestimated the deflection for all beams at $0.3M_n$ load level with an average $\delta_{exp}/\delta_{pred}$ value of 0.89±0.20 and 0.90±0.15, respectively. The ISIS Manual No.3 [2007] equation showed the lowest COV amongst the used equations, namely 15%.

Crack Width

Most of the design codes specify a flexural crack width limit for steel-reinforced concrete structures to protect the reinforcing bars from corrosion and to maintain the structure's aesthetical appearance unlike steel reinforcement, FRP is corrosion resistant. Therefore, the serviceability limits for crack widths in FRP reinforced concrete elements may be directly related to aesthetic considerations.

Table 5-6 compares the measured crack widths to predicted values. The comparison was conducted at three different load levels: at 2,000 microstrains in the reinforcing bars, $0.3M_n$ and $0.67M_n$. The predictions were conducted using a k_b value of 1.4 for ACI 440.1R-06 [2006], and 1.2 for ISIS Manual No.3 [2007]. For CAN/CSA-S6.1S1 [2010], the predictions were conducted using a k_b value of 0.8 for sand-coated FRP bars, and 1.0 for helically-grooved FRP bars. The average $w_{exp.}/w_{pred.}$ at $0.3M_n$ load level calculated according to ACI 440.1R-06 [2006], CAN/CSA-S6.1S1 [2010] and ISIS Manual No.3 [2007] were 0.84±0.32, 1.32±0.56 and 0.73±0.30, respectively. Moreover, there were no significance differences between the $w_{exp.}/w_{pred.}$ at $0.3M_n$ and $0.67M_n$ load level. The degree of conservativeness was higher for the GFRP-reinforced concrete beams with multi-layer reinforcement.

At 2,000 με, both ACI 440.1R-06 [2006] and ISIS Manual No.3 [2007] yielded a good prediction for all beams with an average $w_{exp.}/w_{pred.}$ of 1.03±0.40 and 0.97±0.43, respectively. However, CAN/CSA-S6.1S1 [2010] underestimated the crack widths and the average $w_{exp.}/w_{pred.}$ was 1.74±0.69. Furthermore, ACI 440.1R-06 [2006] prediction equation revealed the lowest COV among all equations at 2000 με, $0.3M_n$ and $0.67M_n$ load levels.

It is worth mentioning that, as shown in Table 5-6, three beams showed crack widths exceeding 0.50 mm. Thus, maintaining the strain level in the GFRP reinforcing bars at 2000 microstrains at service load [ISIS Manual No.3, 2007] may keep the crack width below 0.50 mm. On the other hand, at $0.3M_n$, most of the tested beams showed crack widths exceeding 0.50 mm.

Conclusions

This paper investigated the flexural behaviour of concrete beams reinforced with different grades of GFRP bars that are being used extensively in Canada. Based on the results and discussions concluding remarks could be drawn as follows:

1- Generally, the axial stiffness (E_fA_f) is one of the key factors that govern the flexural behaviour of FRP-reinforced concrete members. The higher the E_fA_f, the better the flexural performance (higher ultimate capacity, lower deflection, smaller cracks widths).
2- Maintaining the same E_fA_f for beams reinforced with the same type of GFRP bars is expected to yield similar behaviour for deflection and ultimate capacity. The larger diameter of GFRP bars, however, is expected to yield fewer numbers of flexural cracks and larger crack widths.
3- At 2,000 microstrains in the GFRP reinforcing bars, some beams showed crack widths larger than 0.5 mm. Limiting the strain to 2,000 microstrains is not an absolute assumption to keep the crack width controlled. The crack widths should be verified at service load levels.
4- The curvature of the GFRP-reinforced concrete members at service may be considered as a limiting parameter to keep the crack width and deflection controlled. The $0.005/d$ provided by Vijay et GangaRao [2001] seems to be feasible for some beams. More verification and refinement, however, are needed.

5- The cracking behaviour of the tested beams tends to confirm that the bond performance of sand-coated GFRP bars is better than the helically-grooved GFRP bars due the bond mechanism difference between the sand-coated and helically-grooved GFRP bars.

6- At 2,000 microstrains in FRP bars, both ACI 440.1R-06 [2006] and ISIS Manual No.3 [2007] yielded good crack-width predictions, on average. However, CAN/CSA-S6.1S1 [2010] underestimated the crack widths. At $0.3M_n$, ACI 440.1R-06 [2006] and CAN/CSA-S6.1S1 [2010] showed un-conservative values of crack widths, while ISIS Manual No.3 [2007] showed good agreement with experimental results. The degree of conservativeness for all predictions was higher for the GFRP reinforced concrete beams with multi-layer reinforcement.

7- The predicted deflections ISIS Manual No.3 [2007] and CAN/CSA-S806 [2012] were in reasonable agreements with the experimentally measured values.

8- Newhook *et al.* [2002] deformability index definition seems feasible for GFRP-reinforced concrete beams. Governing limits, however, need to be provided.

CHAPTER 6

CONCLUSION AND RECOMMENDATIONS FOR FUTURE WORK

6.1 Summary

This research program aimed at investigating the flexural behaviour and serviceability performance of concrete members reinforced with different types and ratios of carbon and glass FRP bars and fabricated using normal-and high-strength concretes. In addition, it evaluates the bond-dependent coefficient (k_b) of glass and carbon FRP bars in normal- and high-strength concretes. This study included an experimental program for fabricating and testing of thirty three full-scale simply-supported beams measuring 4250-mm long × 200-mm wide × 400-mm deep. Twenty seven concrete beams were reinforced with glass FRP bars, four concrete beams were reinforced with carbon FRP bars and two control beams reinforced with steel. All beams were tested in four-point bending over a clear span of 3750 mm. The main variables considered in the study were reinforcement type and ratio, FRP bar diameter, surface configurations, number of layers, and concrete strength. The FRP properties were obtained from testing of five samples for each FRP type and diameter according to ASTM D7205 [2011]. The test results of the beam specimens were presented and discussed in terms of flexural capacity and mode of failure, concrete and reinforcement strains, deflection, and crack widths through three journal papers presented in the course of this thesis.

Among the three papers presented in this thesis, two investigated the flexural behaviour and serviceability performance of carbon and glass FRP-reinforced concrete beams fabricated with normal- and high-strength concretes. The two papers investigated GFRP bars of different grades, diameters, and surface configurations. While the third one evaluated the current design recommendations for bond-dependent coefficient (k_b) values and checked the dependency of the k_b values on FRP bar type (glass and carbon), diameter, and concrete type and strength. The cracking moments and flexural capacity were compared against the provisions of the North American codes and guidelines [ACI 440.1R-06, 2006; ISIS Manual No.3, 2007; CAN/CSA-S6.1S1, 2010; CAN/CSA-S806, 2012]. In addition, the experimental results were employed in assessing the accuracy of the current deflection and crack-width prediction equations and the k_b values in the FRP design codes and guidelines in North America [ACI 440.1R-06, 2006; ISIS Manual No.3, 2007; CAN/CSA-S6.1S1, 2010; CAN/CSA-S806, 2012]. The results introduced the effect of different parameters on the flexural behaviour and serviceability performance of the FRP- reinforced concrete members. Furthermore, the findings did not support the unique k_b value for FRP bars of different types (carbon and glass) with similar surface configurations and was found to be dependent on bar diameter.

6.2 Conclusions

Based on the results of this study and considering the used materials, the findings of this investigation can be summarized as follows:

6.2.1 Flexural behaviour of FRP reinforced beams

- All the GFRP- reinforced concrete beams showed typical bi-linear load-deflection relationships until failure. Both NSC and HSC evidenced reduced stiffness after cracking.

The NSC and HSC beams showed similar behaviour until failure. The post-cracking flexural stiffness of the HSC was higher than that of the NSC when the same axial-reinforcement stiffness (E_fA_f) was provided.

- The E_fA_f is one of the key factors that govern the flexural behaviour of FRP-reinforced concrete members. The higher the E_fA_f, the higher the ultimate capacity.
- Concrete strength and reinforcement ratio have an influence in the flexural behaviour. Using HSC led to increase in the flexural capacity of ≈ 30% than the NSC.
- ACI 440.1R-06 [2006] predicted the flexural capacity with reasonable tolerance of 10 to 12 %. This is attributed to reasonable assumption of ultimate concrete strain (3,000 microstrains) for the unconfined concrete.

6.2.2 Concrete strain

- The concrete stain at the extreme compressive fibre showed typical bi-linear relationship against the moment until failure. The concrete strains were affected by the reinforcement ratio and the concrete strength. Increasing the reinforcement ratio or the concrete strength reduced the concrete strain at the same load level.
- The ultimate concrete strain was lower than expected due to the absence of stirrups in the critical flexural zone of the beams. This led to that concrete's compression failure in some beams was triggered by the buckling of the compression steel reinforcement. This premature buckling was due to a large unsupported length of compression bars (300 mm). This confirms Park et Paulay [1975] and Rasheed *et al.* [2005] conclusions that a maximum spacing between closed ties of $d/4$ in the plastic hinge zone of a RC member is required for proper moment redistribution and to ensure realization of full potential with

respect to ductility. This will prevent premature disintegration of the confined concrete core in the compression zone due to bucking of compression reinforcement.

6.2.3 FRP Strains

- After cracking state, the strains in the FRP bars increase linearly till failure. As the bar diameter and the $E_f A_f$ decreases, the strains increased at the same load level. The surface configuration also indicated some effects on the measured strains.
- The NSC and HSC beams with low reinforcement ratios, ρ_f, (0.56% or less) showed very sharp increases in reinforcement strains at cracking of over 3,000 microstrains. While the beams were designed as over-reinforced sections, this did not prevent the large strain increase due to poor energy absorption at cracking.
- At $0.3M_n$, the strains in the FRP bars were around 4,000 microstrains. This is agreement with the findings of Vijay et GangaRao [1996].

6.2.4 Cracking behaviour and bond-dependent coefficient (k_b)

- Using HSC increased the cracking moment of the GFRP- reinforced concrete beams compared to the NSC beams. The CAN/CSA-S806 [2012] modulus of rupture equation seems applicable for both NSC and HSC in the range of the tested concrete strengths.
- Maintaining the same $E_f A_f$ with larger diameter of GFRP bars yielded fewer numbers of flexural cracks and larger crack widths.
- Increasing the reinforcement ratio and concrete strength resulted in a larger number of cracks and smaller crack widths.

- Beams reinforced with sand-coated GFRP bars produced larger numbers of cracks and smaller crack widths than those reinforced with helically-grooved GFRP bars. This tends to confirm the better flexural bond characteristics of the sand-coated bars.
- Bar diameter had an effect on crack width as evidenced by the NSC and HSC beams reinforced with GFRP bars. Employing the same $E_f A_f$ with two different diameters of GFRP bars (No. 15 and No. 25) yielded higher crack widths with the No. 25 than with the No. 15. The effect was higher in NSC than in HSC.
- At 2,000 microstrains in the GFRP reinforcing bars, some beams showed crack widths larger than 0.5 mm. limiting the strain to 2,000 microstrains is not an absolute assumption to keep the crack width controlled. The crack widths should be verified at service load levels.
- Maintaining minimum practical reinforcement may be of interest to ensure that the section behaves reasonably after cracking and the sudden increase in the strains is minimized. This may have an impact on the current test method in CAN/CSA-S806 [2012], *Annex S*, to determine the k_b values when only two bars are recommended.
- The calculations of k_b values determined at crack width (w) = 0.7 mm, $0.30M_n$, and $0.25f_G$ were somewhat close. This supports using any of those limits as the recommended level at which the k_b values should be determined. The $0.30M_n$ value may be recommended as it has been used by many researchers as a service-load level. Moreover, at $0.30M_n$, the crack width was less than 0.7 mm in all the beams tested, except 3#13G1 and 2#13G2, which implicitly satisfies the requirements of CAN/CSA-S806 [2012], *Annex S*, of keeping 0.7 mm as the maximum crack width that could be used in determining k_b values.

- The bond-dependent coefficient (k_b) is dependent not only on bar surface configuration, but also on bar diameter and material type. Providing one value for k_b based solely on surface configuration was not supported by the test results. The results indicated that concrete strength (normal- and high-strength) had an impact, yet no trend or clear relationship was evidenced.
- At 2,000 microstrains in FRP bars, both ACI 440.1R-06 [2006] and ISIS Manual No.3 [2007] yielded good crack-width predictions, on average. However, CAN/CSA-S6.1S1 [2010] underestimated the crack widths.
- At $0.3M_n$, ACI 440.1R-06 [2006], and CAN/CSA-S6.1S1 [2010] showed un-conservative values of crack widths, while ISIS Manual No.3 [2007] showed good agreement with experimental results. The degree of conservativeness for all predictions was higher for the GFRP reinforced concrete beams with multi-layer reinforcement.
- The small k_b values of CAN/CSA-S6.1S1 [2010] compared to those of ACI 440.1R-06 [2006] and ISIS Manual No.3 [2007] contributed to underestimating crack widths.
- With the helically-grooved GFRP bars (G3: No. 15 and No. 25), employing a k_b of 1.2 in the ISIS Manual No.3 [2007] equation yielded very good agreement with the experimental results. The ACI 440.1R-06 [2006] equation, however, underestimated the crack width of No. 15 GFRP bars, while yielding good agreement for No. 25 GFRP bars.
- The bond coefficient (k_b) value of 1.4 is very conservative for both of sand-coated and helically-grooved GFRP bars in NSC and HSC. Reasonable crack-width predictions were obtained from ACI 440.1R-06 [2006] and CAN/CSA-S6 [2006] using a k_b factor of 1.2 for the helically-grooved GFRP bars and 1.0 for the sand-coated bars in NSC and HSC. A k_b of 0.8 provided by CAN/CSA-S6 [2006] yielded very un-conservative predictions, on

average, for sand-coated and helically-grooved GFRP bars in NSC and HSC. This value (k_b=0.8), however, yielded good yet conservative crack-width prediction for multi-layer sand-coated GFRP bars in NSC and HSC.

- With the sand-coated CFRP bars (C1: No. 10 and No. 13), ACI 440.1R-06 [2006] and ISIS Manual No.3 [2007] showed reasonably close predictions using k_b values of 1.4 and 1.2, respectively. On the other hand, the predictions were reasonable with some diameters and showed discrepancies for the others with the sand-coated GFRP bars type (G1 and G2).
- Using a k_b of 0.8 for the sand-coated FRP bars (carbon and glass) with the CAN/CSA-S6.1S1 [2010] equation underestimated the predicted crack widths in most of the tested beams fabricated using normal- and high-strength concretes.
- The bond-dependent coefficient (k_b) introduced by FRP design codes and guidelines should be revised to include the effect of bar diameter, FRP material type, and concrete strength, in addition to the surface configuration.

6.2.5 Deflection and curvature

- Except beams with low reinforcement ratios, ρ_f, the curvature at $0.30M_n$ was $0.004/d$. The GFRP beams satisfied deflection and crack-width serviceability limits ($L/240$ for deflection and 0.7 mm [0.03 in.] for crack width). This partially confirms Vijay et GangaRao [1996] findings. A minimum reinforcement ratio, however, has to be maintained to generalize this phenomenon.
- The curvature of the GFRP-reinforced concrete members at service may be considered as a limiting parameter to keep the crack width and deflection controlled. The $0.005/d$

provided by Vijay et GangaRao [2001] seems to be feasible for some beams. More verification and refinement, however, are needed.

- After cracking phase, defection and flexural curvature follow a linear relationship till failure, which indicates that bar strain has more contribution to curvature than concrete strains.
- Higher values of concrete strength and reinforcement-to-balanced ratio led to higher *c/d* ratio, smaller compressive concrete strains and thus, smaller curvature and deflections.
- The test results did not support any effect of bar diameter or surface configuration of the GFRP bars on the deflection of the NSC and HSC beams.
- ACI 440.1R-06 [2006] and ACI 440-H [2010] yielded un-conservative deflection values at the $0.3M_n$ and $0.67M_n$. While CAN/CSA-S806 [2012] and ISIS Manual No.3 [2007] yielded conservative deflection predictions at the $0.3M_n$.
- At load levels beyond the cracking, the load-deflection responses predicted by ACI 440.1R-06 [2006]; ACI 440-H [2010]; CAN/CSA-S806 [2012]; ISIS Manual No.3 [2007] are noticed to have large increase in deflection and rapidly approach the behaviour of fully cracked section. This sudden loss in stiffness, however, was not observed during any experimental test and can be attributed to misevaluation of the tension stiffening phenomenon.

6.2.6 Deformability

- The stirrups' spacing in the flexural zone is an important factor to provide appropriate deformability at service load. The absence of the transverse reinforcement (stirrups) may initiate the concrete failure due to buckling of the compression reinforcement.

- Deformability could depend on the concrete strains or the FRP strains, however, a well definition to service load state in term of load or strains in FRP or concrete will properly adjust predicting the deformability.

6.3 Recommendation for future work

Based on the findings of this study, the following suggestion for future work could be introduced:

- Deformability of FRP reinforced members should be further investigated.
- The effect of lateral reinforcement (stirrups) on the flexural behaviour and serviceability of FRP reinforced members should be investigated.
- Serviceability (deflection and cracking) study should be extended to include the FRP-prestressed concrete members.
- Shear induced deflection may be investigated considering different types of FRP stirrups as shear reinforcement.
- Different concrete types may also be investigated such as self-consolidated concrete and high performance concrete.
- Performance of FRP reinforced members subjected to fatigue and cyclic loads at service conditions should be investigated.

CHAPTER 7

CONCLUSIONS, RECOMMANDATIONS ET DES TRAVAUX FUTURS

7.1 SOMMAIRE

Ce programme de recherché focalise sur l'investigation du comportement à la flexion et de la performance en service d'éléments en béton renforcés avec différents types et différents pourcentages de barres d'armature à base de fibres de verre et de fibres de carbone et fabriqués avec un béton normal et un béton à haute performance.

Ce programme évalue aussi le coefficient d'adhérence (k_b) de barres d'armature en fibres de verre et de carbone et fabriqué avec du béton normal et du béton à haute performance. Cette étude inclue un programme expérimental pour la fabrication et les essais de 33 poutres à grande échelle de 4250 mm de long, 200 mm de largeur et 400 mm m de profondeur. 27 poutres en béton étaient renforcées de barres en PRFV (verre), 8 poutres étaient renforcées de barres en PRFC (carbone) et 2 poutres en béton renforcés d'acier.

Toutes les poutres ont été testées en flexion quatre points sur une portée libre de 3750 mm. Les paramètres d'essai étaient: le type de renfort et ratio, le diamètre des barres d'armature, la configuration de surface, l'épaisseur et la résistance du béton. Les propriétés des barres en PRF étaient obtenues à partir des essais sur 5 échantillons pour chaque type de barre et chaque diamètre selon la norme ASTM D7205 [2011].

Les résultats des essais effectués sur ces poutres sont présentés et analysés en termes de résistance à la flexion et mode de rupture, de déformations du béton et des renforcements, de déflection, et de largeur de fissures, à travers 3 articles scientifiques présentés dans cette thèse.

Parmi les trois journaux présentés dans cette thèse, deux ont étudié le comportement en flexion et les performances en service de membrures de béton armé de barres de PRFC et de PRFV fabriqués avec du béton normal ou à haute résistance

Les deux articles ont portés sur des barres de PRFV de différents grades, diamètres et configurations de surface. Le troisième article a, quant à lui, évalué les recommandations actuelles de conception liées au coefficient d'adhérence (k_b) et vérifié la dépendance des valeurs de k_b en fonction du type de barre (PRFV ou PRFC), du diamètre des barres et du type et de la résistance du béton.

Les moments de fissuration et la capacité de flexion ont été comparés aux codes de conception et guidelines nord-américains [ACI 440.1R-06, 2006; ISIS Manuel No.3, 2007; CAN/CSA-S6.1S1, 2010; CAN/CSA-S806, 2012]. En outre, les résultats expérimentaux ont été utilisés pour évaluer l'exactitude de la déflection et des équations de prédiction de largeur fissures et les valeurs du coefficient k_b disponibles dans les codes de conception en Amérique du Nord [ACI 440.1R-06, 2006; ISIS Manuel No.3, 2007; CAN/CSA-S6.1S1, 2010; CAN/CSA-S806, 2012].

Les résultats introduisent l'effet de différents paramètres sur le comportement en flexion et la performance en service des éléments de béton armé à l'aide de PRF. En particulier, les conclusions n'adhèrent pas à l'hypothèse d'une valeur unique de k_b pour les barres en PRF de

différents types (carbone ou verre) avec des configurations de surface similaires, k_b s'étant avéré être dépendant du diamètre de la barre.

7.2 Conclusions

À la lumière des résultats de cette étude et en considérant les matériaux utilisés, les conclusions peuvent être résumées comme suit:

7.2.1 Comportement en flexion de poutres renforcées de PRF

- Toutes les poutres renforcées de barres en PRFV ont montré un comportement charge-déflection typiquement bilinéaire jusqu'à la rupture. Le béton normal et le béton à haute performance réduisent la rigidité après fissuration. Les boutres fabriquées avec un béton normal et un béton à haute performance ont montré un comportement similaire jusqu'à la rupture. La rigidité de flexion après fissuration du béton à haute performance était plus élevée que celle du béton normal.
- La rigidité axiale $E_f A_f$ est l'un des facteurs clé qui gouverne le comportement en flexion des éléments en béton renforcés de PRF.
- En utilisant un béton à haute performance, il y a augmentation de la capacité de flexion d'environ 30% que le béton normal.
- Le code ACI 440.1R-06 [2006] prédit la capacité en flexion avec une tolérance raisonnable de 10 à 12%. Ceci est attribué à la supposition raisonnable de la déformation ultime du béton (3,000 microstrains) pour un béton non-confiné.

7.2.2 Déformation du béton

- La déformation du béton sur la fibre comprimée montre un comportement typiquement bilinéaire jusqu'à la rupture. Les déformations du béton étaient affectées par le pourcentage d'armature et la résistance à la compression du béton. L'augmentation du pourcentage d'armature et de la résistance du béton réduit les déformations du béton pour un même niveau de chargement.
- La déformation ultime du béton était plus basse que celle attendue et est due à l'absence d'étriers dans la zone critique de flexion des poutres. La rupture en compression du béton dans certaines poutres était contrôlée par le flambement de l'armature en compression d'acier. Ce flambement prématuré était dû au non support de barres en compression (300 mm). Cela confirme les conclusions de Park et Paulay, [1975] et Rasheed *et al.*, [2005] que l'espacement maximum de *d*/4 entre les étriers fermés dans la zone plastique d'un élément est requis pour le moment de redistribution et pour assurer le plein potentiel par rapport à la ductilité. Cela préviendra la désintégration prématurée du béton confiné dans la zone de compression du au flambement de l'armature de compression.

7.2.3 Déformations des PRF

- Après fissuration, les déformations dans les barres d'armature en PRF augmentent linéairement jusqu'à la rupture. Comme le diamètre de la barre et le rapport $E_f A_f$ diminuent, les déformations augmentent pour un même niveau de chargement. La configuration de surface indique aussi quelques effets sur les déformations mesurées.

- Les poutres fabriquées avec un béton normal et un béton à haute performance avec un bas pourcentage d'armature ρ_f, (0,56 % ou moins) montrent une augmentation des déformations de l'armature à la fissuration de plus de 3000με. Même si les poutres sont sur-renforcées, cela ne prévient pas l'augmentation de larges déformations dues à une faible énergie d'absorption à la fissuration
- À $0.3M_n$, les déformations dans les barres d'armature en PRF étaient d'environ 4000με. Ce qui est en accord avec les conclusions de Vijay et GangaRao [1996].

7.2.4 Comportement à la fissuration et coefficient d'adhérence (k_b)

- L'utilisation d'un BHP augmente le moment de fissuration des poutres en PRFV comparativement aux poutres avec un béton normal. L'équation du module de rupture du code canadien CAN/CSA-S806, [2012] semble applicable pour les deux types de bétons (BHP et normal) dans les limites des résistances des bétons testés.
- En maintenant le même rapport E_fA_f avec des barres en PRFV de plus grand diamètre, il y a peu de fissures de flexion et des fissures plus larges
- L'augmentation du pourcentage d'armature et de la résistance du béton résulte en un plus grand nombre de fissures et des largeurs de fissures plus petites.
- Les poutres renforcées de barres en PRFV saupoudrées de sable produisent un plus grand nombre de fissures et des largeurs de fissures plus petites que celles renforcées de barres en PRFV avec des rainures hélicoïdales. Cela tend à confirmer de meilleures caractéristiques d'adhérence en flexion des barres saupoudrées de sable.
- Le diamètre de la barre a un effet sur la largeur des fissures pour les poutres renforcées de barres en PRFV. En utilisant le même E_fA_f avec deux diamètres differents de barres en

PRFV (No. 15 et No. 25), des largeurs de fissures plus grandes avec le diamètre No. 25 qu'avec le diamètre No. 15. L'effet est plus prononcé avec le béton normal qu'avec le BHP.

- Pour des déformations de l'ordre de 2000με dans les barres en PRFV, certaines poutres montrent des largeurs de fissures plus grandes que 0,5 mm. La limitation de la déformation à 20000 με n'est pas une supposition absolue pour contrôler la largeur des fissures. Les largeurs de fissures devraient être vérifiées aux niveaux de la charge de service.
- Le maintien d'armature minimale peut être d'un intérêt pour assurer que la section se comporte raisonnablement après fissuration et que l'augmentation soudaine dans les déformations soient minimisées. Cela peut avoir un impact sur la méthode d'essai dans le code CAN/CSA-S806, [2012], *Annexe S*, pour déterminer les valeurs de k_b lorsque seulement deux barres sont recommandées.
- Le calcul des valeurs de k_b déterminé pour une largeur de fissures (w) = 0,7 mm, $0.30M_n$, et $0.25f_G$ étaient quelque peu proches. La valeur de $0.30M_n$ devrait être recommandée, comme elle l'a été utilisée par plusieurs chercheurs à un niveau de chargement en service. En outré, à $0.30M_n$, la largeur des fissures était moins que 0,7 mm pour toutes les poutres testées, sauf la 3#13G1 et 2#13G2, lesquelles implicitement satisfont les exigences du code CAN/CSA-S806, [2012], *Annexe S* en gardant 0,7 mm comme la largeur maximale des fissures qui devrait être utilisée dans la détermination des valeurs de k_b.
- Le coefficient d'adhérence (k_b) est dépendant, pas seulement de la configuration de la surface de la barre, mais aussi du diamètre de la barre et du type de matériau. Les

résultats montrent que la résistance du béton (normal et à haute performance) a un impact.

- Pour des déformations de l'ordre de 2000με des barres en PRF, le code de l'ACI 440.1R-06 [2006] et le manuel d'ISIS No.3, [2007] donnent, en moyenne, de bonnes prédictions de la largeur des fissures. Cependant, le code CAN/CSA-S6.1S1 [2010] sous-estiment les largeurs de fissures.
- À $0.3M_n$, le code de l'ACI 440.1R-06 [2006] et le code CAN/CSA-S6.1S1 [2010] montrent des valeurs non conservatrices des largeurs de fissures, alors que le manuel ISIS No.3 [2007] est en parfait accord avec les résultats expérimentaux. Le degré de conservation pour toutes les prévisions est plus élevé pour les poutres en béton renforcées de barres en PRFV avec plusieurs lits d'armature.
- Les petites valeurs de k_b du code CAN/CSA-S6.1S1 [2010] comparées à celles de l'ACI 440.1R-06 [2006] et du manuel d'ISIS No.3 [2007] contribuent à la sous-estimation des largeurs de fissures.
- Pour les barres en PRFV avec des rainures hélicoïdales (G3: No. 15 et No. 25), utilisant un k_b de 1,2 du manuel d'ISIS No.3 [2007], l'équation est en accord avec les résultats expérimentaux. Cependant, l'équation du code de l'ACI 440.1R-06 [2006] sous-estiment la largeur des fissures avec les barres en PRFV No. 15, alors qu'elle est en parfait accord avec les barres en PRFV No. 25.
- La valeur du coefficient d'adhérence (k_b) de 1,4 est très conservatrice pour les deux types de barres (recouvertes de sables et avec rainures hélicoïdales) dans des bétons normaux et des bétons à haute performance. Les prédictions raisonnables des largeurs de fissures

étaient obtenues du code de l'ACI 440.1R-06 [2006] et du code CAN/CSA-S6 [2006] en utilisant un facteur k_b de 1,2 pour les barres PRFV avec des rainures hélicoïdales et un facteur de 1,0 pour les barres saupoudrées de sable dans des bétons normaux et des bétons à haute performance. Un facteur k_b de 0,8 fourni par le code CAN/CSA-S6 [2006] montre, en moyenne, des prédictions non conservatrices pour les barres saupoudrées de sable et les barres avec des rainures hélicoïdales dans des bétons normaux et des bétons à haute performance. Cependant, cette valeur de 0,8 montre encore une prédiction conservatrice de la largeur des fissures pour les barres en PRFV saupoudrées de sable dans des bétons normaux et des bétons à haute performance.

- Avec des barres en PRFC saupoudrées de sable (C1: No. 10 et No. 13), le code de l'ACI 440.1R-06 [2006] et le manuel d'ISIS No.3 [2007], montrent des prédictions proches en utilisant des valeurs de k_b de 1,4 et 1,2 respectivement. D'un autre côté, les prédictions sont raisonnables avec certains diamètres, mais sont contradictoires avec d'autres barres en PRFV saupoudrées de sable (G1 et G2).
- En utilisant un facteur k_b de 0,8 pour les barres en PRF saupoudrées de sable (carbone et verre) avec le code CAN/CSA-S6.1S1 [2010], l'équation sous-estiment les largeurs des fissures prédites dans la plupart des poutres testées, et fabriquées avec des bétons normaux et des bétons à haute performance.
- Le coefficient d'adhérence (k_b) introduit par les codes de design et les guidelines de calcul devrait être révisé pour tenir compte de l'effet du diamètre de la barre, du type de matériau, de la résistance à la compression du béton ainsi que la configuration de surface.

7.2.5 Déflection et courbure

- Mis à part les poutres avec un bas pourcentage d'armature ρ_f, la courbe était, à $0.30M_n$, de 0,004/*d*. Les poutres en PRFV satisfont la déflection et la largeur des fissures à l'état limite de service (*L*/240 pour la déflection et 0,7 mm [0,03 in.] pour la largeur des fissures). Cela confirme partiellement les conclusions de Vijay et GangaRao, [1996]. Cependant, un minimum de pourcentage d'armature doit être maintenu pour généraliser ce phénomène.
- La courbure des éléments en béton renforcés de barres en PRFV, en service, doit être considérée comme un paramétré limite pour contrôler la largeur des fissures et la déflection. Le rapport 0.005/*d* proposé par Vijay et GangaRao, [2001] semble être adéquat pour certaines poutres. Cependant, plus de verifications sont utiles.
- Après la zone de fissuration, la courbe de la déflection suit une relation linéaire jusqu'à la rupture, ce qui indique que la déformation de la barre a contribué beaucoup plus que les déformations du béton.
- Les valeurs les plus élevées de la résistance à la compression du béton et du pourcentage d'armature correspondent au plus élevé du pourcentage *c/d* et aux plus petites déformations du béton en compression et par conséquent aux plus petites courbures et déflections.
- Les résultats d'essais ne montrent aucun effet du diamètre de la barre ou de la configuration de surface des barres en PRFV sur la déflection des poutres en béton normal ou en béton à haute performance.

- Le code de l'ACI 440.1R-06 [2006] et celui de l'ACI 440-H [2010] fournissent des valeurs non conservatrices de la déflection à $0.3M_n$ et à $0.67M_n$. Cependant, le code CAN/CSA-S806 [2012] et le manuel d'ISIS No.3 [2007] fournissent des prédictions conservatrices de la déflection à $0.3M_n$.
- Au-delà des niveaux de chargement de fissuration, les réponses charge-déflection prédites par l'ACI 440.1R-06 [2006]; l'ACI 440-H [2010]; le code CAN/CSA-S806 [2012] et le manuel d'ISIS No.3 [2007] montrent une importante augmentation de la déflection et se rapproche rapidement du comportement de la section pleinement fissurée. Cependant, cette perte soudaine en rigidité n'était pas observée durant les essais expérimentaux et peut être attribuée à la mauvaise évaluation du phénomène de la rigidité en tension.

7.2.6 Déformabilité

- L'espacement des étriers dans la zone de flexion est un facteur important pour assurer la déformabilité appropriée à la charge de service. L'absence d'armatures transversales (étriers) peut initier la rupture du béton à cause du flambement de l'armature en compression.
- La déformabilité peut dépendre des déformations du béton ou des déformations des PRF, cependant, une bonne définition de l'état de la charge de service en termes de charge ou de déformation dans les PRF ou dans le béton ajustera convenablement la prévision de la déformabilité

7.3 Recommandations pour des travaux futurs

À la lumière des résultats de cette étude, les suggestions suivantes pour des travaux futurs sont proposées.

- La déformabilité des éléments renforcés de PRF devrait être investiguée plus profondément.
- L'effet du renforcement latéral (étriers) sur le comportement en flexion des éléments en béton renforcé de PRF devraient être analysés plus en profondeur.
- L'étude de la déflection et la fissuration devrait inclure les éléments en béton précontraints de PRF.
- Le cisaillement induisant la déflection devrait être investigué en considérant diffèrent types d'étriers comme renforcement de cisaillement.
- Différents types de béton doivent être aussi investigués comme le béton auto plaçant et le béton à haute performance.
- La performance des éléments renforcés de PRF soumis à des charges cycliques dans les conditions de service devrait être investiguée.

LISTE DES RÉFÉRENCES

Abdalla, H. A. (2002). Evaluation of deflection in concrete members reinforced with fibre reinforced polymer (FRP) bars. *Composite Structures,* volume 56, numéro 1, p. 63-71.

ACI 318 (1999). *Building code requirements for structural concrete.* American Concrete Institute (ACI). (1999), Farmington Hills, Mich.,

ACI 318 (2008). *Building code requirements for structural concrete.* American Concrete Institute, Farmington Hills, Mich.,

ACI 440.1R-03 (2003). *Guide for the Design and Construction of Structural Concrete Reinforced with FRP Bars.* American Concrete Institute, Farmington Hills, Mich, 44 p.

ACI 440.1R-04 (2004). *Guide for the Design and Construction of Structural Concrete Reinforced with FRP Bars.* American Concrete Institute, Farmington Hills, Mich, 44 p.

ACI 440.1R-06 (2006). *Guide for the Design and Construction of Structural Concrete Reinforced with FRP Bars.* American Concrete Institute, Farmington Hills, Mich, 44 p.

ACI 440.6M-08 (2008). *440.6M-08 Specification for Carbon and Glass Fiber-Reinforced Polymer Bar Materials for Concrete Reinforcement.* American Concrete Institute, Farmington Hills, U.S.A., 10 p.

Aiello, M. A. et Ombres, L. (2000). Load-deflection analysis of FRP reinforced concrete flexural members. *Journal of Composites for Construction,* volume 4, numéro 4, p. 164-170.

Alsayed, S. H. (1998). Flexural behaviour of concrete beams reinforced with GFRP bars. *Cement and Concrete Composites,* volume 20, numéro 1, p. 1-11.

Al-Sunna, R. A. S. (2006). *Deflection behaviour of FRP reinforced concrete flexural members.* University of Sheffield,

Ashour, A. F. et Family, M. (2006). Tests of concrete flanged beams reinforced with CFRP bars. *Magazine of Concrete Research,* volume 58, numéro 9, p. 627-639.

ASTM D7205 (2011). *Tensile Properties of Fiber Reinforced Polymer Matrix Composite Bars.* American Society for Testing and Materials, Conshohocken, USA, 12 p.

Baena, M., Torres, L., Turon, A. et Barris, C. (2009). Experimental study of bond behaviour between concrete and FRP bars using a pull-out test. *Composites Part B: Engineering,* volume 40, numéro 8, p. 784-797.

Bakis, C., Ospina, C., Bradberry, T., Benmokrane, B., Gross, S., Newhook, J. et Thiagarajan, G. (2006). Evaluation of Crack Widths in Concrete Flexural Members Reinforced with FRP Bars, Dans *Third International Conference on FRP Composites in Civil Engineering*

Barris, C., Torres, L., Turon, A., Baena, M. et Catalan, A. (2009). An experimental study of the flexural behaviour of GFRP RC beams and comparison with prediction models. *Composite Structures,* volume 91, numéro 3, p. 286-295.

Beeby, A. W. (2004). The influence of parameter φ/ϱ_{eff} on crack widths. *Structural Concrete,* volume 5, numéro 2, p. 71-83.

Beeby, A. W., Alander, C., Cairns, J., Eligehausen, R., Mayer, U., Lettow, S., Ferretti, D., Iori, I., Gambarova, P., Bamonte, P. et Others (2005). The influence of parameter φ/ϱ_{eff} on crack widths. *Structural concrete,* volume 6, numéro 4, p. 155-165.

Benmokrane, B., Chaallal, O. et Masmoudi, R. (1996a). Flexural response of concrete beams reinforced with FRP reinforcing bars. *ACI Structural Journal,* volume 93, numéro 1, p. 46-55.

Benmokrane, B., Chaallal, O. et Masmoudi, R. (1996b). Flexural response of concrete beams reinforced with FRP reinforcing bars. *ACI Structural Journal,* volume 93, numéro 1, p. 46-55.

Bentz, E. C. (2005). Explaining the riddle of tension stiffening models for shear panel experiments. *Journal of Structural Engineering,* volume 131, numéro 9, p. 1422-1425.

Bischoff, P. H., Gross, S. et Ospina, C. E. (2009a). The story behind proposed changes to ACI 440 deflection requirements for FRP-reinforced concrete. Dans *ACI Spring 2009 Convention, March 15, 2009 - March 19.* American Concrete Institute, San Antonio, TX, United states, p. 53-76.

Bischoff, P. H., Gross, S. et Ospina, C. E. (2009b). The story behind proposed changes to ACI 440 deflection requirements for FRP-reinforced concrete. Dans *ACI Spring 2009 Convention*p. 53-76.

Bischoff, P. H. et Paixao, R. (2004). Tension stiffening and cracking of concrete reinforced with glass fiber reinforced polymer (GFRP) bars. *Canadian Journal of Civil Engineering,* volume 31, numéro 4, p. 579-588.

Bischoff, P. H. et Scanlon, A. (2007a). Effective moment of inertia for calculating deflections of concrete members containing steel reinforcement and fiber-reinforced polymer reinforcement. *ACI Structural Journal,* volume 104, numéro 1, p. 68-75.

Bischoff, P. H. et Scanlon, A. (2007b). Effective moment of inertia for calculating deflections of concrete members containing steel reinforcement and fiber-reinforced polymer reinforcement. *ACI Structural Journal,* volume 104, numéro 1, p. 68-75.

Bischoff, P. H. (2005). Reevaluation of deflection prediction for concrete beams reinforced with steel and fiber reinforced polymer bars. *Journal of Structural Engineering,* volume 131, numéro 5, p. 752-762.

Bischoff, P. H. (2007). Deflection calculation of FRP reinforced concrete beams based on modifications to the existing branson equation. *Journal of Composites for Construction,* volume 11, numéro 1, p. 4-14.

Bouguerra, K., Ahmed, E. A., El-Gamal, S. et Benmokrane, B. (2011). Testing of full-scale concrete bridge deck slabs reinforced with fiber-reinforced polymer (FRP) bars. *Construction and Building Materials,* volume 25, numéro 10, p. 3956-3965.

Branson, D. E. (1968). Design procedures for computing deflections. *Journal of the American Concrete Institute,* volume 65, numéro 9, p. 730-742.

Brooks, A.E., and K. Newman (1968). Proceedings International conference Structure Concrete. *Cement and Concrete Association,*

CAN/CSA-A23.3 (1994). *CAN/CSA-A23.3 Design of concreete structures for buildings.* Canadian Standsrds Association, Ontario,Canada, 220 p.

CAN/CSA-A23.3 (2004). *CAN/CSA-A23.3 Design of concreete structures for buildings.* Canadian Standsrds Association, Ontario,Canada, 220 p.

CAN/CSA-S6 (2002). *CAN/CSA-S6 Canadian Highway Bridge Design Code.* Canadian Standards Association, Mississauga, Ontario, Canada, 800 p.

CAN/CSA-S6 (2006). *CAN/CSA-S6 Canadian Highway Bridge Design Code.* Canadian Standards Association, Mississauga, Ontario, Canada, 800 p.

CAN/CSA-S6.1S1 (2010). *CAN/CSA-S6.1S1 Canadian Highway Bridge Design Code.* Canadian Standards Association, Mississauga, Ontario, Canada, 800 p.

CAN/CSA-S806 (2002). *CAN/CSA-S806 Design and construction of building components with fibre-reinforced polymers.* Canadian Standards Association, Ontario, Canada, 177 p.

CAN/CSA-S806 (2012). *CAN/CSA-S806 Design and Construction of building components with fibre-reinforced polymers.* Canadian Standards Association, Ontario, Canada, 187 p.

CAN/CSA-S807 (2010). *CAN/CSA-S807 Specification for fibre-reinforced polymers.* Canadian Standards Association, Mississauga, Ontario, Canada, 44 p.

CEB-FIP. (1990). *Model code 1990, Design code.* Comité Euro-International Du Béton, Thomas Telford Services Ltd, London,

CEN. (2004). Part 1.1: General rules and rules for buildings (EN 1992-1-1:2004). Dans Comité Europeen De Normalisation, *Eurocode 2: Design of concrete structures*Brussels, p. 225.

Ceroni, F., Cosenza, E., Gaetano, M. et Pecce, M. (2006). Durability issues of FRP rebars in reinforced concrete members. *Cement and Concrete Composites,* volume 28, numéro 10, p. 857-868.

Chang, K. K. (2001). Aramid Fibers. Dans ASM International, *ASM Handbook.* Material park, Ohio, p. 41-45.

Chen, W. F., and A. F. Saleeb (1982). Constitutive Equations for Engineering Materials. Dans *Plasticity and Modeling, Vol. 2.* Wiley, New York,

Claudio E. Todeschini, Albert C. Bianchini, and Clyde E. Kesler, (1964). Behaviour of Concrete Columns Reinforced with High Strength Steels. *American Concrete Institute -- Journal,* volume 61, numéro 6, p. 701-716.

CNR-DT 203. (2006). *Guide for the Design and Construction of Concrete Structures Reinforced with Fiber-Reinforced Polymer Bars.* Advisory Committee on Technical Recommendation for Construction, 39 p.

El-Gamal, S., El-Salakawy, E. et Benmokrane, B. (2005). Behaviour of concrete bridge deck slabs reinforced with fiber-reinforced polymer bars under concentrated loads. *ACI Structural Journal,* volume 102, numéro 5, p. 727-735.

El-Nemr, A., Ahmed, E. et Benmokrane, B. (2011). Instantaneous deflection of slender concrete beams reinforced with GFRP bars. Dans *Annual Conference of the Canadian Society for Civil Engineering 2011, CSCE 2011, June 14, 2011 - June 17,* volume 2. Canadian Society for Civil Engineering, Ottawa, ON, Canada, p. 1685-1694.

El-Salakawy, E., Kassem, C. et Benmokrane, B. (2002). Flexural behaviour of concrete beams reinforced with carbon FRP composite bars. Dans *Canadian Society for Civil Engineering - 30th Annual Conference: 2002 Chellenges Ahead, June 5, 2002 - June 8,* volume 2002. Canadian Society for Civil Engineering, Montreal, QB, Canada, p. 2025-2033.

Feeser, W. et Brown, V. (2005). SP-230-53: Guide Examples for Design of Concrete Reinforced with FRP Bars. *ACI SPECIAL PUBLICATIONS,* volume 230, numéro 2, p. 935.

fib. (2007). *FRP reinfrocement in Rc structures.* Féderation International Du Béton, Fib Task Group 9.3, Fib Bulletin 40, Lausanne, Switzerland, 147 p.

fib. (2010). *Model code 2010. First complete draft,* Fib Bulletin 56 édition. Féderation International Du Béton, 288 p.

Frosch, R. J. (1999). Another look at cracking and crack control in reinforced concrete. *ACI Structural Journal,* volume 96, numéro 3, p. 437-442.

GangaRao, H. V. S. et Faza, S. (1991). Bending and bond behaviour and design of concrete beams reinforced with fiber reinforced plastic rebars. *Final report to the Federal Highway Administration, West Virginia University,* p. 159.

GangaRao, H., Faza, S. (1992). *Bending and Bond Behaviour of Concrete Beams Reinforced with Plastic Rebars.* Technical Report, Phase I, West Virginia University, Morgantown, West Virginia, USA,

Gergely, P., and Lutz, L.A. (1968). Maximum Crack Width in Reinforced Concrete Flexural Members volume SP-20, numéro 6, p. 87-117.

Gergely, P. et Lutz, L. R. A. (1968). *Maximum crack width in reinforced concrete flexural members,*

Ghali, A. et Azarnejad, A. (1999). Deflection prediction of members of any concrete strength. *ACI Structural Journal,* volume 96, numéro 5, p. 807-816.

Grace, N. F., Soliman, A., Abdel-Sayed, G. et Saleh, K. (1998). Behaviour and ductility of simple and continuous FRP reinforced beams. *Journal of Composites for Construction,* volume 2, numéro 4, p. 186-194.

Hognestad, E. (1951). Study of combined bending and axial load in reinforced concrete members.

Hognestad, E., Hanson, N. W. et McHenry, D. (1955). Concrete stress distribution in ultimate strength design. *American Concrete Institute -- Journal,* volume 27, p. 455-479.

ISIS Manual No.3 (2007). *Design Manual No. 3: Reinforcing Concrete Structures with Fibre Reinforced Polymers.* The Canadian Network of Centres of Excellence on Intelligent Sensing for Innovative Structures, University of Manitoba, Winnipeg, Manitoba, Canada, 151 p.

IStructE. (1999). *Interim guidance on the design of reinforced concrete structures using fibre composite reinforcement.* Institution of Structural Engineers (IStructE), STEDO Ltd., London,

JSCE. (1997). *Recommendation for design and construction of concrete structures using continouous fiber reinforcing materials*, 23 édition. Japan Society of Civil Engineering, Tokyo, Japan, 325 p.

Kassem, C., Farghaly, A. S. et Benmokrane, B. (2011). Evaluation of flexural behaviour and serviceability performance of concrete beams reinforced with FRP bars. *Journal of Composites for Construction,* volume 15, numéro 5, p. 682-695.

MacGregor, J. G. (1997). Reinforced concrete: Mechanics and design. Prentice Hall Upper Saddle River, NJ, pp. 450

Masmoudi, R., Benmokrane, B. et Chaallal, O. (1996). Cracking behaviour of concrete beams reinforced with fiber reinforced plastic rebars. *Canadian Journal of Civil Engineering,* volume 23, numéro 6, p. 1172-1179.

Masmoudi, R., Thériault, M. et Benmokrane, B. (1998). Flexural behaviour of concrete beams reinforced with deformed fiber reinforced plastic reinforcing rods. *ACI Structural Journal,* volume 95, numéro 6, p. 665-676.

Mathys, S., and Taerwe, L., (2000). Concrete slabs reinforced with FRP grids, I: One-way bending. *Journal of Composites for Construction,* volume 4, numéro 3, p. 145-153.

McCallum, B. E. C., et Newhook, J. P. (2012). Evaluation of the bond dependent coefficient and parameters which influence crack width in GFRP reinforced concrete. Dans *Proceedings of the Sixth International Conference on Advanced Composite Materials in Bridges and Structures*. ACMBS VI, Kingston, Ontario, Canada, May 22-25, p. 8.

Mota, C., Alminar, S. et Svecova, D. (2006a). Critical review of deflection formulas for FRP-reinforced concrete members. *Journal of Composites for Construction,* volume 10, numéro 3, p. 183-194.

Mota, C., Alminar, S. et Svecova, D. (2006b). Critical review of deflection formulas for FRP-reinforced concrete members. *Journal of Composites for Construction,* volume 10, numéro 3, p. 183-194.

Nanni, A. (2003). North American design guidelines for concrete reinforcement and strengthening using FRP: Principles, applications and unresolved issues. *Construction and Building Materials,* volume 17, numéro 6-7, p. 439-446.

Neville, A. M. (1970). *Creep of Concrete: Plain, Reinforced, and Prestressed*North-Holland, Amsterdam,

Newhook, J., Ghali, A. et Tadros, G. (2002). Concrete flexural members reinforced with fiber reinforced polymer: Design for cracking and deformability. *Canadian Journal of Civil Engineering,* volume 29, numéro 1, p. 125-134.

Newman, K. (1966). Composite Materials. *Concrete systems,* p. 336-452.

OSPINA, C. E. et BAKIS, C. E. (2007). Indirect Flexural Crack Control of Concrete Beams and One-Way Slabs Reinforced with FRP Bars. *Proceedings of FRPRCS,* volume 8,

Parkyn, B. (1970). *Glass Reinforced Plastics*. Iliffe, London,

Pecce, M., Manfredi, G. et Cosenza, E. (2000). Experimental Response and Code Modelsof GFRP RC Beams in Bending. *Journal of Composites for Construction,* volume 4, numéro 4, p. 182-190.

Pecce, M., Manfredi, G., Realfonzo, R. et Cosenza, E. (2001). Experimental and analytical evaluation of bond properties of GFRP bars. *Journal of Materials in Civil Engineering,* volume 13, numéro 4, p. 282-290.

Pilakoutas, K., Guadagini, M. Neocleous, K. and Taerwe, L. (2007). Design guidelines for FRP reinforced concrete structures. Dans *Proceedings of Advanced Composites in Construction*University of Bath, Bath, UK.,

Pilakoutas, K., Guadagnini, M., Neocleous, K. et Taerwe, L. (2007). Design guidelines for FRP reinforcement concrete structures.

Pilakoutas, K., Neocleous, K. et Guadagnini, M. (2002). Design philosophy issues of fiber reinfored polymer reinforced concrete structures. *Journal of Composites for Construction,* volume 6, numéro 3, p. 154-161.

Rafi, M. M., Nadjai, A. et Ali, F. (2007). Experimental testing of concrete beams reinforced with carbon FRP bars. *Journal of Composite Materials,* volume 41, numéro 22, p. 2657-2673.

Rafi, M. M., Nadjai, A., Ali, F. et Talamona, D. (2008). Aspects of behaviour of CFRP reinforced concrete beams in bending. *Construction and Building Materials,* volume 22, numéro 3, p. 277-285.

Rasheed, H. A., Nayal, R. et Melhem, H. (2004). Response prediction of concrete beams reinforced with FRP bars. *Composite Structures,* volume 65, numéro 2, p. 193-204.

Rashid, M. A., Mansur, M. A. et Paramasivam, P. (2005). Behaviour of aramid fiber-reinforced polymer reinforced high strength concrete beams under bending. *Journal of Composites for Construction,* volume 9, numéro 2, p. 117-127.

Razaqpur, A. G., Švecová, D. et Cheung, M. S. (2000). Rational method for calculating deflection of fiber-reinforced polymer reinforced beams. *ACI Structural Journal,* volume 97, numéro 1, p. 175-184.

Shah, S. P. (1980). High Strength Concrete. Dans *University III Proceeding Workshop Chicago*. Pitman, University of Illinois, Chicago, USA,

Theriault, M. et Benmokrane, B. (1998). Effects of FRP reinforcement ratio and concrete strength on flexural behaviour of concrete beams. *Journal of Composites for Construction,* volume 2, numéro 1, p. 7-16.

Tighiouart, B., Benmokrane, B. et Gao, D. (1998). Investigation of bond in concrete member with fibre reinforced polymer (FRP) bars. *Construction and Building Materials,* volume 12, numéro 8, p. 453-462.

Toutanji, H. A. et Saafi, M. (2000). Flexural behaviour of concrete beams reinforced with glass fiber-reinforced polymer (GFRP) bars. *ACI Structural Journal,* volume 97, numéro 5,

Vijay, P. V. et GangaRao, H. V. S. (1996). Unified limit state approach using deformability factors in concrete beams reinforced with GFRP bars. Dans *Part 1 (of 2), November 10, 1996 - November 14.* Proceedings of the 1996 4th Materials Engineering Conference, volume 1. ASCE, Washington, DC, USA, p. 657-665.

Wallenberger, F. T., Watson, J. C., and Hong, L. (2001). Glass Fibers. Dans ASM International, *ASM Handbook.* Material Park, Ohio, p. 27-34.

Walsh, P. J. (2001). Carbon Fibers. Dans ASM International, *ASM Handbook.* Material Park, Ohio, p. 35-40.

Yost, J. R. et Gross, S. P. (2002a). Flexural design methodology for concrete beams reinforced with fiber-reinforced polymers. *ACI Structural Journal,* volume 99, numéro 3, p. 308-316.

Yost, J. R. et Gross, S. P. (2002b). Flexural design methodology for concrete beams reinforced with fiber-reinforced polymers. *ACI Structural Journal,* volume 99, numéro 3, p. 308-316.

Yost, J. R., Gross, S. P. et Dinehart, D. W. (2003). Effective Moment of Inertia for Glass Fiber-Reinforced Polymer-Reinforced Concrete Beams. *ACI Structural Journal,* volume 100, numéro 6, p. 732-739.